PLASMA STUDIES WITH THE IMP-2 SATELLITE

by

JOSEPH HERBERT BINSACK

B.E.E., Manhattan College
1958

M.S., Massachusetts Institute of Technology
1960

SUBMITTED IN PARTIAL FULFILLMENT OF THE

REQUIREMENTS FOR THE DEGREE OF

DOCTOR OF PHILOSOPHY

at the

MASSACHUSETTS INSTITUTE OF TECHNOLOGY
August, 1966

Signature of Author _____
Department of Electrical Engineering, August 22, 1966

Certified by _____
Thesis Supervisor

Accepted by _____
Chairman, Departmental Committee on Graduate Students

PLASMA STUDIES WITH THE IMP-2 SATELLITE

by

JOSEPH HERBERT BINSACK

Submitted to the Department of Electrical Engineering on August 22, 1966 in partial fulfillment of the requirements for the degree of Doctor of Philosophy.

ABSTRACT

The IMP-2 satellite was launched on 4 October 1964 into the subsolar region with an apogee of nearly 96,000 km. The M.I.T. plasma experiment on this satellite made extensive measurements of the solar plasma in the vicinity of the earth. The nearly five months of useful data included some measurements of the interplanetary solar wind, but the vast majority of the data covered the magnetosphere and the transition region.

An investigation of the spatial and temporal behavior of the boundaries of the transition region has been conducted. Both long term (hours) and short period (minutes) vibrations have been observed. The structure of the solar plasma in the interplanetary medium has been studied from the viewpoint of contact discontinuities associated with recurrent M-region storms on the sun. In the transition region, it is shown that the large isotropic fluxes are due to refracted electrons rather than hot protons. Estimates of the electron thermal energy show it to be below 50 e.v. The refraction of electrons permits the detection of electron fluxes in the magnetosphere. In the dawn hemisphere, electron thermal energies of 1 Kev are common. Finally, it is shown that the detector is sensitive to the near-earth plasmasphere of dense thermal ions. The "knee" boundary is mapped and its response to solar activity is studied.

Thesis Supervisor: Bruno B. Rossi
Title: Institute Professor

ACKNOWLEDGEMENT

I would like to express my appreciation to Professor Rossi for his supervision of this thesis. I am particularly indebted to Dr. H.S. Bridge for his assistance, guidance and encouragement during the entire course of this study. Sincere thanks are also due Professors Olbert and Lazarus for their helpful suggestions and stimulating discussions. The preflight preparation of the instrument and the postflight data editing was carried out by Dr. E.F. Lyon to whom I would like to express my sincere appreciation. I also wish to express my thanks to V. Vasyliunas for the many helpful suggestions and discussions.

I would like to thank Dr. Fairfield and Dr. Ness of the Goddard Space Flight Center for many interesting discussions and permission to use some of their data prior to publication.

Finally, I cannot express enough gratitude for all the love, patience and understanding given me by my wife and three girls during this period.

TABLE OF CONTENTS

To My

FATHER

and

MOTHER

CHAPTER I

INTRODUCTION

A. Historical Development

In addition to a steady emission of black body radiation characteristic of a surface temperature near 6000°K, the sun produces other "radiations" of a more unsteady nature which produce a number of conspicuous effects near and at the earth. The aurora and the geomagnetic storm were the two principal terrestrial effects on which early investigations of solar-terrestrial relations were based: their simple observations required little more than the naked eye and crude magnetometers. More recently, as a wide variety of instruments had permitted observation of a broader range of phenomena, it has been found that radio storms, modulation of the galactic cosmic ray intensity, solar cosmic ray enhancement, variations in trapped radiation belts and certain aspects of the terrestrial weather are evidently to be regarded as manifestations of a solar influence.

Perhaps the first serious attempt to understand the nature of the solar-terrestrial relations was the work of Störmer just after the turn of the century (Störmer, 1955 and references therein)*. He suggested that the auroral forms are produced by charged particles which propagate from a point on the sun and are deflected in the dipole magnetic field

---

*References will be found in the bibliography. In some cases the origin work is not referenced directly, but rather a more convenient work is quoted which is more in the context of the particular discussion.

of the earth. Of particular importance are his calculations of the orbits of charged particles in a dipole magnetic field. These trajectories have become of fundamental importance in modern studies of cosmic rays.

The current view that the aurora and geomagnetic storm are the result of plasma from the sun begun with Chapman in 1927. He and Ferraro set out to illustrate, through a sequence of idealized examples, that a cloud of ionized gas emitted from the sun at the time of a solar flare will produce many of the observed effects as it sweeps past the earth a day or two later (Chapman and Ferraro, 1930). They were able to show that the pressure of this gas flow on the geomagnetic field could produce the sudden commencement and initial phase of the geomagnetic storm, and they speculated as to how the passage of this gas might lead to the main and recovery phases of the storm. The point of view of Chapman and Ferraro has become widely accepted, and essentially all the modern ideas are stated in the context of their ideas first proposed 35 years ago.

Since the work of Chapman and Ferraro, there has been a great proliferations of ideas, usually each separate idea propounded as an attempt to explain some fact of the increasing store of observational information.

Biermann (1951) pointed out several properties of Type I comet tails which appear to indicate that they result from the interactions of a fast moving solar plasma with the cometary material. He suggested that gas is often streaming radially outward from the sun in all directions with the velocities ranging from 500 to 1500 km/sec and that there is no

indication that the gas ever has any inward motion. Biermann concluded that the solar ejection of particles is a continuing process and not limited to solar eruption at the time of a large flare. This solar corpuscular radiation is much more violent when the sun is active, but apparently continues at a lower level during the quiet periods of the solar cycle.

In 1956, Parker began his studies of the solar corona by considering the possibility that the corona may not be in hydrostatic equilibrium, but rather that it may be expanding hydrodynamically, and flowing outward in a form which he called the "solar wind" (Parker, 1958). Since the interplanetary gas is very tenuous, it is not obvious that a fluid-like picture can be applied. The condition for the validity of such a fluid model is that the mean free path for collision of the particles be small compared to the dimensions of the system, or to relevant lengths which are of importance such as the scale height.

At the time Parker brought out his hydrodynamic solar wind theory, the solar wind was far from being considered a demonstrated fact. Several years were to pass before the first, tentative direct observations of the solar wind were reported. Meanwhile, a controversy developed when Chamberlain (1960 , 1961) proposed that the subsonic solution of the hydrodynamic equations are chosen by nature. The resulting expansion velocities were more than an order of magnitude lower than Parker's estimates. The controversey between a solar "breeze" and solar "wind" was not resolved until the direct observations of the high velocity solar wind by satellite experiments (see the summary by Parker, 1965).

Excellent reviews of the early work in the field of solar plasma and of the observations leading to the concept of a solar wind are presented by Lüst (1962), Rossi (1963), and most recently by Dessler (1966).

B. The Solar Wind and Interplanetary Magnetic Fields

The development of the solar wind concept by Parker (1963 , 1965) was based on the hydrodynamic expansion of the solar corona. He showed that the thermal energy of expansion exceeds the gravitational energy of confinement, and that the corona expands continuously. Parker's solution to the hydrodynamic equations indicated that the expansion became supersonic beyond a critical radius from the sun. The equations governing the expansion are similar to those describing the flow of gas through a deLaval nozzle (Clauser, 1960) and the analogy has proven helpful in subsequent studies.

One of the principal problems related to the study of the interplanetary medium has been its microscopic physical properties. If a body of gas is to be treated as a hydrodynamic fluid, then there must be a communication process among the particles so that they may act as a group. For the corona, the hydrodynamic approximation is expected to be valid since the collision mean free path is less than the local scale height. However, beyond several solar radii, the solar plasma must be considered to be essentially collisionless, because the mean free path of the individual particles are very large compared to the scale of the phenomena being studied.

In the interplanetary medium, the mechanism by which the various particles interact and propagate disturbances is related to the presence of the interplanetary magnetic field. In effect, the information is propagated by waves with wave lengths predominantly near some typical dimensions of the disturbance or obstacle. The critical communication

scale is not the collision mean free path, but is on the order of the proton gyroradius.*

On a scale of 1 A.U.** the solar wind can be considered as a collisionless plasma; in addition on this scale it is also a very highly conducting medium. A consequence of this fact is that the magnetic field will be "frozen in" the plasma and move in unison with it. (Alfven, 1950). This yields a magnetic field topology which is completely determined by the motion of the plasma.*** Parker (1958) used this result and showed that the solar plasma leaving the sun would carry with it the "frozen in" solar magnetic fields. These field lines are stretched out along the Archimides spiral that represents the locus of a continuous stream of solar wind plasma as seen in a non-rotating reference frame.

The first experimental verification of this predicted spiral structure was obtained by McCracken (1962) using solar-flare cosmic

---

*For a 200 km/sec proton in a 10 gamma magnetic field (10^{-4} Gauss), the gyroradius is 200 km.

**The astronomical unit (A.U.) is 1.5×10^8 km or roughly 210 solar radii.

***The interplanetary fields are carried with the plasma since the plasma kinetic energy density greatly exceeds the magnetic energy density in the interplanetary medium. If the converse were true, then the magnetic fields would confine and trap the plasma causing it to corotate with the sun to an appreciable distance (Dungey, 1958; Alfven, 1950 ; Gold, 1959).

ray data obtained at the earth's surface. Direct measurements made in interplanetary space (Ness, et al., 1964 ; Wilcox and Ness, 1965 ; Davis et al., 1966 ; Coleman et al., 1966[a]) have conclusively demonstrated the solar origin of the interplanetary magnetic field, and its general alignment with the Archimedes spiral. The magnitude lies in the neighborhood of 5 gamma during quiet times. Ness, et al., (1964) have commented on the extraordinary steadiness of the interplanetary field during the flight of IMP-1, but other experiments find that from time to time, the field is strongly enhanced (Coleman, et al., 1961 ; Sonett, et. al., 1964).

The fields appear to have a large scale sector structure (Wilcox and Ness 1965) the pattern of which has changed over the last several years (Coleman, et al., 1966[b]). The division of the structure into regions of oppositely directed magnetic fields suggests that the different sectors are separated by neutral sheets. The sheet model provides the possibility, but it has not yet been experimentally shown, that local heating of the solar wind could take place in the neutral sheet region. For this to happen, disipative mechanisms must operate, extracting energy from annihilation of the field to produce heating of the gas by the released energy (Sonett, et al., 1962). The mechanism would be either ohmic heating, an unlikely occurrence because of the extreme mean free path, or some form of magnetohydrodynamic turbulence leading to diffusion of the solar wind across the field lines. The latter process has been suggested by Petschek (1963) as a source of entropy generation behind collision-free shock waves, and in the neutral sheet region of the earth's

magnetic tail (Levy, Petschek and Siscoe, 1963 ; Ness, 1965).

Parker's hydrodynamic model of the solar wind predicted that the expansion of a solar corona at 10^6°K would produce a plasma flow at the orbit of the earth near 500 km/sec. For the solar wind, the important waves are the magneto-acoustic waves which travel at a phase velocity $\sqrt{V_A^2 + V_S^2}$ where V_A is the Alfven speed and V_S is the local speed of sound in the medium. Since V_A and V_S are roughly comparable*, the plasma velocity is nearly 5 V_A to 10 V_A, it is clear that the solar wind must be considered to be supersonic (Bonetti, et al.,1963 : Snyder and Neugebauer, 1964 ; Ness, 1964 ; Lyon, 1966).

As long as the solar wind remains supersonic, the earth's magnetosphere cannot make its presence felt upstream in the wind; and in order to make the solar wind flow around the obstacle, nature takes a drastic step. A shock wave forms on the upstream side of the magnetosphere and produces subsonic flow behind it. The shock is a collision-free phenomenon and its thickness is expected to be of the order of a hybrid proton-electron gyroradius (Levy, Petschek, and Siscoe, 1963).

As the solar plasma crosses the shock wave, the directed wind velocity is expected to become subsonic and the random energy of the particles should increase. The energy density of the solar magnetic field embedded in the plasma stream is also expected to increase and the field should become more turbulent than in the free stream. The plasma is then expected to flow around the magnetospheric cavity in a transition region that lies between the boundary of the cavity and the

*For a 5 gamma magnetic field and a plasma density of 5 cm^{-3}, $V_A \approx 50$ km/sec.

undisturbed plasma stream. As the plasma moves in this channel, away from the stagnation point (the "nose" of the magnetospheric cavity) the directed velocity should steadily increase until the fluid again becomes supersonic. In the flanks of the magnetosphere, a "flag waving" type of instability is expected, as suggested by Dungey, (1955) and discussed recently by Hines (1963) and probably observed by Explorer 10 (Bonetti, et al., 1963).

Observations to date are in very good agreement with the above model (see the reviews of Obayashi, 1964 ; Ness, 1965_a; Hess and Mead, 1965). The observed standoff distance of the shock from the magnetopause is approximately 3.5 Re* (Ness, 1965a; Lyon, 1966). The theoretical predictions of the topology of the solar wind - geomagnetic field interaction region require a knowledge of the radius of curvature of the boundary, the Mach number of the fluid flow, ratio of specific heats of the fluid, and the effects of viscous interactions across the boundary. Theoretical shapes have been investigated by a number of workers; Beard (1960), Midgley and Davis (1962), Slutz (1963), Spreiter and Briggs (1962), Mead and Beard (1964), and all results are in generally good agreement as long as the region near the null points in the polar region is not considered. A very detailed numerical study has recently been conducted by Spreiter, Summers, and Alksne (1966) for the location of bow shock wave, and the density, velocity and temperature of the flow in the transition region for various Mach numbers and specific heat ratios.

---

*The earth's radius (1 Re) is a convenient scale length to use. It is usually taken as 6371 km.

The three regions of near earth space are depicted schematically in Fig. 1 . The shock boundary separates interplanetary space from the transition region. The magnetopause is the boundary between the transition region and the magnetosphere.

Extensive plasma measurements in the interplanetary region have now shown that the solar wind is continually flowing from the sun at very high velocities, generally ranging from 360 to 700 km/sec for Mariner 2 (Snyder and Neugebauer, 1964), 250 to 450 km/sec for IMP-1 (Lyon, 1966), and 300 to 525 km/sec for Mariner 4 (Lazarus, et al., 1966a). The flow is nearly radial from the sun and ion temperatures of the order of 10^5 °K have been reported (Neugebauer and Snyder, 1964). More recently measurements on the Vela satellites by the Los Alamos group indicate that the temperature of the ion component can be below 10^4 °K (Strong, et al., 1966b). The various experimenters have reported average densities in the neighborhood of 5 protons/cm, with frequent rapid excursions beyond 20 protons/cm^3.

C. Outline of the Present Study

In this study, the principal results of the M.I.T. plasma experiment on the IMP-2 (Explorer 21) satellite will be presented. The plan of this report is first to briefly describe the satellite and the instrument in Chapter 2, and then to proceed in Chapter 3 to a discussion of the methods used in analyzing the data. The principal results are presented and discussed in Chapter 4. Finally, Chapter 5 summarizes the main conclusions of the study.

CHAPTER II

THE M.I.T. PLASMA EXPERIMENT ON IMP-2

A. Description of the Satellite and Orbit

The IMP (Interplanetary Monitoring Platform) series of satellites is a continuation and extension of the NASA Explorer series of satellites. IMP-1 (Explorer 18), launched on 26 November 1964, attained an apogee of 195,000 km (31.7 earth radii) which carried it well into interplanetary space. IMP-2, (Explorer 21), was launched slightly more than ten months after IMP-1 on 4 October 1964. A malfunction of the third stage rocket resulted in reduced performance and an injection velocity 1.8% below nominal. The apogee achieved was 95,000 km (15.9 earth radii) which was less than half of the planned distance. In addition, the dynamic perturbations introduced by the malfunction caused a shift of the spacecraft spin axis of about 78 degrees resulting in a wider range of incident sun angles. This ultimately shortened the spacecraft lifetime by reducing the available power supplied through the solar paddles. The spacecraft was inoperative from 5 Dec through 13 Dec 64, from 9 Feb through 5 Mar 65, and for all practical purposes after 4 April 65.*

Because of the reduced apogee the primary objectives of the mission could not be accomplished, and IMP-2 is officially classed as a "Mission Failure". Nevertheless, the nine experimenters were able to obtain nearly five months of useful data while the satellite explored the

---

* Intermittent operation permitting some data acquisition occurred from July through October after which no further attempt was made to acquire data (Carr, 1966).

magnetosphere and transition region. A limited amount of data was also obtained in the interplanetary region during portions of the first 40 orbits.

The IMP-2 orbital parameters are given in Table 1 and the changes in the attitude and spin period are depicted in Figs. 2 and 3 . The non-nominal range for these quantities is directly attributable to the malfunctions of the third stage rocket. The effect of these non-nominal values on the performance of the M.I.T. plasma experiment will be discussed later in this chapter.

The region of space scanned by the IMP-2 satellite as projected onto the solar ecliptic plane* is illustrated in Fig. 4 which also includes a representation of the average magnetopause and shock boundaries as seen by IMP-1. The velocity vector at injection placed the apogee of the orbit some 5 Re below the ecliptic plane. As a consequence all outbound passes through the magnetosphere and transition region occurred at high ecliptic latitudes in the Southern hemisphere, whereas the inbound passes were very close to the ecliptic plane.

An interesting feature of the orbit is the relationship of the period to the apparent solar day. Because two orbital periods are very nearly equal three days, alternate orbits of the satellite will be essentially the same when viewed in a coordinate system depending on the earth's rotation. One such coordinate system is the geocentric solar

---

* For a description of frequently used coordinate systems, see Appendix A.

TABLE 1

IMP 2 Parameters

Launch: 0345:00.4, UT, 4 October 1964, out of Pad 17A Cape Kennedy, Florida by the Thor Delta rocket #26

Injection: 0351:29.5, UT, 4 October 1964, at approximately 23.3 degrees North and 66.7 degrees West at an altitude of 197 km and velocity of 35,023 ft/sec (nominal 35,591 ft/sec).

Orbit	Nominal	Actual
Apogee (km)	205,000	95,569
Perigee (km)	194	193
Period (hrs.)	98.6	34.94
Inclination (Deg.)	33.0	33.53
Eccentricity	0.939	0.88

Spin and Attitude: (4.5 days after launch)

Spin axis	R.A. (Deg.)	37.0	41.4
	Dec. (Deg.)	-30.7	47.4
Spin axis - sun angle (Deg.)		105	130
Spin rate rpm		23	14.25

magnetic system described in Appendix A. This feature can be effectively used in discussing some data from the magnetosphere and especially in the magnetosphere tail near the midnight local time meridian.

B. Description of the Plasma Experiment

1. General

The M.I.T. plasma probe flown on IMP-2 was essentially the same design as that flown on IMP-1,* with two significant modifications: the noise level of the instrument was reduced by about a factor of eight and a photoeffect from the front grid was eliminated.

The instrument, shown schematically in Fig. 5 and described in more detail in Appendix C, was a "Faraday Cup" designed to measure the flux of charged particles within energy windows determined by the potential on the modulator grid (grid #2). The trajectories of these particles as they pass through the cup are altered by the square wave voltage applied to this grid. Only those particles reaching the collector contribute to the measured current. The difference between the currents measured during each half cycle of the square wave constitutes the A.C. signal which is processed by the measurement chain.

Five of the six measurement channels (hereafter referred to as the "positive" channels) employed positive modulator voltages. The remaining channel (the "negative" channel) used negative voltages. The exact voltages used, and a listing of some of the pertinent characteristics of the instrument are included in Table 2.

The instrument was operated in synchronism with the spacecraft's telemetry system. One complete spectrum (5 positive and 1 negative

---

* For a thorough description of the instrument and scientific results of the M.I.T. plasma experiment see Lyon, E.F., Ph.D. Thesis (1966).

Table 2

M.I.T. IMP-2 Plasma Probe Characteristics

Channels	Lower Mod. Voltage	Upper Mod. Voltage
1	40	90
2	95	230
3	265	650
4	700	2000
5	-130	-265
6	1800	5400

Sensitivity	$7. \times 10^{5}$ $(cm^{2}- sec)^{-1}$	$(3. \times 10^{-12}$ amps)
Dynamic Range	4 decades	
Effective Area	24.25 cm^{2}	
Solid Angle	~ 1 ster.	
Noise Bandwidth	~ 150 cps.	
Type of Demodulation	amplitude (halfwave rectification)	

channels) was accomplished within 2.87 minutes every 5.45 minutes (see Fig. 6). Data for each channel were taken within 3.52 seconds (22 separate measurements of current taken by a "sample and hold circuit" every 0.16 seconds). Since the 3.52 second interval of data collection was shorter than the spin period during the major portion of the satellite's lifetime (Fig. 3), the measurements taken in any single channel did not cover a complete revolution. The missing azimuthal coverage exhibited a beat phenomenon due to the commensurability, N, of the spin period, T, and the period between successive spectrum measurements, (5.45 min).

$$N = \frac{5.45}{T} \qquad \text{revolutions/beat}$$

Since the spin period varied from 4.2 sec to 3.3 sec, the beat phenomenon was most apparent when N became equal to the integers between 78 and 100 (see Fig. 3). During these times (about every seven days) a particular segment of the azimuthal scan was lacking for several hours. Often times this effect occurred in one or more channels within a segment of prime interest and precluded useful analysis of data during these periods.

2. Sources of Spurious Currents

One of the most troublesome problems on IMP-1 was a photoelectric current resulting from electrons emitted by the front grid. These electrons were modulated by the electric fields near that grid, and eventually reached the collector and gave rise to a spurious A.C. signal. The fact that this problem (and many others) was eliminated

on IMP-2 and subsequent flights is due to the efforts of Dr. E.F. Lyon (1966b). Extensive analysis and testing demonstrated that reducing the potential of this front grid from -36 to -18 volts was a sufficient modification to eliminate this type of photocurrent.

There were, however, other contributions to the measured current which IMP-2, in part, helped to distinguish due to its improved sensitivity:

(a) A photocurrent which appears in the negative channel.

(b) The refraction of the trajectories of both positively and negatively charged particles.

(c) The scattering of particles by the strong electric fields surrounding the wires of the modulator grid.

Each of these mechanisms will now be discussed briefly.

(a) The Photocurrent in the Negative Channel

The photoeffect that became apparent in the negative channel also existed on IMP-1, but was usually barely above the noise level. With IMP-2, however, it stood out by a factor of ten or more above the noise and could not be ignored.

The source of this photocurrent is the electrons emitted by the second grid, the modulator grid. As in the case of the photocurrent from the front grid on IMP-1, the modulation of these electrons is due to the electric fields about the wires of the grid liberating the photoelectrons. The fields on either side of the modulator grid are inherently asymmetrical. Both the unequal spacing between the grids and the different

potentials on grid #1 and #3 combine to produce the asymmetry. This results in stronger fields between grids #2 and #3. Furthermore the grids are not truly planar, so that the field strength and direction will vary slightly throughout the grid structure. As the square wave voltage on the modulator grid varies, so will the probability of accelerating toward the rear of the cup those electrons born on that grid. Since there is no potential barrier for these electrons, a large majority of them will reach the collector.* The phasing of the resultant alternating current is such as to be out of phase with the normal flux of plasma electrons recorded in the negative channel. When the two components are comparable, a near cancellation occurs. This, indeed, is often observed when the plasma electrons produce a current near 5×10^{-11} amps.

(b) The Refraction Effect

A significant contribution to the better understanding of the functioning of the instrument was made in the analysis of the IMP-2 data through the demonstration of the importance of particle trajectory refraction within the cup. Although this effect has long been known

*An estimate of the currents involved can be made as follows: The photoelectric current density from tungsten due to solar ultraviolet is approximately 4×10^{-9} amps/cm^2 (Hinteregger, et al. 1959). The effective area of the tungsten mesh on grid #2 is about 2 cm^2. One needs only to introduce a modulation efficiency of less than one percent to produce the measured currents. Calculations based on fringing electric fields near the wires show that this is a reasonable estimate of the efficiency.

to exist, its contribution to the data was considered to be minor. Indeed on IMP-1 this was the case due to the higher noise level (although it did lead to the initial misinterpretation of the nearly isotropic component in the positive channels within the transition region as being solely due to very hot protons (Olbert and Moreno, 1964 ; Lyon, 1964)).

A qualitative understanding of the effect can be obtained with the aid of Fig. 7 which is a schematic view of the cup showing for positive modulator voltages the trajectories of an electron and ion each with a given initial velocity vector and point of entry. It is seen that for the higher voltage of the square wave modulation more electrons and fewer ions are collected compared to the amount collected for the lower voltage. Both effects constitute an alternating current in phase with the normal ion current.

This latter current usually constitutes the bulk of the measured current and results from the direct modulation of those ions with

$$Z_i e V_j \leq \frac{1}{2} m_i (v \cos\theta)^2 \leq Z_i e V_{j+1}$$

where V_j and V_{j+1} are the lower and upper modulator voltages respectively, Z_i and m_i are the charge and mass of the ion, and v is the velocity of the ion incident upon the cup at the polar angle, θ , with respect to the axis of symmetry of the cup.

It should be noted that the presence of a sufficient flux of electrons can cause a significant if not dominant current to be measured in the positive channels. The nearly isotropic current in the transition region, originally interpreted as hot ions on IMP-1, was primarily due

to the refraction of isotropic electrons in the positive channels. (Lyon, 1966a).

(c) Scattering

There is another mechanism which can modulate the flow of charged particles to the collector. It is the scattering of the particles when they are in the vicinity of the modulator grid wires. When the modulator voltage is at its higher level for a particular channel, the electric field curvature is greater near the wires and thus an enhanced scattering mechanism is achieved. This scattering also included a modification of the effective cross section of the wires for absorption and will increase (decrease) the cross section if the charge of the particle is opposite to (same as) the sign of the modulator voltages.

The entire process can be viewed as a modulation of the effective transparency of the modulator grid, since the effect is to remove particles, independent of sign, from the incoming stream of plasma. However, due to their smaller mass, electrons will be more easily accelerated than protons. The residual electron modulation has been investigated (Vasyliunas,1964) and found to be less than one percent of the electron flux. The major effect is to slightly reduce the transparency for electrons in the higher channels. This has been noted in the refracted electrons which appear in the positive channels. The isotropic background appearing in channel 6 tends to be lower than that expected if the transparency were indepdendent of the channel voltages.

For the majority of the data, scattering will be ignored since refraction contributes the greatest percentage of extraneous signals in the positive channels. This particular circumstance is due to the fact that most of the electrons have low energy and their trajectories are determined primarily by the dominant intergrid electric fields, rather than the intragrid fields. The quantitative study of refraction and its inclusion in the analysis of the IMP-2 data will be given in the next chapter.

CHAPTER III

ANALYSIS OF THE DATA

This chapter will deal with models and techniques used in the analysis and interpretation of the data. The principal results of the analysis will be presented in the next chapter.

A. Introduction to the Models

It is useful to start from first principles and consider exactly what the instrument measures.

Consider the local coordinate system of the cup: the positive Z axis is along the axis of symmetry of the cup with the direction of the outward normal (henceforth referred to as the "cup normal", or "axis of the cup"), the positive X axis is arbitrarily taken to be coincident with the spin axis of the satellite, and θ and ϕ, are the polar and azimuthal angles in this coordinate system (see Appendix A, Fig. A-5).

Let $N_i\left[E, \theta, \varphi, \hat{m}(t), \vec{\pi}(t)\right]$ be the number of particles per second of species, i, per unit energy - area - solid angle (arriving from direction θ, ϕ). The cup normal is pointing in the direction specified by the unit vector $\hat{n}$ and the satellite is in position $\vec{\pi}$ at time t.

Let $f_i(\vec{\pi}, \vec{v}, t)$ be the phase space distribution function for species i as seen in the reference from of the cup.

Then from conservation of particles we have

$$N_i\left[E, \theta, \varphi, \hat{m}(t), \vec{\pi}(t)\right] dE\, dA\, d\Omega\, dt = f_i(\vec{\pi}, \vec{v}, \tau)\, d^3\pi\, d^3v \qquad (3.1)$$

from which it is easily shown that for non-relativistic particles

$$N_i\left[E, \Theta, \Phi, \hat{m}(t), \vec{n}(t)\right] = \frac{v^2 \cos\Theta}{m_i} f_i(\vec{n}, \vec{v}, t) \qquad (3.2)$$

The instrument registers these particles with an efficiency $H(v_z, v_t)$ depending only upon the normal component of velocity $v_z = v\cos\Theta$ and the tangenial component $v_t = v\sin\Theta$ *. With $Z_i e$ being the charge of the species ($e = +1.6 \times 10^{-19}$ coulomb) and A_g the geometrical area of the cup's collection, the direct current measured for the modulator voltage V_j is

$$I_j\left[\hat{m}(t), \vec{n}(t)\right] = \sum_i Z_i e \int_{A_g} dA \int_{4\pi} d\Omega \int_0^\infty v_z H_{ij}(v_z, v_t)\, v^2 f_i(\vec{n}, \vec{v}, t)\, dv \qquad (3.3)$$

This is the basic relationship between the particle distribution function and the particle current. The measured A.C. signal is the difference between the currents for lower (j) and higher ($j+1$) modulator voltages for a particular channel:

$$I_{measured} = I_j - I_{j+1} \qquad (3.4)$$

---

* Two exceptions which are discussed elsewhere: The response to solar photons is dependent upon $\hat{n}(t)$; and the response to "scooped positive ions" depends on both $\hat{n}(t)$ and $\vec{n}(t)$.

To permit (3.3) to be manageable in the models, three simplifying assumptions will be made:

Assumptions:

1) Only singly ionized positive ions, and electrons are considered:

$$Z_i = \pm 1 \qquad (3.5a)$$

2) The efficiency consists of a constant transparency of the grids at normal incidence, T, and a normalized efficiency η_{ij} . The transparency has been measured optically and experimentally and was found to be approximately 25%. (Lyon, 1966).

$$H_{ij}(v_z, v_t) = T\,\eta_{ij}(v_z, v_t) \qquad (3.5b)$$

$$T = 0.25$$

3) The normalized efficiency can be expressed as

$$\ln\left[\eta_{ij}(v_z, v_t)\right] = v_t^2\,\Psi_{ij}(v_z) \qquad (3.5c)$$

With these assumptions, and designating the effective area as $A_e = TA_g$, and now using a Cartesian velocity space

$$I_j\left[\hat{n}(t), \vec{\pi}(t)\right] = e A_e \sum_i Z_i \int_{-\infty}^{\infty} dv_x \int_{-\infty}^{\infty} dv_y \int_{-\infty}^{\infty} dv_z \; v_z \in^{-(v_x^2 + v_y^2)\,\Psi_{ij}(v_z)} f_i(\vec{\pi}, \vec{v}, \tau) \qquad (3.6)$$

To proceed further, one must make some assumptions concerning the form of the distribution functions as seen in the frame of reference to the cup.

B. Plasma Models

Ideally, one would like to invert equation (3.6) and solve for the distribution function in the cup frame in terms of the measured currents, and then transform the distribution to the plasma's center of mass frame.* In principle this can be done by expansions in terms of orthogonal functions (spherical harmonics and Mellin transforms appear to be the natural ones to use (Vasyliunas, 1966a)). However, the amount of effort required is beyond the scope of this work, and so the simpler method of parameter fitting to a particular model distribution function has been pursued.

The choice of the model distribution function must be done carefully, lest the physics of the problem be lost in the study. One must use as much $\bar{a}$ priori information as possible, yet in those areas where no information is available one should maximize the vagueness of the model, i.e., include no built in biases and be least committal.

In the study of positive ions, from the class of distribution functions isotropic in the center of mass frame of the plasma, only those with a single parameter, w_o, will be considered. As viewed in the local coordinate system of the cup, this distribution will have two parameters: V, the velocity of the center of mass with respect to the cup frame, and w_o, a measure of the shape of the isotropic distribution

*The "Center of Mass" frame is defined as that frame of reference in which there is no net mass flow. The relative velocity of this frame with respect to a particular observational frame is called the "bulk velocity", V, of the plasma.

in the center of mass frame. The assumption of an isotropic distribution of particles in the center of mass frame is based on the following considerations:

1) In the interplanetary region, even though the ion-ion collision mean free path is of the same order as the dimensions of the system (1 A.U.), irregularities in the interplanetary magnetic field, low frequency MHD waves, and various instabilities which develop when the distribution becomes too anisotropic, will all tend to randomize and redistribute any distribution so that it will relax toward an isotropic function.

2) In the transition region, the passage of the plasma across the shock boundary increases the entropy and rapidly randomizes the distribution. (While the exact mechanism for accomplishing this randomization is still not clear, low frequency waves certainly contribute).

3) In the magnetosphere, the spiraling of the particles about the magnetic lines of force combined with the wide range of their pitch angle distribution will tend to give a high degree of isotropy to the distribution function as seen by the cup.

For these reasons, as well as the reduced complexity of the mathematics, an isotropic model will be assumed.

It can be shown (Jaynes, 1957) that from the class of two parameter distributions, the one which maximizes the vagueness (by maximizing entropy) is the Maxwellian distribution:

$$f_m(\vec{v}) = C_m \in^{-\frac{(\vec{v}-\vec{V})\cdot(\vec{v}-\vec{V})}{w_o^2}}$$

$$C_m = \frac{N}{\left(\pi w_o^2\right)^{3/2}} \tag{3.7}$$

where N is the density of particles in real space.

In the following sections the most probable thermal speed or simply thermal speed, w_o (km/sec), will be used to describe the spread of the distribution, rather than the temperature, simply to avoid any direct implication that the particles are in true thermodynamic equilibrium. It is true, of course, that for the Maxwellian distribution the temperature T is meaningful and related to w_o by

$$kT = \frac{1}{2} m_i w_o^2 = E_o \tag{3.8}$$

where k is Boltzmann's constant, and m_i, is the mass of the species. We shall also frequently use the thermal energy, E_o (ev), which is related to w_o by (3.8).

If the model is developed assuming that the bulk velocity is directly from the sun, then any offset in the data (due, for example to aberration in the interplanetary region, or confined flow in the transition region) will be easily determined from the data.

Let us define a satellite - sun coordinate system (see Appendix A and Fig. A- 6)such that the positive Z axis is along the spin axis, the X-Y plane is the plane traced out by the rotating cup normal, and the positive X half of the X-Z plane contains the satellite-sun line at a lattitude of α degrees. The azimuthal angle of the cup normal is β. As shown in Appendix A, the velocity streaming from the sun will have

coordinates in the frame of the cup:

$$V\Big]_{cup} = \begin{bmatrix} V_x \\ V_y \\ V_z \end{bmatrix} = V \begin{bmatrix} \sin\alpha \\ \cos\alpha \sin\beta \\ \cos\alpha \cos\beta \end{bmatrix} \qquad (3.9)$$

so that (3.7) becomes

$$f_\lambda(\vec{n}, \vec{v}, t) = C_m \exp\left\{ - \frac{(v_x - V_x)^2 + (v_y - V_y)^2 + (v_z - V_z)^2}{w_0^2} \right\} \qquad (3.10)$$

When this function is substituted into (3.6), the three dimensional integral factors; two of the integrals can be done analytically, and the expression reduces to a one-dimensional integral. The ion current for modulator voltage j in terms of these parameters is:

$$I_j\left[\vec{n}(t), V, w_0^2, \alpha, \beta\right] = N C_1 \int_0^\infty dv_z \, \frac{v_z}{1 + \Psi_{ij}(v_z) w_0^2} \exp\left\{ - \frac{(v_z - V_z)^2}{w_0^2} - \frac{(V_x^2 + V_y^2)\,\Psi_{ij}(v_z)}{1 + \Psi_{ij}(v_z)\, w_0^2} \right\} \qquad (3.11)$$

where

$$C_1 = \frac{e A_e}{w_0 \sqrt{\pi}}$$

This integral can readily be evaluated by a computer once an analytic expression for $\Psi_{ij}(v_z)$ is obtained. The method of finding this expression is outlined in the next section, but first, let us continue the discussion, now considering electrons.

The electrons are almost certainly isotropic, even in the frame of reference of the cup.* In this case Eq.(3.11) reduces to:

$$I_j\left[\bar{\pi}(t), w_o^2\right] = N C_i \int_o^\infty dv_z \frac{v_z}{1+\Psi_{ij}(v_z) w_o^2} \epsilon^{-\left(\frac{v_z}{w_o}\right)^2} \qquad (3.12)$$

It is also advantageous to investigate a three parameter model for use in regions where there is an abundance of high energy electrons in a so called "Non-Maxwellian tail". A useful distribution is the Kappa distribution**:

---

*The mean free path for electron-electron collisions is much smaller that 1 A.U. and thus the electrons will be almost Maxwellian in their own frame. Theoretical calculations (Sturrock and Hartle, 1966) show that the electrons cool very little from the corona temperature of 2×10^6 °K. The thermal speed is approximately 6000 km/sec which is much greater than the 200-700 km/sec convective motion. Thus the slight anisotropy in the frame of reference of the cup can be ignored in the first approximation.

**Introduced by Prof. Olbert of M.I.T. in his studies of IMP-1 (Olbert, 1966).

$$f_K(w^2) = \frac{C_K}{\left(1 + \frac{1}{K}\,\frac{w^2}{w_0^2}\right)^{K+1}}$$

$$C_K = C_m \frac{\Gamma(K+1)}{K^{3/2}\,\Gamma(K-\frac{1}{2})} \qquad (3.13)$$

Appendix B discusses this distribution function in detail, and outlines its relation to the Maxwellian function.

Both models have been explored and in particular the Kappa distribution for K = 4 has been applied to the transition retion.***

*** Based on the data from OGO-1, Vasyliunas (1966c) has suggested that in most cases Kappa lies between 3 and 5.

C. The Cup Response Including Refraction

In this section, the paths of charged particles will be studied in order to determine the appropriate analytical expression for $\Psi_{ij}(v_z)$ appearing in (3.5c).

If an "allowed trajectory" is defined as the path of a particle with certain initial conditions which intersects the collector plate without striking any other structure of the cup*, then from simple electrostatics one can determine the region in phase space in which these initial conditions lie. For each of the 12 modulator voltages, and for each species of particles considered, an effective collection area in configuration space can be determined for intercepting particles at a particular point in velocity space.

An extensive computer analysis was performed to determine the allowed trajectories for the following cases:

1) Protons in the five positive channels
2) Electrons in the five positive channels
3) Electrons in the one negative channel

The fourth combination, protons in the negative channel, was not explored in detail due to the character of the data in the negative channel (a photocurrent in large part destroyed any detectable proton produced current); also the effect can be shown to be minor compared to the electron current.

---

* This includes the four grid meshes, whose effective transparency changes with the angle of view approximately as 1.4 - 0.4 sec θ.

When the effective area is normalized to normal incidence and the logarithm of the resulting normalized efficiency is plotted against $v_t^2 = v^2 \sin^2\theta$, the result is nearly a straight line for constant v_z and V_j (the j^{th} modulator voltage). This substantiates the choice of writing (3.5c) as

$$\ln\left[\eta_{ij}(v_z, v_t)\right] = v_t^2\, \psi_{ij}(v_z)$$

The slopes of these lines as a function of v_z for a particular V_j were then fitted by the method of least squares to an appropriate analytic function.

For cases (1) and (3), i.e. for the cases where the charge of the particle agreed with the sign of the modulator voltage, the form of the expression was

$$\psi_{ij}(v_z) = \frac{1}{v_z^2}\left[\frac{A_{ij}}{B_{ij} + \sqrt{1 - \frac{2eV_j}{m_i v_z^2}}} + C_{ij}\right] \qquad (3.14)$$

for case (2) for electrons in positive channels the best expression was of the form

$$\psi_{ij}(v_z) = \frac{1}{v_z^2}\left[\frac{D_{ij}}{\sqrt{1 + \frac{2eV_j}{m_i v_z^2}}} + E_{ij}\ln\left(1 + \frac{2eV_s}{m_i v_z^2}\right) + C_{ij}\right] \qquad (3.15)$$

where V_s = -36 volts is the voltage of the suppressor grid. This would have been the form for studying protons in the negative channels had it been pursued. For completeness, the three least squared fitted parameters for each of the three cases are given in Table 3. The accuracy of this method is quite good resulting in relative error in $\eta_{ij}(\bar{v}_3, \bar{v}_t)$ of usually less than 2% over a wide range of interest.

While the experimental verification of this model has not yet been undertaken in the laboratory, the applicability to the actual data can readily be demonstrated. The approach is to use the expressions for $\Psi_{ij}(\bar{v}_3)$ and calculate the measured current in each channel according to (3.11), (3.12) and (3.4) for various values of the parameters N, V, w_o, α and β as defined previously. By normalizing the current to unit density, and noting that α changes slowly throughout the life of the satellite (see Fig. 2) one needs only to concentrate on V, w_o and β for selected values of α.

These calculations have been made using the IBM-7044/Calcomp Plotter combination to display the results for a wide range of the parameters. It is not possible to include even a small fraction of these results here. As an illustration Fig. 8b displays the log of the current per unit density due to Maxwellian protons in each of the positive channels for the parameters α = 40 ; V = 800 km/sec. and w_o = 50 km/sec. For each channel the azimuthal angle is displayed running from - 180 to + 180 with the center mark being the "sun time", i.e. the time when the cup normal vector is closest to the sun-satellite

TABLE 3

LEAST SQUARE FITTED PARAMETERS FOR $\psi_{ij}(v_z)$

Particle, i	Modulator Voltage j	A_j	B_j	C_j	D_j	E_j
Protons	40	0.46277	0.19038	0.74290		
	90	0.64604	0.17234	0.58058		
	95	0.64318	0.16453	0.57934		
	230	0.68704	0.12730	0.52219		
	260	0.67528	0.11870	0.52802		
	650	0.66372	0.09140	0.52351		
	700	0.66876	0.09178	0.51911		
	2000	0.66895	0.08173	0.51324		
	1800	0.66697	0.08224	0.51536		
	5400	0.65240	0.07104	0.52252		
Electrons	-130	0.90726	0.15619	0.33280		
	-265	0.87948	0.19252	0.38000		
Electrons	40			0.68324	0.44841	-0.45114
	90			0.59338	0.53827	-0.35372
	95			0.59054	0.54111	-0.34463
	230			0.49853	0.63312	-0.27790
	260			0.49405	0.63760	-0.26697
	650			0.43584	0.69581	-0.22421
	700			0.43409	0.69756	-0.22096
	2000			0.38942	0.74223	-0.20033
	1800			0.39576	0.73589	-0.20038
	5400			0.36088	0.77077	-0.19166

line. These calculations were made for the bulk velocity vector parallel to the sun-satellite line, the actual data may be shifted in β from this by a small but measurable amount due to aberration and other causes, e.g. confined flow of the transition region.

To illustrate the importance of considering the refraction effect, calculations were made using the approximation previously used in some of the IMP-1 analysis (Lyon, 1966b):

$$\Psi_{ij}(v_3) = \frac{1.5}{v_3^2} \qquad (3.16)$$

The results are shown in Fig. 8c and as a comparison a sample of actual data from Orbit 1, interplanetary region, is included as Fig. 8a. It is seen that refraction completes the model. The necessity of including refraction in the analysis of IMP-1 was not apparent because the actual signals which appear in the lower channels were usually below the noise level. The apparent discrepancy in the bulk velocity can easily be resolved simply by lowering it to 750 km/sec for the particular example.

For electrons in the positive channels the analysis is similar. Fig. 9b shows the calculated contribution of electrons to the positive channels using a Kappa distribution (K = 4) and w_o = 4000 km/sec. The results are compared to a sample transition region spectrum from Orbit 2, Fig. 9a. The isotropic background in the positive channels is explained well by this model by an electron density of 12 cm^{-3}.

As an additional check, the measured current in the negative channel can be compared to that predicted by the model for these

parameters, and again the agreement is quite good. It should be noted that the slight roll modulation near the sun time in the positive channels is due to the presence of an additive ion current with moderate directed flow velocity.

The typical spectrum in the magnetoshpere has higher thermal speeds. Fig. 10a shows an example from Orbit 15, and Fig. 10b shows the model currents computed for the K = 5 Kappa distribution with E_o = 2.5 Kev.

D. Methods of Presentation of the Data

In principle one could plot all the data in as fine detail as in Fig. 8, 9 , and 10, choose the best fitting set of curves based on the plots of model currents, and thus determine the parameters of the plasma. However, the generation of such detailed data plots and determination of the parameters by this method would simply be too costly and time consuming. For these reasons, a simplified method of analysis was pursued.

A type of summary plot of the data (see Figures 37-44) was developed which would highlight the isotropic component primarily due to electrons, and the flowing component primarily due to protons. This plot displays the maximum current in each channel, and the arithmetic average current measured in a $\pm$ 60 degree sector centered in the anti-solar direction. Since the negative channel was contaminated by a photocurrent, only the latter data points were plotted for this channel. In addition the plots indicate the roll azimuthal angle, β, (measured from the time of closest approach of the cup normal to the sun-satellite line) for the largest of the five channel maximum currents, and numbers that channel to which it corresponds.

An important precaution was taken in determining the maximum current in each channel. Since the spin period was usually longer than the time data were measured in a particular frame, a gap in the data occurred frequently just at the point where the maximum current would have been expected. To avoid registering the boundary of the gap as the true maximum, a procedure was employed to ensure that legitimate, smaller

(but non-zero) currents existed on either side of any accepted maximum. In essence, this required that the true maximum have a zero first derivative.

With this type of summary plot and with the experience and cross checks provided by sample details plots such as in Figure 8 , 9 , and 10 one can determine the behavior of the plasma during the lifetime of the satellite.

E. Calculation of Plasma Parameters

In order to obtain the parameters of the proton component of the plasma, a procedure was developed whereby the data from the summary plots can be compared with the model. Using the summary plots, the ratio of the peak currents in adjacent channels is determined for all available channels. These ratios determine lines in the graphs in Figs. 11 and 12 which are computed from the model. The two parameters, bulk velocity V, and thermal speed w_o, are then estimated from the intersection of the lines. The density is determined by the absolute value of the current and is computed from Fig. 13.

A similar procedure was used for the isotropic component due to electrons (Fig. 14 and 15) and possibly due to subsonic protons, Fig. 16 and 17 . Where electrons are involved, one can cross-check with the negative channel currents, Fig.18 , to increase confidence in the estimates of density and thermal speed.

This procedure was applied to the data for selected times of interest. In general, the agreement of the model and the data was very good, especially in the interplanetary regions for α less than 50 degrees. In the transition region the separation of the isotropic electrons from the protons could not always be done unambiguously. The data from the magnetosphere can be fitted quite well with a model assuming contributions from electrons alone, however, the contribution of protons is not always negligible and had to be considered. The principal results of the analysis of the data will be described in the next chapter.

CHAPTER IV

PRINCIPAL RESULTS OF THE PLASMA EXPERIMENT

A. Introduction

During the first six months in orbit, the IMP-2 satellite explored a vast region of near-earth space and sampled some interplanetary space (see Figures 1 and 4). As noted by earlier satellites, particularly its sister satellite IMP-1, there exist three generally well defined and permanent regions in the space surrounding the earth:

Region I: Interplanetary space, where the plasma flux and magnetic fields are undisturbed and undistorted by the presence of the earth.

Region II: Transition region (alternately termed the Magnetosheath), the interaction region between the streaming solar plasma and the geomagnetic field. It is the space between Region I and Region III.

Region III: Magnetosphere, the geomagnetic cavity which contains the geomagnetic field.

These regions are separated by boundaries which are variable in space and time:

Magnetopause: the outer boundary of the Magnetosphere; the boundary between Region II and III.

Bow Shock*: the outer boundary of the transition region; the boundary between Region II and I.

---

*The term Bow Shock is used as a definition of a boundary and does not necessarily imply the de facto existence of a standing shock wave, collionless or otherwise. This is still a topic under active discussion, and this work will attempt to treat the boundary objectively, as it presents itself in the plasma data.

In the next few sections, the findings of the M.I.T. Plasma Experiment on the IMP-2 Satellite will be discussed in terms of these regions and boundaries, and comparisons will be made with previous results and theories.

B. The Boundaries of the Transition Region

The existance of two generally well defined and permanent boundaries of the transition region had been established by previous satellites (Cahill and Amazeen, 1963 ; Obayashi, 1964 ; Ness, 1964). In these measurements it was found that the boundaries generally responded to solar wind activity, and that is some sense the planetary index, K_p, was a measure of this activity. The theoretical shape of these boundaries and the topology of the magnetic field configuration is quite sensitive to the model taken for the connection of the geomagetic field (Axford, 1962 ; Levy, Petschek and Siscoe, 1963 ; Dessler, 1961 ; Mead and Beard, 1964 ; Spreiter and Jones, 1963). However, most all theories agree on the approximately 10 Re geocentric distance to the magnetopause and 14 Re to the shock in the subsolar region.

1. General Character of the Boundaries

IMP-2 was able to penetrate the magnetopause during nearly all of the first 70 orbits, and reached the shock boundary during its first 41 orbits. In Fig. 19 , these boundaries are shown as the terminal points of the portion of the satellite's trajectory through the transition region. Each pass through the transition region is numbered corresponding to the orbit number, and the magnetopause is indicated by a cross, the shock boundary by a dot. A solar ecliptic coordinate system is used to display the trajectories (see Appendix A). The X_{se} axis is considered an axis of symmetry and all points are rotated about this axis into the ecliptic plane for the illustration. The average

location of these boundaries as determined by IMP-2 are also shown in the diagram.

The average positions of the boundaries for IMP-2 agree remarkably well with those computed for the IMP-1 data, a year earlier (Ness, et al. 1964 ; Lyon, 1966b). However, comparing the deviations about the means shows that the spreads are greater for the IMP-2 data. This almost certainly reflects the increased activity at the start of solar cycle 20 beginning in October 1964 (Dept. of Commerce, 1965).

Before these boundaries are discussed further, the criteria for determining the boundaries from the plasma data, and a few examples will be presented.

(a) Bow Shock

In general, the plasma data from the interplanetary region is strongly roll modulated and appears in only a few positive channels. The modulation is indicative of a highly directed proton flow streaming away from the sun. A low nearly isotropic background above the noise level is sometimes present. As the satellite crosses the shock boundary into the transition region, the character of the plasma signals changes dramatically. Refracted electrons cause a large isotropic signal to appear in all channels. When there is still a flow of protons above the high isotropic background signal, it has changed its direction compared to the interplanetary flow.

The outbound pass of Orbit 15 (Fig. 40) shows several widely separated shock crossings. Between 1500 and 1718 hours* on 24 October

*All times will be given in Universal Time expressed as a four digit number; e.g. 1718 hours will be used to express 18 minutes past 5 PM Greenwich Mean Time.

1964 (The 298th day of the year), the satellite was in the transition region. At 1718 hours the satellite crossed the shock boundary into interplanetary space: The average currents in the antisolar direction dropped by more than a factor of 20; directed flow appeared mainly in channel 2; and the direction of flow also changed as is indicated by the azimuthal angle β of the maximum current.

At 1740 hours another shock crossing occurred; this time the transition region overtook the satellite. The satellite did not emerge from Region II until 1925 hours where again the shock boundary was encountered. This process was repeated several times as the satellite was alternately in Regions I and II.

Most shock crossings are not as easily discernable as in the preceding case. The outbound and inbound passes of Orbit 2 and 3 (Fig. 37 & 38) illustrate examples of multiple shock crossings which occur on a very short time scale. Approximately 70% of the shock traversals exhibit multiple crossings.

(b) Magnetopause

The outer boundary of the magnetosphere was sometimes difficult to distinguish from the transition region. Both regions are characterized by nearly isotropic signals in all positive channels. The features which distinguish the two regions are that Region III currents are more isotropic with no apparent flow component, less variable on a short time scale, and always smaller in all channels. An extremely sharp megnetopause crossing occurred at 1340 hours on 25 Oct 64 on the inbound portion of Orbit 15 (see. Fig. 40). Motion of this boundary

is illustrated in the next hour when the transition region surrounds the satellite twice; briefly at 1435 and again from 1441 through 1443 hours.

2. Diffuse Magnetosphere Boundaries

On perhaps 10% of the traversals of the magnetopause, a weak, diffuse boundary was observed. The outbound portion of Orbit 15 (Fig. 40) illustrates this type of behavior. Here, the actual magnetopause crossing was taken to occur at 1455 hours although there exists only a gradual change in character of the signals from 1230 through 1500 hours. An even more extreme example is shown in Fig. 39 for the outbound portion of Orbit 12. The actual crossing was taken at 0645 hours on 20 Oct 64.

The diffuse nature of this type of boundary is also evident in the magnetic field measurements on IMP-2 (Fairfield, 1966). The outbound portion of Orbit 12, and three other orbits for which the plasma data show a diffuse boundary, were jointly reviewed with the GSFC magnetometer group. In all cases there was only a gradual change in the direction of the magnetic field across the magnetopause. This is in contrast to the abrupt change in direction and magnitude normally encountered at the magnetopause (Ness, 1964 ; Cahill and Amazeen, 1963). In the case of Orbit 12, the magnitude of the field began to vary from 20 to 40 gamma* starting at 0645 hours with a high variance, but the field

*one gamma = 10^{-5} Gauss.

direction remained essentially unchanged for another hour.

The exact nature of this diffuse boundary is not clearly understood. There is no obvious correlation between the occurrence of a diffuse boundary and either K_p or the position of the satellite in space. The near continuity in angles across the magnetopause suggests that there is a good topological connection between the geomagnetic field lines in the magnetosphere and the lines of force in the transition region. Particles could diffuse more readily from the transition region into the outer magnetosphere. Indeed electron densities just inside the magnetosphere are a factor of ten higher than normally encountered at a sharp magnetopause (see Table 4). The increase in the number density of electrons* in the magnetosphere is a general feature associated with all the diffuse boundaries observed by the plasma experiment.

A direct comparison with fluxes of high energy electrons is possible on Orbit 15. Comparing the diffusive boundary of this orbit with the University of California's Geiger counters on IMP-2 (Anderson, 1965a), reveals that the flux of electrons above 45 Kev shows a smooth and gradual decrease from 1200 to 1445 hours on 24 Oct 64 (Fig. 20). During the same time, the M.I.T. plasma experiment (Fig. 40) shows a smooth and gradual increase leading right into the

---

* Presumably the number density of protons equals that of the electrons to preserve plasma neutrality. Protons are not observed since their fluxes would be well below that of the electrons if one assumes equal thermal energies.

TABLE 4

ELECTRON PARAMETERS ACROSS THE MAGNETOPAUSE

		Magnetosphere	Transition
Diffuse Magnetopause (Orbit 12 outbound)	N	1 ± 0.1 cm^{-3}	> 10 cm^{-3}
	E_o	1 ∓ 0.2 Kev	< 150 ev
Sharp Magnetopause (Orbit 15 inbound)	N	0.12 ± 0.02 cm^{-3}	> 10 cm^{-3}
	E_o	1.5 ∓ 0.5 Kev	< 70 ev

transition region. This diffuse boundary on the outbound portion is to be contrasted with the sharp boundary in both experiments on the inbound portion of this same orbit.

The inverse correlation of the measured fluxes by these two experiments is taken as evidence of an inward diffusion within the magnetosphere of low energy electrons ($E \sim 1$ Kev at the magnetopause). Observations of energetic electrons above 1.6 Mev on Explorer 14, have also shown an inward diffusion (Frank, 1965).

The diffusion theories of Nakada and Mead (1965), Kaufman (1965) and Dungey (1964) require a source of particles near the magnetopause. Assuming violation of only the third adiabatic invarient (Northrop and Teller, 1960), but conservation of the first two, they show how this mechanism can adiabatically increase the energy of the particles which diffuse inward from the magnetopause.

As electrons diffuse inward, a greater percentage will have energies above the threshold of the 45 Kev geiger tubes. Calculations, based on the Kappa distribution described in Appendix B, were made using the parameters derived from Orbit 15 at 1200 hours and also 1430 hours on 24 Oct 64. These calculations predict within a factor of two the observed counting rates of the University of California's experiment at these times. Furthermore, the cube of the distance ratio (6.5 Re/ 10 Re) is very nearly equal the inverse ratio of the thermal energies (2.5 Kev/0.5 Kev) at these respective times. This supports the constancy of the first adiabatic invariant during the diffusion process.

3. Boundary Response to Solar Activity

During the lifetime of the IMP-2 satellite, solar cycle number 19 was waning and the new cycle was just becoming established. The recurrent pattern activity that had persisted since late 1962 began to break up starting with solar rotation (SR) number 1797 (14 Nov 64). Bartel's daily character figure C-9 and the general behavior of the K_p index (Lincoln, 1965), reproduced here as Figs. 21 and 22, provide a vivid indication of these features. IMP-2 was able to provide information on the behavior of the boundaries during two solar rotations, from the latter half of SR 1795 through the first half of SR 1797. This section will discuss some of the recurrent events listed in Table 5 and their effect on the boundaries of the transition region.

It is quite apparent from Fig. 19 that each of the IMP-2 orbits listed in Table 5 shows a boundary compressed with respect to the average location. Particularly prominent are orbits 16, 20, 25, and 30. It is fortunate that for these orbits data are also available from the M.I.T. Plasma Experiment on the OGO-1 satellite. This satellite was exploring the dusk side of the magnetopause and transition region (local time approximately 1800 hours) during these particular times (Fig. 23). Limited data are also available from IMP-1 which resumed operation on 12 Nov 64 and continued through its first anniversary to 15 Dec 64. During this period IMP-1 was near the subsolar region (local noon).

The data from IMP-1 can be used in the study of the 15 Nov 64 event as a monitor of the interplanetary conditions since IMP-2 could

TABLE 5

Day of Solar Rotation	Day	Orbit Number		
		IMP-2	OGO-1	IMP-1
14 - 15	3-5 Oct. 64	1		
	1 Nov. 64	20	22	
	28-29 Nov. 64	39		*
21 - 22	11-12 Oct. 64	6		
	8 Nov. 64	25	25	
2	19 Oct. 64	11		
	15 Nov. 64	30	27	*
9	26 Oct. 64	16	20	
	22 Nov. 64	35		*

* The exact orbit number of IMP-1 is unknown; but data is available for analysis.

not provide this information.*

(a) 4-5 October 1964 Event

Just prior to the launch of the IMP-2 satellite there was a large magnetic storm with sudden commencement at 1243 hours on 3 Oct. The magnetic storm lasted well into 5 Oct. (Lincoln, 1965). While IMP-2 was unable to investigate the onset of this storm, it did explore the subsolar region very shortly thereafter. The limited sampling of the interplanetary region from 1200 hours on 4 Oct to 0600 hours of the following day showed that the bulk velocity was near 725 $\pm$ 25 km/sec and that the densities ranged from 5 to 10 cm^{-3}. The thermal energy, E_o, was in the range of 30 e.v. During succeeding orbits the velocity decreased from a value of 700 $\pm$ 25 km/sec at 0300 on 6 Oct, to 500 $\pm$ 25 km/sec at 1500 on 7 Oct; the density remained nearly constant at 4 cm^{-3}. The Ames group (Wolfe, et al. 1965) have reported similar plasma parameters for this same time period based on their electrostatic analyzer on IMP-2.

As a simple model of magnetospheric compression, one can take the change in boundary position to be inversely proportional to the sixth

*The plasma experiment on IMP-2 could not effectively monitor the interplanetary conditions after approximately Orbit 18. The large sun-satellite - cup normal angle (angle α in Fig. 2) placed the experiment near cutoff for directed flow from the solar direction. Thus it provided no data concerning conditions in Region I after 28 Oct 64. The instrument was, however, very capable of defining boundaries and other changes in the character of the plasma.

root of the change in the normal component of plasma pressure on that boundary. This relation arises from equating the external dynamic plasma pressure (neglecting the small contribution of the interplanetary magnetic field pressure) to the internal pressures which are predominantly those of the geomagnetic field whose intensity is taken to fall off as the inverse cube of the geocentric distance. Using the IMP-1 average boundary positions, and the corresponding values of the plasma parameters (bulk velocity of 300 km/sec and density of 6 cm^{-3}) (Lyon, 1966), one finds that the magnetopause should have been compressed from the average 11 Re to 8.3 Re. The actual 9.7 Re on the inbound pass is primarily attributable to the expansion of the magnetosphere as it enters the main phase of the storm (Sugiura and Heppner, 1965) at the time of the measurement.

(b) Multiple Shock Crossings During the First Seven Orbits

The period following this storm is particularly interesting since it is rich in shock boundary motion. The geometry of the orbit was very favorable since apogee for the first seven orbits occurred some 2.5 Re beyond the average shock location and was nearly at the constant sun-earth-satellite angle of 20°. It would therefore be expected that near apogee, the plasma would be typical Region I and only near the actual shock boundary would Region II plasma be encountered. Fig. 24 shows that even at apogee, plasma characteristic of the transition region was found. This figure displays the times and the corresponding geocentric distance when the plasma exhibited a high isotropic background

(presumably due to refracted electrons) and no appreciable flow component or protons in the positive channels. The data included in this diagram were from 8 second samples taken at an average rate of 33 samples per hour (see Appendix C). Regions where data is missing are enclosed in curly brackets.

First, it should be noted that in a gross fashion both boundaries of the transition region appear at further geocentric distances on each succeeding orbit from 1 through 5, which follow the storm on 3 Oct 64. When the recurrent disturbance associated with the 21st day of the solar rotation produces a magnetic storm with some suggestion of a sudden commencement at 1049 hours on 12 Oct 64, the shock boundary is again depressed during the inbound pass of Orbit 6. The inbound pass of Orbit 7 shows the beginning of the expansion which is further evident in Orbits 8 and 9 (not shown).

Second, considering the finer details depicted in the figure, one notices first the increase, and then the decrease in the number of observances per orbit of the transition-like plasma at large distances from the shock boundary. If one considers only the number of occurances beyond one earth radius from the first (last) shock crossing on the outbound (inbound) pass, then the number distribution for Orbits 1 through 5 are: 1, 5, 9, 5, and 3. The interplanetary plasma conditions do not correlate with this pattern. The plasma bulk velocity for instance is slowly decreasing over the eight day period to a value of 500 km/sec, while the density remains nearly constant at 4 cm^{-3}.

Upon comparing observations with the GSFC magnetometer group (Fairfield, 1966), a nearly perfect one-to-one correspondence was found

between the periods of observing transition-like plasma and the occurrence of a disordered highly variable magnetic field.

These regions of transition-like plasma are quite suggestive of the energetic electron spikes which have been reported in and beyond the transition region (Fan et al., 1966 ; Anderson et al., 1965b; Frank and Van Allen, 1964 ; Anderson, 1965c). Observation of energetic electron spikes during the flight of IMP-2 has also been reported (Anderson, 1965a), and Figures 25 and 26 illustrate the data from the University of California Geiger tubes for Orbits 1 and 2. While there appears to be no correlation between the observations of spikes of energetic electrons and a change in the M.I.T. plasma data for Orbit 1, the following orbit shows the contrary. Despite the poor time resolution available from Fig. 26 several cases of simultaneous observation of spikes and transition like plasma (Fig. 24) can be noted, e.g. 0545, 0645, 1330 and 1500 hours and those within the region labeled "S".

The time between 1500 and 1700 hours on 6 October is quite rich in multiple shock crossings as evident in the plasma data (Fig. 24 and 37). During this same time period, a build up in spike activity is clearly evident from Fig. 26. The University of California group has studied this period from the standpoint of a possible periodic modulation of the energetic electrons (Lin and Anderson, 1966). Their detailed data are shown in Fig. 27. Drawn to the same time scale in this figure is a representation indicating the periods of time when the M.I.T. experiment was encountering transition-like plasma. There appears to be quite

good correlation* between the appearance of energetic electron spikes and the occurrence of plasma characteristic of the transition region. Indeed, the spikes seem to be observed preferentially at those times when the plasma data indiate a change in character, i.e. a shock boundary traversal. Furthermore there is a noticeable lack of spike activity once the multiple shock crossings have ceased and the continued transition region is encountered after 1700 hours.

Anderson, et al. (1965b) suggested that the electrons spikes observed beyond the bow shock were of magnetospheric origin and had escaped outward beyond the boundary of the outer radition belts. Fan, et. al. (1964 and 1966) have argued against this interpretation in favor of a local acceleration mechanism, principally the first order Fermi mechanism (Fermi, 1954). They believe this mechanism to be

*Some of the apparent lack of correlation may simply be due to the different data taking duty cycles of the two experiments. Each period of observation for the M.I.T. experiment lasted at most 8 seconds, and was separated from other samples by 81.8 seconds (twice this value during the Rubidium vapor magnetometer sequence; see Appendix C for details). When two adjacent samples indicated no change in character of the plasma, the samples were joined in the figure (except when interrupted by the magnetometer sequence indicated by a gap).

The U. of C. experiment accumulated counts for approximately 40 seconds prior to a brief 1.6 second readout. Due to the impulsive character of the spikes, some inconsistencies will develop in the comparison of the two experiments from this point alone.

active between the trap formed by the bow shock and the approaching magnetic irregularities carried by the solar wind. Fermi acceleration increases the longitudinal component of the electron's velocity (with respect to the local magnetic field), which results in a decrease in the pitch angle, allowing the particle to escape from the trap. However, in the presence of small irregularities between the confines of the trap, magnetic scattering will randomize the pitch angles so that the electrons may remain inside the trap for further acceleration.

Variations of the above qualitive descriptive have been quantitatively studied by Jokipii and Davis (1964) and Jokipii (1966) outside the bow shock, and by Shen and Chang (1965) within the transition region. Electron acceleration by ion acoustic waves generated by plasma instabilities has been investigated by Scarf, et al. (1965). All of these models have some merit, and all can explain some of the past observations.

The data presented here for the inbound pass of Orbit 2, give better support for the local acceleration models rather than the magnetospheric origin model:

1) There is an abrupt termination of the occurrence of spikes at the same time as the last shock boundary is encountered. If these large fluxes of energetic electrons were shaken off the magnetosphere during this disturbed period, it would seem highly unlikely that the generation process would cease exactly as the satellite penetrated the transition region.

2) The spikes appear to be associated with rapid boundary motion and occur predominantly at the time of a shock boundary corssing. There is some indication that more spikes are observed when the shock boundary moves inward, i.e. when the satellite goes from Region II to Region I. These spikes may possibly be due to an increase in energy and/or density (a form of "snowplow" pile up) of the electrons on the transition side of the shock as it recedes and passes the satellite.

3) A slowly varying shock boundary does not produce any spikes. This will be discussed further in section (e)of this chapter: see also Fig.20 and 40 for the example of Orbit 15.

4) The magnetopause boundary is also frequently in motion. Most of the apparent spikes seen near the magnetopause boundary can be directly associated with times when the satellite briefly was inside the magnetosphere. The motion of the magnetopause permits the sampling of the high fluxes typical of the magnetosphere and these appear as spikes when compared to the low fluxes as seen in the transition region. This feature is apparent when comparing Fig.20 with Fig.40 and . Further comment is made for Orbit 15 in section (e)of this chapter.

In summary, the rapid motion of the shock appears to have produced either the local acceleration of electrons or an increase in their density. This increase in flux of electrons was detected by the Geiger counters as energetic spikes of electrons above 45 Kev.

(c) 26 October 1964 Event

A magnetic storm with sudden commencement at 0009 hours occurred

while the IMP-2 satellite was in the magnetosphere at 9.0 Re and at a sun-earth-satellite angle of 55 during the outbound portions of Orbit 16 (Fig. 41). Immediately following this event, the satellite entered the transition region after encountering a very sharp magnetopause at a distance of 9.2 Re. The shock boundary was encountered shortly thereafter (0210 hours) at 11.2 Re which is the closest every observed on IMP-2 at any sun-earth-satellite angle. Both boundaries are quite definitely compressed (see Fig. 19) probably due to the arrival of a front of energetic plasma from the sun associated with the recurrent storm of the 9th day of solar rotation.

The pre-storm conditions are taken to be those available from Orbit 15 at 1030 of 25 Oct 1964 (Fig.40) which was some 14 hours preceding the storm. The plasma parameters were varying slightly about the following averages: bulk velocity 250 km/sec, density 10 cm^{-3}, thermal energy a cold 2 ev. Fig. 28 displays the post-storm interplanetary conditions obtained from the detailed data plot of Orbit 16. These parameters were determined by comparing the data with a model plasma using the measured $\alpha = 52^{\circ}$ (see Chapter 3). When the satellite just enters the interplanetary region at 0210 hours, there is only a trace of the front that passed from two hours earlier which caused the sudden commencement and compressed both the shock and magnetopause. Clearly shown in the figure, however, is the arrival of enhanced plasma some seven hours after the sudden commencement. The bulk velocity reaches a maximum of 700 km/sec while the density climbs to 40 cm^{-3}. The thermal energy also rises to approximately 80 ev.

(x) 13 November 1964 Event

On this night (Friday, the thirteenth), my third lovely daughter was presented to be by my wonderful wife, Barbara. To permit needed rest for father and girls, interplanetary conditions were exceptionally quiet the following day: the 24 hour sum of K_p was only 1_o.

(d) 15 November 1964 Event

Another disturbance of special interest occurred at 1009 hours on this date. Unfortunately, the sun-satellite-cup normal angle, α. (Fig. 2), for IMP-2 was at its worst in the entire flight with regard to the M.I.T. plasma experiment. Boundary crossings could be identified but only limited information concerning the plasma properties could be obtained.

On the other hand, fortune was with us since the IMP-1 satellite, launched a year earlier, resumed operating on 12 Nov 1964 after a five month "rest". This satellite was well into the interplanetary medium in the subsolar direction before and during this event*. The spin axis on IMP-1 was also very favorable resulting in an angle $\alpha = 13^{\circ}$. The data from IMP-1 will be used to monitor the interplanetary plasma conditions during this time.

Immediately preceding the sudden commencement IMP-2 was in the transition region at 13.3 Re. The sun-earth-satellite angle was 50°

---

*At 1000 hours this satellite was outbound at a 17 Re geocentric distance.

in the dawn hemisphere. At 1018.4 hours ** the shock boundary crossed the satellite and IMP-2 emerged into the interplanetary medium. The magnetometer measurements concur with this time (Fairfield, 1966).

The IMP-1 plasma data (Fig. 30 and 42) indicates an increase in density from 20 to 30 cm^{-3} at roughly 1010, with an additional increase to 50 cm^{-3} at 1020 hours. The development of the event then proceeds with erratic increases in density reaching a maximum of 100 cm^{-3} between 1325 and 1405 hours. Thereafter the density drops to a level of 60 cm^{-3} after 1430 hours. A sudden increase to 100 cm^{-3} at about 1440 appears to have stimulated the magnetosphere resulting in a sudden impulse on the magnetograms at 1443 hours (Lincoln, 1965). A sudden drop to 40 cm^{-3} at 1525 also appears to have resulted in another sudden impulse registered at 1529 hours. (The magnetograms for this period have not been studied, but it is interesting to speculate that these two sudden impulses should have opposite polarity; one due to the sudden increase in plasma density, the other due to its sudden decrease). Subsequent to this last impulse, the density gradually returned to more normal values near 15 cm^{-3} and remained at this level at least up to 2000 hours (data are lacking from this time until 0400 of the next day).

All during the period that the density was appreciably varying, the plasma velocity was nearly constant at 300 - 325 km/sec. However, starting at roughly 1740 hours the velocity increased to 400 km/sec, and was found to have climbed to 500 km/sec from 1830 up to 2000 hours. Data for eight hours from the next day indicate that the velocity remained

---

** This precision in time is attainable since the boundary crossing occurred during the time data was being received from channel 3 and 4 (Appendix C). Thus the time is known to within $\pm$ 3 seconds.

high at a constant 450 km/sec, while the density had subsided to 5 to 10 cm^{-3}.

A discussion of the development of this event from the standpoint of interplanetary dynamical process will be postponed to section C of this chapter. A few comments remain to be made in this section concerning the boundary motions related to this event.

At the time (1018.4 hours) the shock boundary passed IMP-2, the satellite was located at a geocentric distance of 13.3 Re and the 0845 hour local time meridian. The average shock location in this vicinity is 15.5 Re. The measured compression to 86% of the average distance is an upper limit since the boundary could have been pushed well below the satellite.

It one adopts the same model of compression as used for the 4-5 Oct 64 event, then, since the external pressure increased by a factor of 2.5, the boundary should have been compressed to 85% of the average, which is in excellent agreement with the measurements.

The dusk side of the transition region was also compressed as measured by the M.I.T. electron experiment on OGO-1 (Vasyliunas, 1966a). This satellite was at 20 Re on the 1800 hour local time meridian when the shock boundary overtook the satellite on the inbound pass at 1017 hours. The multiple corssings seen by OGO-1 in the following hour probably indicate that 20 Re was the limit of compression at this time. Using 24 Re (Ness, 1966) as an estimate of the average boundary on this meridian, the OGO-1 data indicate a shock compression to about 84% of the average.

The sudden rise in interplanetary plasma density to 65 cm^{-3}

(IMP-1, Fig. 30) at 1120 and 100 cm^{-3} at 1325, pushed the shock front far enough in front of the OGO-1 satellite so that it remained in the interplanetary medium until it reached about 17 Re.

(e) Evidence for Long Period Vibrations of the Shock Boundary

An instance of extremely simple expansion and contraction of the shock boundary was observed between 1600 hours of 24 October and 0300 of the next day. The satellite was outbound on its 15th orbit (Fig. 40) during a geomagnetically quiet period ($K_p \leq 1$). A small disturbance occurred at 1606 hours, followed by a sudden impulse in the magnetograms at 1739 hours. While the exact magnitude of the disturbance is not available at this time, it appears to have been slight enough so as to excite only the simplest of response modes in the outer extremities of the magnetosphere and transition region. Evidence for this is available from the limited number of observatories which reported the disturbance (Lincoln, 1965) and the wave-like phenomenon which it excited in the outer transition region. This is to be contrasted with the single shock crossing observed from the strong storm of 15 Nov and to some extent that of 26 Oct (Fig.41).

The periods of time when the satellite was periodically engulfed by the transition region are shown in Fig. 40. By displaying these periods on a distance versus time diagram (Fig. 29), one can obtain a view of the event. Here one can visualize the shock boundary executing a quasi-oscillatory motion, excited by the disturbance at 1609 hours. It is not possible to distinguish from this data, whether the entire magnetosphere is taking part in the pulsations, or whether there exist

waves confined to the shock boundary and convected passed the satellite. Any frequency measured by the satellite becomes doppler shifted due to the relative motion of the satellite through the medium supporting the wave. Dual satellite observations of this type of phenomenon would be required to distinguish between the possibilities.

The actual event was most likely rich in many frequencies, both those which are constant but harmonically related as well as those which are variable in time. It is a remarkable feature of this event that just a single sinusoid can adequately describe the shock crossing (see Fig. 29). The frequency that was most natural to the data, corresponded to a period of oscillation of 2.72 hours and a small amplitude of 1.7 Re about a mean geocentric distance of 14.2 Re. This average distance is the same value as the average shock crossing in this region.

The boundary motion might be expected to locally accelerate particles by a form of the Fermi process. However, the calculated boundary velocities are only a few kilometers per second and are probably insufficient to supply enough energy within these timespans to locally accelerate particles to any appreciable flux level. Indeed, the Geiger counters on IMP-2 with flux threshold of about 100 $cm^{-2}sec^{-1}$ for electrons about 45 kev, report an extremely quiet region with an absence of spikes during the period of 1500 hours through 0900 hours of 25 Oct (Fig. 20) (Anderson, 1965a).

The spikes which are seen after 1000 hours on the inbound pass of Orbit 15 appear to be associated with the more rapid motion of the shock boundary. This feature exhibits the same correlation between

multiple shock crossings derived from the plasma data, and the occurrence of energetic electron spikes that was discussed earlier in connection with Orbit 2 (section (b)).

The sharp rise in the counting rates of the Geiger tubes after 1300 hours (Fig. 20) coincides with the satellite entering the magnetosphere as indicated by the plasma (Fig. 40). The several marked decreases in the Geiger counting rates near 1500 hours are most likely due to the satellite being momentarily enveloped by the transition region.

C. Plasma Patterns in Interplanetary Space

1. Introduction

The unfortunate circumstances which severely limited the ability of the IMP-2 experiments to observe conditions in the interplanetary space, were discussed in Chapter II. For these reasons an extensive study of solar wind parameters similar to that conducted using the Mariner 2 data (Neugebauer and Snyder, 1964 , 1966) and the IMP-1 data (Lyon, 1966b) could not be performed for IMP-2. Some solar wind parameters could be derived for specific times and are presented elsewhere in this work. In part 4 of this section we will discuss a particular pattern which was apparent in the plasma data after many of the geomagnetic disturbances which occurred in the early orbits of IMP-2. First, a review will be given of the general average structure of the interplanetary medium as observed by previous satellites.

2. Recurrent Patterns of 27 Days Observed by Mariner 2

Perhaps the most extensive analysis of the interplanetary plasma that has been published to date is the Mariner 2 observation of the solar wind (Neugebauer and Snyder, 1964 , 1966). During the Mariner 2 flight to and past Venus in 1962, several streams of hot, high velocity plasma were observed to recur at 27 day intervals, with peak velocity and thermal speeds of 830 km/sec and 125 km/sec, respectively. It was estimated that one of the observed streams persisted for at least 18 months. Between streams the velocity dropped to as low as 310 km/sec while the thermal speed was 25 km/sec. Near 1 A.U. the average density was approximately 5 protons/cm^3. The density was highest at the leading

or western edge of each stream with a maximum value of 80 protons/cm^3.

The 27 day recurrence pattern of high velocity plasma can be associated with the so-called M-regions which are assumed to exist on the surface of the sun and which emit enhanced solar plasma (Bartels, 1949). An attempt was made to trace the plasma observed by Mariner 2 back to its origin on the sun's surface. However, the calculated position of the sources of the high velocity plasma did not correlate well with any features (sunspots, flares or plages) on the surface of the sun. The conclusion reached was that the M-regions are not visible on the surface of the sun (Snyder and Neugebauer, 1966).

With regard to the effect of the solar plasma on geomagnetic disturbance, Snyder, et al. (1963) found a high correlation between the plasma bulk velocity and the planetary indices of geomagnetic activity, K_p or A_p (See also Maer and Dessler, 1964).

3. The Sector Structure Observed by IMP-1

The magnetic field measurements on the IMP-1 satellite revealed another average pattern in the interplanetary medium. The direction of the interplanetary magnetic field was repetitive on a time scale of 27 days in a very dramatic way and showed the existence of four distinct sectors (Ness and Wilcox, 1965). Within each sector the magnetic field is directed either away from or towards the sun within the entire sector. Three of the sectors have a time interval of approximately 7.6 days, while the fourth sector shows a time interval corresponding to 3.8 days at 1 A.U.

It was found that the field magnitude, solar wind velocity and geomagnetic activity as indicated by K_p all had the same average behavior within a sector. The solar wind density, however, was slightly different: its average maximum in the sector accurred about one day sooner than the velocity and exhibited a general minimum half way within the sector (Wilcox and Ness, 1965 ; Lyon, 1966b).

Ness and Wilcox (1964 , 1965) also demonstrated the solar origin of the interplanetary field. They also attempted to identify the region on the sun's surface responsible for the 2 Dec 1963 geomagnetic storm. By using the plasma velocity and the observed time of the storm, they suggest that in this one case a region preceding a unipolar magnetic region (a "ghost UMR", Bumba and Howard, 1965) is to be identified with Bartel's M region. They speculate that the weak magnetic fields of the ghost UMR might be such as not to interfer with the escape of solar wind plasma from the sun.

4. The Structure of High Velocity Plasma Streams

In this part, we report on a particular pattern of the interplanetary plasma that was frequently observed during the flight of IMP-2. The observation of this pattern by previous satellites and a possible mechanism for this structure are discussed.

On four out of the five occasions when IMP-2 was in interplanetary space following the occurrence of a geomagnetic disturbance with sudden commencement, a definite pattern was observed in the plasma structure. While the detailed features were not always easily discernable for each

event*, the general pattern was apparent and is best illustrated by the 15 Nov 64 event, as monitored by IMP-1 (Fig. 30 and 42):

(a) An enhancement in the number density of the plasma, precedes by about a third of a day the arrival of the high velocity plasma stream. The first increase in density can cause geomagnetic storms with sudden commencement; subsequent sudden changes in plasma density seem to be associated with sudden impulses observed in ground station magnetograms.

(b) During the period before the arrival of the high velocity stream, the plasma density generally continues to rise toward a plateau several times its initial value. However, the plasma velocity shows little, if any, increase during this same period.

(c) Upon the arrival of the high velocity stream, there is generally a marked decrease in plasma density.

The general behavior outlined above has also been observed in some of the data from Mariner 2 (Neugebauer and Snyder, 1964 , 1966). The density was generally observed to reach a maximum on the leading edge

*Observations on the other occasions were incomplete as follows: For the event on 26 Oct, and for the events of 8 and 15 Nov 64, IMP-2 did not enter the interplanetary region until several hours after the sudden commencement. For the 1 Nov event, however, the satellite was over one earth radius beyond the shock. In all but the 8 Nov event, there was an indication of the arrival of very enhanced plasma some seven or eight hours after the sudden commencement. For this event it is conceivable that the increase in velocity was merely undetectable due to the extremely high value for α at the time. The 3 Oct event was only samples some 22 hours after it occurred, and presumably the high velocity plasma stream had already arrived.

of a high velocity stream before the velocity maximum was reached. The density then reached very low values in the center of the high velocity peak.

This same feature has also been frequently observed in the data from Mariner 4 (Lazarus, et al., 1966a) and Pioneer 6 (Lazarus, et al., 1966b). The time delay between the increase in density and the arrival of an enhanced velocity stream is typically less than 12 hours.

A review of the early IMP-1 data indicates that most of the large sudden increases in density and velocity follow the behavior outlined above. The changes in plasma parameters were not as dramatic as observed by other satellites. Several exceptions are also apparent most notably when the incremental change in velocity was less than 50 km/sec.

The averaging technique used to correlate plasma parameters with time within a particular sector structure (Wilcox and Ness, 1965) gives the misleading result that the time delay between the peak in density and the peak in velocity is more than a day. These authors used a sliding 24 hour average of the one hour plasma parameters computed at 3 hour intervals. For the plasma structure being considered, it is easy to demonstrate that an eight hour delay between the density increase and the velocity increase will result in an apparent separation of about 24 hours between peaks in the averages.*

*As a simple approximation, consider the density profile to be a square pulse starting at 00XX hours ending at 08XX hours; the velocity profile is also square starting at 08XX hours and lasting some 30 hours. The density and velocity averages obtained by this technique would be trapezoidal with an apparent "peak" separation of 27 hours.

The structure of solar disturbance patterns has been investigated by many workers (Parker, 1963 ; Gold, 1963 ; Dessler, 1966 , and references therein). In view of the observations by IMP-1 and 2, Mariner 2 and Pioneer 6, the recent studies by Hirshberg (1965a, and 1965b) Razdan, et al., (1965), Dessler and Fejer (1963), Colburn and Sonett (1966), Sturrock and Spreiter (1965) are of special interest. They consider the structure within the solar wind that would be expected to develop when a fast plasma stream is embedded in a slower ambient wind.

Sturrock and Spreiter develop the shock relations which are expected if the high velocity stream is supersonic with respect to the ambient plasma. They, and also Razdan, and Colburn and Sonett attempt to apply the resulting fast and slow shock fronts to the positive and negative impulses occurring in certain geomagnetic storms. Hirshberg considers the steady state structure of recurrent, M-region, high velocity streams. She finds the associated geomagnetic storms follow the expected structure of these high velocity streams. Dessler and Fejer attempt to interpret the K_p index in view of the structure of M-region geomagnetic storms.

The structure can be briefly described with the aid of Fig. 31 a and b. The top figure shows the idealized flow across the shocks that may form when two streams of gas come into contact at a supersonic relative velocity. The standoff distance between the fast shock and the tangential discontinuity depends on the radius of curvature of the front of the high velocity stream, and Mach number of the flow, and the ratio of specific heats of the gas (Landau and Lifshitz, 1959).

The coordinate system is one in which the observer travels with the high velocity stream. The lower figure is the same flow transformed to a coordinate system in which the observer is at rest with respect to the sun.

If we postpone for the moment consideration of the effect that aberration* has on the solar ecliptic longitude of the observed plasma flow, then at the position of the satellite the following observations should be recorded (assuming that the relative velocities of the two streams are high enough to form shocks):

(a) The ambient plasma in front of the fast shock would appear to be flowing radially away from the sun (0^{o} solar ecliptic longitude).

(b) In the standoff region between the fast shock and the tangential discontinuity, there is an increase in pressure and density, and the velocity changes. The change in magnitude of the velocity is not great (Fig. 31 c); the velocity direction changes to positive longitudes in order to allow mass flow around the oncoming discontinuity.

(c) There is no change in pressure at the tangential discontinuity; the density may change by any amount: the magnitude of the velocity is that of the high velocity stream but it would appear to be flowing from negative longitudes.

---

*Aberration simply shifts the apparent direction of flow by a few degrees toward more negative longitudes. The effect is a function of the plasma velocity and the heliocentric distance at which the co-rotation of the source of the plasma can be considered terminated. The shift due to wind aberration normally amounts to less than 5 degrees.

(d) The enhanced stream of plasma finally arrives after the passage of the slow shock, and flows radially from the sun.

The above is a summary of the expected pattern as outlined by Hirshberg (1965a). She has found very good agreement with the development of M-region magnetic storms and the structure expected from a recurrent fast stream of particles embedded in the solar wind. The observations of the IMP satellites in late 1964 also are consistent with the above structure. The velocity and density profiles for the 26 Oct and 15 Nov have been presented as Figures 28 and 30 , respectively. Listed in Table 6 are the approximate solar ecliptic longitudes of the observed plasma velocity for these two events. The order of the data listed corresponds to the four regions discussed above.

For both events, the shift in the direction of plasma velocity is in accordance with the model. The 15 Nov 64 event observed by IMP-1 has a larger change in direction within the interplanetary medium. On the other hand, the 26 Oct event seen by IMP-2 apparently has changes in velocity within the standoff region, as well as in the high velocity stream driving it.

Some suggestion that the 15 Nov event actually involved some type of tangential discontinuity is available from the GSFC magnetometer data (Fairfield, 1966). When the plasma velocity begins to increase rapidly at about 1745 hours (see Fig. 30) the magnetic field measurements by the IMP-2 satellite reveal a sudden reversal in field direction (it is uncertain whether the field magnitude went to zero from its 18 gamma value, so that no comment can be made with regard to the passage of a neutral

TABLE 6

Region*	IMP-2		IMP-1	
	Time Day Hour	Solar Ecliptic Longitude of Plasma Velocity**	Time Day Hour	Solar Ecliptic Longitude of Plasma Velocity**
(a)	25 Oct 07xx	- 8°	15 Nov 0950	-4°
(b)	26 Oct 0400	- 3°	15 Nov 1045	+6°
(c)	26 Oct 0830	-14°	15 Nov 1915	-6°
(d)	27 Oct 20xx	- 4°	16 Nov 0530	-4°

* See section C-4 of Chapter 4 for description of regions

** Velocity directions are known to within $\pm 2^{\circ}$ due to the technique of superposing many spectra.

sheat). Before the high velocity stream became established at 1830 hours, the field reversed four additional times, and then remained quiet at a reduced magnitude of 10 gamma. Further study and collaboration on these measurements may yield more insight into this and other interplanetary structures.

D. The Transition Region

1. Introduction

The space between the shock boundary and the outer boundary of the magnetosphere is termed the "transition" region (sometimes referred to as the magnetosheath, Dessler, 1964). Due to the very complex interaction between the solar wind, the interplanetary magnetic field, and the geomagnetic cavity, it is difficult to define the transition region in any more exact terms than simply a region of interaction located between Region I and Region III. The many probes and the dozen or more satellites which have explored this region have found it to be generally turbulent and also responsive to solar wind activity.

The magnetopause separates the transition region and the magnetosphere. It has nearly a spherical shape on the day side with radius of about 10 Re during geomagnetically quiet periods. On the dawn and dusk sides the magnetospheric cavity flares out to some 14 Re and in the night hemisphere an elongated magnetospheric tail developes. (Ness, 1965a). There is some suggestion of a dawn/dusk asymmetry in the shape of the cavity (Ness, 1966) but further data is needed to show that the effect is larger than that expected to be caused by the aberration of the solar wind.

The transition region is separated from the interplanetary region by the shock boundary, which is located approximately 3.5 Re in front of the magnetopause along the earth-sun line. The general shape of the boundary resembles a hyperboloid of revolution and was found to extend to beyond 20 Re at the dawn meridian (Ness, 1964 ; Lyon, 1966), by the IMP-1 satellite. The magnetic field measurements on IMP-3 have

shown that the shock boundary continues to flare out to beyond 30 Re at the 1900 hour dusk meridian (Ness, 1966). The recently launched Anchored IMP (July, 1966; apogee 70 Re) will hopefully provide data concerning the possible extension of the shock and magnetospheric tail to beyond the orbit of the moon.

The boundaries of the transition region have already been discussed in Section B and are displayed in Fig. 19. In this section some of the measurements made in the transition region by IMP-2 are presented.

2. Electrons and/or Protons in the Transition Region

The refraction of electrons* in the positive channels resulted in almost a complete loss of information about the protons in the transition region. The important theoretical questions on the density, velocity, and temperature profiles near the stagnation point, the validity of the fluid model as expressed by the Rankine-Hugoniot shock relations; and many other theoretical hypotheses could not be tested by this experiment.

The currents due to refracted electrons were in phase with the proton currents. Only when the signal was roll modulated to a sufficient degree that the proton component was clearly distinguishable, could an unambiguous separation be accomplished. Even then, there were often inconsistencies in the parameters determined by the process outlined in Chapter 3.

*The refraction effect is discussed in detail in Chapter 2.

The flux measured in the antisolar direction was taken to be due solely to the refraction of isotropic electrons in the positive channels. The currents predicted by a K = 4 Kappa distribution of electrons were compared with the data. An electron thermal energy near 300 E.V. usually offered the best fit in the four lowest positive channels. The current predicted for the negative channel by this electron spectrum was always more than a factor of ten greater than measured.

Whenever the roll modulation within the measurements permitted the abstraction of the proton component, the proton density was always nearly a factor of ten greater than the electron density determined by fitting a 300 e.v. electron spectrum to the four lowest positive channels. This accentuates even more the discrepancy in the negative channel.

On the other hand, if one invokes plasma neutrality by setting the electron density equal to the proton density determined for that set of measurements, then thermal energies below 50 e.v. are obtained. The agreement between the predicted and measured currents in the negative channel is significantly improved, and although the fit in the positive channels is poorer, it is still tolerable.

Part of the discrepancy can be attributed to the fact that the model current ratios are rather insensitive to change in thermal energy below 300 e.v. (Fig. 14). Furthermore, some additional refinements in the model (scattering, grid wire absorption, more accurate transparency measurements, possible variations from the assumed -36 volts on the suppressor grid, etc.) could alter the current ratios the

slight amount which would be required to fit the data and satisfy plasma neutrality as well. Since it is difficult to conceive how the plasma could not be neutral over scales of the order of the standoff distance (about 20,000 km) in the transition region*, it is believed that the thermal energy of the electrons is indeed below 50 e.v.

In view of the above discussion, it was quite difficult to analyze effectively the data in a large portion of the transition region. The following observations and conclusions, however, have been made:

(a) The electron thermal energy is most likely below 50 e.v. in the portion of the transition region explored by IMP-2. This energy is consistent with the Vela results (Strong, et al., 1966) and the OGO-1 observations (Vasyliunas, 1966b). All three measurements are at variance with the hot electrons observed by Freeman, Van Allen and Cahill (1963) on Explorer 12.

(b) In the region near the stagnation point no appreciable roll modulation is observed. This is attributed to a predominance of refracted isotropic electrons** with thermal energies near 50 e.v. The

---

*The Debye length, the distance over which appreciable departure from plasma neutrality can occur, is of the order of 10 meters for thermal energies near 50 e.v. and densities of 50 cm^{-3}.

**The possibility that the effect is solely protons can be excluded. Calculations show that in order for protons to produce signals of somewhat the same nature (still a poor fit) they would require the highly unlikely parameters of $V < 25$ km/sec, $\omega_o > 250$ km/sec, $N \sim 2000$ cm^{-3}.

very slight (less than 20%) roll modulation in the higher channels would not be inconsistent with protons having comparable thermal and bulk velocities. A non-Maxwellian proton distribution with a high energy "tail" could also be made to fit the data. No definitive conclusions, however, can be made.

(c) In the flanks of the transition region the roll modulation increased as it did in IMP-1 (Egidi, 1965 ; Lyon, 1966b). Near the 0600 local time meridian, the proton velocity was between 200 to 250 km/sec and the density was approximately 40 cm^{-3}. The interplanetary conditions were unknown at these times, but the period referred to (31 Dec 64) had very low K_p values and were designated as two successive quite (Q) days (Lincoln, 1965). After the onset of a storm on 2 Jan 65 (Fig. 43) the data from this region indicated the unusually high density of 300 protons/cm^3, and a plasma bulk velocity of 350 km/sec. The thermal speed remained at 125 km/sec.

A comparison of proton spectral observations with the IMP-2, OGO-1, and Vela-2B satellites has been made by Wolfe, et al. (1965). The satellites were widely separated in solar ecliptic longitude and latitude within the transition region. The data were also not taken simultaneously but were gathered during the disturbed period between 4 and 5 October 1964. Their analysis of the spectra indicates that there is a strong (25% of the total number density) non-Maxwellian component in the proton distribution above about 3000 volts. Based on the spectral data near the peak of the energy distribution, they determined a convectice velocity of 434 km/sec with an associated temperature of approximately 1 x 10^6 °K ($w_p \sim 125$ km/sec). The similarity

of the spectra from the three satellites leads them to conclude that the characteristics of the ionic component of the plasma in the transition region was apparently independent of the point of observation with respect to the subsolar region.

The Vela-2 satellite observations of strongly streaming plasma in the dawn and dusk portions of the transition region have been reported elsewhere by the Los Alamos group (Gosling, et al., 1966a). However, since these satellites are in a 17 Re nearly circular orbit, they cannot sample the transition region near the stagnation point.

The M.I.T. plasma data from IMP-2 were reviewed for the same period reported by the Ames group (Wolfe, et al., 1965). No suggestion of such high velocities is apparent in the data. The roll modulated component of the signals is consistent* with nearly equal thermal and convective velocities of about 200 km/sec.

Both the IMP-1 (Olbert and Moreno, 1964 ; Lyon, 1966) and the IMP-2 M.I.T. plasma experiments have shown a change in directed flow of the plasma and an increase in roll modulation at larger angles from the subsolar region. It is still an unresolved question whether the plasma near the stagnation point is subsonic. However, we conclude that there is definitely an increase in flow velocity as the plasma moves around the magnetospheric cavity.

---

*The addition of a high energy non-Maxwellian "tail" component in the proton distribution improves the agreement between model and measured currents.

E. The Magnetosphere

The spurious signal caused by the refraction of electrons in the positive channels permitted the measurement of electrons in the magnetosphere. Due to the higher thermal energies of the electrons in this region, the parameters of the electron distribution could be determined with good precision in contrast to the difficulty encountered with the transition region data. The currents predicted by the model agreed with the measured currents in all six channels. A model using only protons would require unrealistic densities and thermal energies, and then would only duplicate the data in some of the channels. Protons were thus excluded in the limited amount of analysis that was conducted.

In general, it was found that the electron density ranged from 0.1 to 1 electron/cm^3. The density varied with radial distance and local time meridian. The thermal energy, however, remains essentially constant near 1 Kev. Fig. 37 through 41 display some typical magnetospheric data (at both the right and left portions of the Figures) when the satellite was less than 10 Re from the earth near the subsolar region. It should be noted that the signals are nearly completely isotropic; no convective flow is seen.

Fig.43 of Orbit 63 displays the data in the dawn hemisphere near the 0600 local time meridian. The magnetosphere extends to further geocentric distances in this region and shows some interesting structure on the outbound pass before the satellite enters the transition region (0300 hours on 2 Jan 65). The fact that this structure is duplicated in all six channels is further evidence for a single mechanism, i.e., refracted electrons.

An example of data taken in the "tail"* of the magnetosphere is shown for Orbit 114 in Fig. 44 . Several interesting features are observed:

(a) For almost the entire first half of the orbit (1200 to 2300 hours), the electron flux is at or below the threshold sensitivity** of the instrument;

(b) Near apogee there are several occurrences of electron fluxes above the noise level (2300 to 0600 hours);

(c) On the inbound pass after 0600 hours, electrons are continuously observed well above the threshold flux levels.

This structure is observed on many of the orbits in this same region. It was found that the behavior can best be explained by the geometry of the orbits.

When the orbits in this region are presented in geocentric solar

---

*The name "tail" arises from the analogy of the extended magnetosphere in the night hemisphere to the tail of a comet. Recent measurements show that the magnetosphere shows no closure out to at least 30 Re (Ness. 1965b) and some authors believe the tail to be swept back from several hundred to a thousand earth radii (Dessler, 1964).

**The threshold flux level for this mechanism is roughly 10^9 electrons cm^{-2} sec^{-1}.

magnetic coordinates* (see Appendix A), the trajectories in the dipole meridian plane are similar on alternate orbits. The similarity is due to the fact that 2 orbits are completed in nearly exactly 3 days. Since the Z axis of this coordinate system is fixed to the geomagnetic dipole axis on the rotating earth, the coordinates of the satellite on every other orbit will be nearly identical. Fig. 32 displays the two types of trajectories in the dipole meridian plane.

---

*The use of geocentric solar magnetic coordinates reflects the important influence that the solar plasma flow has on the geomagnetic field. In the IMP-1 studies of the earth's magnetic tail, Ness (1965b) employed the geocentric solar magnetospheric coordinate system (Appendix A). However, the apogee of IMP-2 (15.9 Re) is nearly half that of IMP-1. The tail structure is not as well developed inside 20 Re as it is out at 30 Re. The use of geocentric solar magnetic coordinates reflects the control of the geomagnetic field in this region by retaining the concept of geomagnetic latitude; in addition, it recognizes the importance of the solar wind flow by introducing the concept of magnetic local time as the longitude in this coordinate system.

The distinction between solar magnetic and magnetospheric coordinate systems is almost academic with regard to IMP-2. When IMP-2 was providing information in the tail region it was the time of the Vernal Equinox. The solar magnetic Z axis was merely coning once per day around the solar magnetospheric Z axis at a cone angle of 11°.

While as yet all the data have not been analyzed, there appears to be a definite correlation between the onset of the electron fluxes and the satellite being very near the solar magnetic equatorial plane. When this occurred the electron fluxes persisted. This is the case for most all the even numbered orbits (such as Orbit 114 after 0600 hours, Fig. 44). During the period when the satellite was 3 Re or more below the solar magnetic equatorial plane, electron fluxes above threshold were not observed (1200 to 2300 hours.) Electron fluxes were also found on odd numbered orbits. The different orbital times of the observations again corresponded to the satellite being within 3 Re of the magnetic equatorial plane.

It is not clear whether the sudden onset of these electron fluxes is due to the satellite penetrating the outer boundary of the trapping region, or the so-called cusp region (Anderson, 1966). There is no apparent correlation with magnetic field measurements (Fairfield, 1966) during these sudden onsets.

Much still reamins in the analysis and interpretation of the M.I.T. data in the magnetosphere and its tail. It has already proved to be quite worthwhile to study the electrons in positive channels using data collected in the magnetosphere by an instrument primarily designed to monitor interplanetary protons.

F. The Plasmapause -- The Near-Earth Boundary of Thermal Ions

1. Introduction

Recent observation and studies (Carpenter, 1963) of a new whistler phenomenon suggest that the distribution of ionization in the magnetosphere may exhibit a pronounced departure from smoothness. The equatorial profile of electron density is shown to have an abrupt decrease, or "knee", at several earth radii.

Observations of a knee were also reported by Gringauz who flew ion traps on Luniks 1 and 2 and found a decrease in ion current at several earth radii (Gringauz et al., 1960). A cold plasma envelope was recorded at up to a height of about 20,000 km by the Russian Zord 3, Venera 2 and 3 in 1965 (Russian Cospar Report, 1966). The first results from the OGO-1 positive ion spectrometer experiment indicate that the ions are distributed in a belt-like region which exhibits a sharp gradient (Taylor, Brinton and Smith, 1965). The ion belt was observed to expand and contract over an altitude range of 8000, to 30,000 km in an inverse relationship with the magnetic activity index A_p.

In a recent paper (Carpenter, 1966) further whistler experiments are discussed and a descriptive model of the distribution of thermal ions around the earth is presented. The term "plasmapause" comes from that paper and is defined as the outer boundary of the plasmasphere, a region of dense ionization greater than 100 cm^{-3}. While the existence of the plasmapause appears to be a permanent feature, the whistler measurements showed that it exhibits both a diurnal variation as well as being

influenced by magnetic disturbances.

In this section, evidence is presented which shows that the M.I.T. plasma experiment on IMP-2 was also able to detect the plasmapause. A thorough mapping of its traversals and variability will be presented.

2. The Detection of Thermal Ions

On all the perigee passes of the IMP-2 satellite, where data were available, a marked increase in the average antisolar directed flux in the negative channel was a consistent feature* (see Fig.37-41). The detailed plots show (Fig. 33) that this current was roll modulated (a function of the azimuthal angle β) with a broad peak which varied with respect to the sun time during the perigee pass. This last characteristic eliminated the possibility that the observed effect was caused by a photoelectron current, while the fact that it would sometimes commence with a 30 fold increase within one format (5.45 minutes) ruled out such pehnomena as earth light and solar-paddle interference.

In this section it will be shown that the measured currents were most likely due to secondary electrons produced by ions bombarding the modulator grid.** This process can produce a roll modulated signal,

---

*The increase in flux in the negative channel near perigee was also observed on IMP-1 (Lyon, 1966[a]) and on the plasma probe on an early Air Force P-11 subsatellite (Bridge, 1966). These fluxes were previously interpreted as due to electrons.

**The suggestion of secondary electrons from positive ions bombarding the modulator grid is due to Vasyliunas (1966a), based on his observations on the OGO-1 satellite. This point will be discussed later.

and it was easily verified that the peak in the measured signals corresponded to that time when the angle between the cup normal direction and orbital velocity vector was at a minimum. This condition presented the maximum cross sectional area of the cup for "scooping up" the ions.

Calculations were made using a secondary emission yield of approximately 0.2 ± 0.1 (Medved and Strausser, 1965 ; Large, 1963) of protons on tungsten. The yield is a monotonically increasing function of the energy of the incident particle in the range of interest (130 to 265 electron volts). This yield variation will produce an A.C. component in the number of secondary electrons. The current is out of phase with the current produced by plasma electrons in this channel.

Since the thermal energy of the ions, and the velocity of the satellite relative to the ions are small compared to the modulator potential energy, the energy with which the ions strike the tungsten modulator grid is essentially the modulator potential itself. The flux of incoming ions can be estimated as the product of the number density, N, and the satellite's velocity (3.6 km/sec at a geocentric distance of 5 Re). The effective area for scooping up the ions is larger than the geometric area due to the focussing effect of the fields near the front grid (at - 18 volts with respect to the spacecraft's frame). There have been several estimates of the enhancement factor. Serbu and Maier (1966) use a factor of 4 as the best value between the minimum value of 1, and the maximum of 10 (based on idealized theoretical studies by L.W. Parker, 1965). This factor will be used in these calculations also.

The capture cross section of the modulator grid is also slightly larger than the true geometrical area. The strong accelerating fields near the wires of the grid enhance the effective area for collisions. An effective area of 10 cm^2 is reasonable for this process.

Combining the incident flux, effective scooping area, capture cross sectional area, and yield, one obtains as an estimate of the expected alternating current due to secondary electrons

$$I_s \sim N\,(3.6\times10^{5})(4)(10)(0.1)(1.6\times10^{-19})$$

$$\sim 2N \times 10^{-13} \text{ amps}$$

This value is quite consistent with the currents measured near the plasmapause. Beyond the boundary the density of ions is less than 1 cm^{-3}; whereas inside of the boundary the density can exceed 10^3 cm^{-3}. The change in density takes place within a spatial separation of less than one earth radius (Taylor, Brinton and Smith, 1965 ; Carpenter, 1966 ; Angerami and Carpenter, 1966). This change in density results in a current in the negative channel which would rise from below the noise level to a value of the order of 10^{-10} amps. This is exactly what is observed. Furthermore, as the satellite penetrates deeper into the plasmasphere, the current rises to nearly 10^{-9} amps, a result of the increase in flux due to the increased ion density at lower altitudes, and the increased orbital velocity nearer perigee.

The time sequence of the signals in the negative channel can be easily traced by referring to Fig. 33. This diagram shows the roll modulated currents resulting from ion produced secondary electrons,

frames (a) through (h) in the figure. The satellite had just passed perigee and was beginning Orbit 8 outbound. Each frame took approximately 4 seconds, and was separated from adjacent frames by 5.45 minutes. Two points are worth noting in these first nine frames.

1) The angle corresponding to the maximum current shifts to the right as time increases. This is directly attributable to the changing direction of the orbital velocity vector as the satellite begins the outbound part of its orbit. The maximum signal occurs when the angle between the cup normal and the velocity vector is minimum.

2) The maximum signal decreases with time as does the front to back ratio of currents. Since the flux of incident ions is proportional to the orbital velocity, the maximum currents will decrease as the satellite's velocity decreases away from perigee.

Between 0733 and 0738 hours on 14 Oct 1964 when the satellite was at an altitude of 15,292 km (3.4 Re geocentric distance), the density of positive ions decreased by more than a factor of ten. This is taken as the location of the plasmapause for this traversal. The photoelectric current in the negative channel (frames i and j) is now clearly seen to be a persistent feature of the signal between $\pm$ 60 about the "sun time".

In reviewing the data from the M.I.T. electron experiment* on the OGO-1 satellite, Vasyliunas (1966c) reported that near perigee, the currents in all four negative channels are clamped below noise level.

*A separate Faraday Cup with four negative channels was used on the OGO-1 satellite.

He attributes this effect to a component of current out of phase with the plasma electron current expected in these channels. The detection system in OGO-1 experiment is a synchronous detector, any spurious signal out of phase from the expected signal will result in an output of opposite polarity from the nominal output; thus, the output below noise level.

The plasma experiment on IMP-2 employed an amplitude detector (see Appendix C) and thus was only sensitive to the magnitude of the difference between normal plasma electron current and the secondary emission electron current. This is apparent in the inbound perigee pass of Orbit 15 (Fig. 40). One observes that the signal in the negative channel first decreases abruptly as the two currents become comparable, and then rises as soon as the secondary electron current predominates.

It is not possible to determine the number density of these ions to any greater extent than merely to indicate consistency with former measurements. However, since the signals are roll modulated one can estimate the thermal temperature of the ions. By comparing the front to back ratio of the measured currents (usually 5 to 10) and knowing the satellites velocity (V) at the time, an approximate* thermal energy $E_o \leq 0.2$ e.v. is obtained assuming the ions are ionized hydrogen

*When $X = \frac{V}{\omega_o} >> 1$, the front to back ratio is approximately $X \exp(X^2)$. Using the results near perigee when $V \sim 10$ km/sec one finds $X \sim 2$ for a measured ratio of 15.

atoms.*

In the next section the location of the boundary of dense ions (the plasmapause) will be mapped, and their response to solar activity as indicated by K_p will be discussed.

3. Mapping the Plasmapause

On all orbits where data were available near perigee, a sharp change in the character of the current in the negative channel was encountered at various geocentric distances from 2.09 to 6.86 Re. Plotting the 130 data points on a distance versus local time diagram produced negligible order in the presentation of the data. However, when the data are displayed on a L vs. magnetic local time (MLT)** plot considerable order was introduced (See Fig.34). These points represent data accummulated over the first six months of IMP-2 (127 orbits, not all of which contained useful data in this region). The scarcity of data on the dusk side simply reflects the lack of trajectories in that region during these six months.

---

*The ratio of H^+ to He^+ was found to be consistently near one percent by the OGO-1 ion spectrometer (Taylor, et al., 1965).

**L is the magnetic shell parameter introduced by McIlwain (JGR, 1961) and the magnetic local time is the azimuthal angle in solar magnetic coordinates (see Appendix A).

Any diurnal variation in the data might not be apparent due to the effects of variations caused by magnetic disturbances. Even the average L values for each 20 degree increment (shown as solid lines in the Figure) do not display any significant diurnal feature.

In order to remove the magnetic disturbance variation, the three hour K_p value at the time of each data point was used as an index of these variations. Fortunately, during the lifetime of IMP-2, the K_p value rarely exceeded the value of 4, and thus many crossings at low values were available. In an attempt to display the boundary as it exists during quiet and undisturbed periods a plot of average L versus MLT was drawn using a total of 63 points when the three hour K_p was less than or equal to one (Fig. 35). Here, it is apparent that the boundary assumes an almost circular appearance with an average L of about 5.5 geocentric earth radii. There is some hint of the beginning of a bulge near the dusk side but the number of measurements here are insufficient for any definite conclusion.

The majority of the whistler data (Carpenter 1966) were taken when K_p was between two and four. The principle features were:

(1) A relatively broad minimum in geocentric distance centered roughly at 0600 LT at about 3 - 3.5 Re.

(2) A maximum geocentric distance at about 2000 LT of 5 - 5.5 Re.

(3) Following the maximum near 2000 LT a decrease in range with time on the nightside of the earth at a rate resulting in a change of 1.5 Re over a period of 10 hours.

(4) A rapid increase in distance near 1800 LT involving a radial variation of about 1 Re in a period of 1 hour.

(5) A gradual outward tendency across the dayside from 0600 LT to midafternoon of about 0.5 Re.

From the limited quantity of data available during magnetically quiet conditions, (K_ρ = 0-1) they conclude that the diurnal curve of equatorial distance versus local time moves outward and becomes more symmetric with respect to the earth. During the quiet interval on 28-29 July 1963, (K_ρ = 0-1) the typical geocentric equatorial distance was between 5 and 6 earth radii, with a slight bulge at 2200 LT.

During magnetically quiet periods, both the whistler knee measurements and the M.I.T. plasma measurements agree remarkably well in the determination of the boundary of dense thermal ionization. Furthermore, a study of the plasma data during times of higher K_ρ values, also yielded extremely good agreement. Fig. 36 , shows the L values (averaged over all angles) as determined by the plasma data plotted as a function of the magnetic disturbance index K_ρ. The relationship can adequately be described by

$$L = 6. - 0.6\ K_\rho$$

The inverse relationship between the knee position and the magnetic activity index (K_ρ or A_ρ) was also shown in the whistler studies (Carpenter, 1966) and the ion spectrometer experiment on OGO-1 (Taylor, Brinton and Smith 1965).

There appears to be little doubt that the M.I.T. plasma experiment can detect the plasmapause, and accurately determine its location.

CHAPTER V

SUMMARY AND CONCLUSIONS

The M.I.T. plasma probe on the IMP-2 satellite was highly successful in exploring the boundaries of the transition region and investigating their response to solar activity. A thorough mapping of the boundaries shows that their average locations have not changed from the time since IMP-1 was in the same vicinity. Because IMP-1 passed through this region less frequently and at faster relative velocities than its sister satellite, IMP-2 was able to explore in more detail the motion of the boundaries and their response to changes in interplanetary plasma conditions.

Both long and short period motions of the shock boundary have been observed. The former displayed a very clean, nearly sinusoidal character on one occasion studied in detail and apparently was not rapid enough to produce any appreciable fluxes of high energy electrons. On the other hand, there were usually spikes of electron fluxes above 45 Kev energy associated with the short rapid shock boundary motions.

During the first few orbits short duration samples of transition-like plasma have been observed several earth radii beyond the normal shock location. These bursts show excellent correlation with the times that the GSFC magnetometer observed turbulent magnetic fields. A limited investigation shows that some of these bursts occur at the time of electron spikes (the converse is not necessarily true).

Local electron acceleration, with possibly some pileup in density, is shown to be a reasonable explanation for the correlation with rapid

boundary motions. It is concluded that a model assuming a magnetospheric origin for the spikes of electrons cannot explain the observed correlations.

Several specific geomagnetic storms are investigated from the standpoint of the resulting magnetospheric compression. The observed compression was in very good agreement with the classical predictions which equate external dynamic plasma pressure and internal geomagnetic pressure. The recurrence cycle of these storms is clearly evident in the compression of the boundaries on certain days of the solar rotation.

A very distinctive type of magnetopause was occasionally observed in the plasma data. The diffusive nature of this boundary was also apparent in the GSFC magnetometer data and on at least one occasion in the U. of Calif. Geiger tube data. An enhanced topological connection of the magnetic field lines between the transition region and the magnetosphere is believed to have resulted in an increased diffusion of low energy, transition region, electrons into the outer magnetosphere. The radial dependence of these energetic electrons is shown to be in good agreement with an inward diffusion of particles while conserving the first adiabatic invariant.

The investigation of the interplanetary medium by IMP-2 was severely limited by a malfunction in the launch and injection sequence. Nevertheless, it is found that the pattern of the plasma behavior followed closely that expected to be produced by recurrent M-region storms on the surface of the sun. The tangential discontinuity between the high velocity plasma stream from the M-region and the slower

ambient interplanetary plasma is believed to have been observed during the 15 Nov 1964 event.

The refraction of the trajectories of charged particles within the detector is shown to constitute an appreciable component of the measured current. This electron component is oftentimes impossible to separate from the proton current in the positive channel especially when the satellite was in the transition region. As a result the shock boundary relations could not be checked and the usefulness of the fluid model could not be tested. Analysis of the electron component in the transition region reveals that thermal energies below 50 e.v. are consistent with the data provided plasma neutrality is assumed. Electrons in the magnetosphere are shown to have generally 1 Kev. thermal energies.

Finally, it is shown that the M.I.T. plasma experiment was sensitive to the region of dense thermal ionization near the earth. The boundaries of this region obtained from the IMP-2 data agree remarkably well with the knee region, or plasmapause, investigated by whistler techniques.

APPENDIX - A

DESCRIPTION OF FREQUENTLY USED COORDINATE SYSTEMS

A. Orbital Coordinate Systems

In the following section $\hat{S}$ is a unit vector pointing from the earth's center to the sun's center, $\hat{\eta}$ is the unit vector of the Vernal Equinox, $\hat{d}$ is a unit vector antiparallel to the geomagnetic dipole moment, $\hat{p}$ is a unit vector pointing in the direction of the earth's spin vector, and $\hat{E}$ is a unit vector in the direction of the North ecliptic pole.

1. Celestial (Geocentric Equatorial) System (Fig. A-1).

The origin of this system is at the center of the earth and its orientation is determined by its X and Z axes. The positive Z axis coincides with the earth's axis of rotation and passes through the North Pole. The positive X axis points in the direction of the Vernal Equinox, i.e., it is defined by the intersection of the earth's equatorial plane with the plane of the ecliptic, at that position in the earth's orbit where the sun's declination (the latitude angle) relative to the earth's equatorial plane changes from south to north. The two angles used to describe a direction are the Right Ascension (the azimuthal angle from the Vernal Equinox) and Declination (the latitude angle from the equatorial plane).

2. Geocentric Solar Ecliptic System (Fig. A-2).

The origin of this system is at the center of the earth and its X and Y axes are in the plane of the ecliptic. The positive X axis points toward the sun; the positive Z axis is perpendicular to the ecliptic plane and points in the direction of the North ecliptic pole; and the Y axis is the third member of the right handed system. The direction of the Y axis is nearly antiparallel to the earth's orbital velocity vector. The solar ecliptic longitude is the azimuthal angle in the ecliptic plane and is measured from the earth-sun line (the positive X axis). It can alternately be described in terms of local time: local noon, 1200 hrs., is 0° solar ecliptic longitude; local dusk, 1800 hours, is 90°; local midnight 2400 hours, is 180°; and local dawn, 0600 hours, is -90° solar ecliptic longitude. The solar ecliptic latitude is measured from the ecliptic plane.

3. Geocentric Solar Magnetic System (Fig. A-3).

The origin is also at the earth's center. The orientation is determined by its X and Y axes. The positive Z axis is coincident with the geomagnetic dipole but in the opposite direction, i.e., it points Northward. The X axis is such that the earth-sun line lies in the positive X half of the X-Z plane, and the Y axis is the third member of the right handed coordinate system. In this system the angle λ, the latitude of the sun, changes daily by approximately $\pm 11^{\circ}$ about a yearly variation of $\pm 23^{\circ}$.

4. Geocentric Solar Magnetospheric System (Fig. A-4).

This is an earth centered system whose orientation is determined by its X and Z axes. The positive X axis is coincident with the earth to sun line; the positive Z axis points Northward such that the X-Z plane contains the geomagnetic dipole moment; and the Y axis forms the third member of the right handed system. In this system the angle χ is the geomagnetic latitude of the sun and has maximum daily excursions of $\pm 11^{\circ}$ about a slow yearly variation of $\pm 23^{\circ}$.

B. Analysis Coordinate Systems

In the following section $\hat{\ell}$ is the unit vector aligned along the satellite spin vector, $\hat{q}$ is the unit vector coincident with the satellite-sun line and $\hat{n}$ is the unit normal vector of the cup.

1. Cup Coordinate System (Fig. A-5).

The center of this coordinate system is on the axis of symmetry of the cup in the plane of the front grid. The positive Z axis is the outward cup normal, and the X-Y plane is parallel to the collector surface. The positive X axis is taken to be parallel to the satellite's spin axis. A particular direction is specified by the polar and azimuthal angles θ and ϕ. Thus a particle with velocity vector V would be specified in the coordinate system by the column matrix.

$$V\Big]_{cup} = \begin{bmatrix} V_x \\ V_y \\ V_z \end{bmatrix} = V \begin{bmatrix} \sin\theta \cos\phi \\ \sin\theta \sin\phi \\ \cos\theta \end{bmatrix} \qquad (A.1)$$

2. Satellite Sun Coordinate System (Fig. A-6).

This system is a satellite centered coordinate system with the positive Z axis coincident with the satellite's spin vector. The X-Y plane is the plane traced out by the rotating cup normal, and the positive X half of the X-Z plane contains the satellite-sun line.

The angle α, the latitude of the sun, is a slowly varying function of season. It is measured directly by the spacecraft's optical aspect sensor (OA). The azimuthal angle of the cup normal, β, for any time t can be computed from the time the optical aspect sensor is in the X-Z plane, t_o, and the spin rate w of the satellite: $\beta = w(t-t_o) + 135^\circ$. The 135° is the mechanical offset between the OA and the cup normal. The transformation from cup coordinates to satellite coordinates is

$$V]_{SS} = \begin{bmatrix} 0 & \sin\beta & \cos\beta \\ 0 & -\cos\beta & \sin\beta \\ 1 & 0 & 0 \end{bmatrix} V]_{cup} = [B]\, V]_{cup} \qquad (A.2)$$

The transformation from satellite sun coordinates to solar ecliptic is done in two rotations. (Translating the origin of the solar ecliptic system from the center of the earth to that of the satellite introduces negligible error, so that one may take $\hat{q} = \hat{s}$).

$$V]_{SE} = \begin{bmatrix} 1 & 0 & 0 \\ 0 & \cos\gamma & -\sin\gamma \\ 0 & \sin\gamma & \cos\gamma \end{bmatrix} \begin{bmatrix} \cos\alpha & 0 & \sin\alpha \\ 0 & 1 & 0 \\ -\sin\alpha & 0 & \cos\alpha \end{bmatrix} V]_{SS} \qquad (A.3)$$

$$= [C][A][B]\, V]_{cup}$$

With λ_ℓ as the solar ecliptic latitude of the spin axis, the angle γ is simply

$$\cos\gamma = \sin\lambda_\ell \cos\alpha \tag{A.4}$$

The inverse is readily obtained which permits determining the velocity as seen by the cup in terms of its components in solar ecliptic coordinates.

$$V]_{cup} = [B^T][A^T][C^T]\ V]_{SE} \tag{A.5}$$

where $[M^T]$ is the transpose of the matrix $[M]$.

APPENDIX B

THE KAPPA DISTRIBUTION FUNCTION

Of the class of three parameter isotropic distribution functions, a convenient and useful one, called the Kappa Distribution*, is defined as

$$f_K(w^2) = \frac{C_K}{\left(1 + \frac{1}{K}\frac{w^2}{w_o^2}\right)^{K+1}} \qquad \text{(B.1a)}$$

with a nomalization constant

$$C_K = \frac{N}{\left(\pi w_o^2\right)^{3/2}} \frac{\Gamma(K+1)}{K^{3/2}\,\Gamma(K-\frac{1}{2})} \qquad \text{(B.1b)}$$

where $\Gamma(y)$ is the Gamma function of the argument y. The three parameters of this distribution function are

- N the density of particles in $(\text{length})^{-3}$
- w_o the most probable speed in length/second
- K^o a dimensionless parameter related to the flux spectral index.

Outlined below are some of the important properties of this distribution which were used in this study.

---

*Introduced by Prof. S. Olbert in his studies of plasmas on IMP-1. (Olbert, to be published in JGR).

A. Relationships to the Maxwellian Distribution

1. Integral Transform

Consider the Laplace Transform*

$$\int_0^\infty t^{k-1} \epsilon^{-at} \epsilon^{-s\tau} dt = \frac{\Gamma(k)}{(s+a)^k} \tag{B.2}$$

By letting

$$k = K + 1$$

$$a = 1$$

$$s = \frac{w^2}{K w_o^2}$$

Then

$$\int_0^\infty t^K \epsilon^{-t} \epsilon^{-\frac{t}{K}\frac{w^2}{w_o^2}} dt = \frac{\Gamma(K+1)}{\left(1 + \frac{1}{K}\frac{w^2}{w_o^2}\right)^{K+1}}$$

so that

$$f_K(w^2) = C_K \int_0^\infty \frac{t^K \epsilon^{-t}}{\Gamma(K+1)} \epsilon^{-\frac{w^2}{\frac{K}{t} w_o^2}} dt \tag{B.3}$$

---

*See, for example, Handbook of Mathematical Functions, p. 1022, Nat. Bur. of Standards AMS 55.

Now, the Maxwellian distribution is defined by

$$f_m(w^2) = C_m \in^{-\frac{w^2}{w_o^2}} \tag{B.4a}$$

where

$$C_m = \frac{N}{\left(\pi w_o^2\right)^{3/2}} \tag{B.4b}$$

and one can designate the Poisson Distribution by

$$P_K(t) = \frac{t^K \in^{-t}}{\Gamma(K+1)} \tag{B.5}$$

then we have the interesting and useful relation

$$\begin{aligned} f_K(w^2) &= \frac{C_K}{C_m} \int_0^\infty P_K(\tau)\, f_m\left(\frac{t}{K} w^2\right) d\tau \\ &= \frac{\Gamma(K+1)}{K^{3/2}\,\Gamma(K-\frac{1}{2})} \int_0^\infty P_K(t)\, f_m\left(\frac{t}{K} w^2\right) dt \end{aligned} \tag{B.6}$$

This expression clearly illustrates that the Kappa Distribution is a Poisson weighted sum of Maxwellian Distributions of all possible temperatures.

2) Large Kappa: Maxwellian Limit

$$\lim_{K \to \infty} f_K(w^2) = f_m(w^2) \tag{B.7}$$

To show this we need Stirling's Formula for the Gamma function.

$$\Gamma(z) = \sqrt{\frac{2\pi}{z}} \left(\frac{z}{\epsilon}\right)^z \qquad \text{for large } z$$

and a frequently used limit

$$\lim_{m \to \infty} \left(1 + \frac{1}{m} A\right)^m = \epsilon^A$$

Using these relations in (B.1) and taking the limit as K approaches infinity, after much algebra one obtains (B.7).

B. Moments of the Kappa Distribution

Define the n^{th} moment as

$$M_K^{(m)} = 4\pi \int_0^\infty w^m f_K(w^2)\ w^2 dw \tag{B.8}$$

In light of (B.6) we can write this as

$$M_K^{(m)} = 4\pi \int_0^\infty dw\ w^{m+2} \int_0^\infty dt\ C_K \frac{t^K e^{-t}}{\Gamma(K+1)}\ \epsilon^{-\frac{t w^2}{K w_0^2}}$$

which upon interchanging the order of integration and evaluating the integrals in terms of gamma functions becomes

$$M_K^{(m)} = N \left(K w_0^2\right)^{\frac{m}{2}} \frac{\Gamma\left(\frac{3}{2}+\frac{m}{2}\right)\Gamma\left(K-\frac{1}{2}-\frac{m}{2}\right)}{\Gamma\left(\frac{3}{2}\right)\ \Gamma\left(K-\frac{1}{2}\right)} \tag{B.9}$$

Examples:

Density, n = 0 $$M_K^{(0)} = N \tag{B.10a}$$

Flux, n = 1 $$M_K^{(1)} = \frac{2}{\sqrt{\pi}} N w_0 \frac{\sqrt{K}\ \Gamma(K-1)}{\Gamma(K-\frac{1}{2})} \tag{B.10b}$$

Energy, n = 2 $$U_K = \frac{1}{2} m M_K^{(2)} = \frac{3}{2} N E_0 \left(\frac{K}{K-\frac{3}{2}}\right) \tag{B.10c}$$

where $E_0 = \frac{1}{2} m w_0^2$

and m = mass of particle

Note, in the limit of large K, the moments approach those of the Maxwellian distribution.

C. Derived Quantities

Consider a particular quantity of interest, $\phi_K(w_o^2, \vec{u})$ derived from the Kappa Distribution, and dependent upon the most probable speed, w_o, and other parameters conveniently represented as a point in some parameter space by the vector, $\vec{u}$. Then

$$\phi_K(w_o^2, \vec{u}) = \int H(\vec{u}, w^2)\, f_K(w^2, w_o^2)\, d^3w \qquad (B.11)$$

formally expresses the relationship through the kernel $H(\vec{u}, w_o^2)$ The explicit form of the dependence on w_o is highlighted here as will be done for the Maxwellians distribution, i.e. $f_m(w^2, w_o^2)$

Now in the light of (B.6), the above relation can be written as

$$\phi_K(w_o^2, \vec{u}) = \int H(\vec{u}, w^2)\left[\frac{C_K}{C_m}\int_o^\infty P_K(t)\, f_m\left(w^2, \frac{K}{t}w_o^2\right) dt\right] d^3w \qquad (B.12)$$

$$= \frac{C_K}{C_m}\int_o^\infty P_K(\tau)\, dt \int H(\vec{u}, w^2)\, f_m\left(w^2, \frac{K}{t}w_o^2\right) d^3w$$

The second integral is clearly the same quantity derived from the use of the Maxwellian Distribution.

$$\phi_m\left(\frac{K}{t}w_o^2, \vec{u}\right) = \int H(\vec{u}, w^2)\, f_m\left(w^2, \frac{K}{t}w_o^2\right) d^3w \qquad (B.13)$$

Thus

$$\phi_K(w_o^2, \vec{u}) = \frac{\Gamma(K+1)}{K^{3/2}\,\Gamma(K-\frac{1}{2})}\int_o^\infty P_K(t)\, \phi_m\left(\frac{K}{t}w_o^2, \vec{u}\right) dt \qquad (B.14)$$

which expresses that quantities based on the use of the Kappa Distribution are merely weighted sums of the same quantities based on the use of the Maxwellian Distribution, with a modified most probable speed. Since it is usually straight forward to derive quantities assuming a Maxwellian distribution, the above offers a convenient transformation for finding the same quantities based on a Kappa distribution.

As an example consider the isotropic pressure

$$P_K(W_o^2) = \frac{\Gamma(K+1)}{K^{3/2}\Gamma(K-\frac{1}{2})} \int_0^\infty \frac{t^K \epsilon^{-t}}{\Gamma(K+1)} P_m\left(\frac{K}{t} W_o^2\right) dT$$

where

$$P_m(W_o^2) = \frac{1}{3} \int_0^\infty m\, w^2 f_m(w^2, W_o^2)\, 4\pi w^2 dw$$

$$= C_m \frac{1}{2} \pi^{3/2} W_o^5$$

then for the Kappa distribution we find

$$P_K(W_o^2) = N E_o \left(\frac{K}{K - 3/2}\right) \qquad \text{(B.15)}$$

where $E_o = \frac{1}{2} m W_o^2$

Note that $P_K = \frac{2}{3} U_K$ as it must for any isotropic distribution, and also that in the limit of large Kappa, one has the Maxwellian pressure NE_o.

D. Related Distributions

a) Speed (Fig. B.1)

$$F_s(w^2)dw = 4\pi w^2 f_K(w^2)dw \tag{B.16a}$$

for $w^2 >> w_o^2$ $\quad F_s(w^2) \propto (w^2)^{-K}$

b) Energy

$$N(E)dE = C_K' \frac{E^{1/2}dE}{\left(1 + \frac{1}{K}\frac{E}{E_o}\right)^{K+1}} \tag{B.16b}$$

for $E >> E_o$ $\quad N(E) \propto E^{-(K+\frac{1}{2})}$

c) Flux

$$\Phi(E)dE = C_K'' \frac{E\,dE}{\left(1 + \frac{1}{K}\frac{E}{E_o}\right)^{K+1}} \tag{B.16c}$$

for $E >> E_o$ $\quad \Phi(E) \propto E^{-K}$

APPENDIX C

DETAILED DESCRIPTION OF THE M.I.T. PLASMA EXPERIMENT

A. The Telemetry System

The M.I.T. plasma experiment was one of nine experiments carried on the IMP-2 satellite (Fig. C-0). The information gathered by these experiments was time multiplexed onto an FM/FM telemetry system. The complete time sharing format was accomplished in 5.45 minutes, and was composed of three identical sequences of the structure shown in Fig. C-1 followed by one sequence devoted to the Rubidium vapor magnetometer. Each sequence consisted of 16 frames some of which were shared among experiments. The frame itself is divided into 32 half channels each of duration 0.160 seconds, so that a complete frame takes 5.12 seconds. Frames 13 and 14 of each standard sequence were assigned to the M.I.T. experiment.

Fig. 6 of the main text illustrates how the M.I.T. experiment utilized the six frames per format, and these are also tabulated below for convenience.

Sequence	Frame	Channel	Modulator Voltages
1	13 14	1 2	40/90 95/230
2	13 14	3 4	260/650 700/2000
3	13 14	5 6	-130/-265 1700/5400
4	(Non Operative)		

Each frame consisted of 26 data samples followed by 4 samples of experimental bookkeeping information. The first two half channels in the frame were devoted to satellite bookkeeping. The functions of the 32 half channels per frame are summarized in Fig. C-2 . Of the 26 data samples available per frame the first 4 were contaminated by a power turn on transient and were discarded in the data analysis.

The output of the M.I.T. experiment was an analog voltage between 0 to 5 volts which was sampled and held in synchronism with the 0.16 second half channel period. The telemetry system encoded the analog voltage into an audio frequency which in turn frequency modulated the r.f. carrier.

At the receiving station the demodulated r.f. was fed into a bank of comb filters. Of the 127 comb filters in the bank the receiver chose that comb filter which possessed the maximum signal as being the best estimate of the transmitted audio frequency. Thus an accuracy of better than 1% could be achieved in specifying an analog voltage, provided the signal did not vary faster than the 0.1 second response time of the comb filters.

B. The Cup

The cup was a 6 inch diameter gold plated magnesium shell approximately 3.3 inches deep. Three of the grids were made of fine tungsten mesh, while the shield grid #3 was made of bronze. A net transparency of 25% at normal incidence for all four grids was determined by optical measurements. (Lyon, 1966)

The detailed response to protons was measured in an evacuated chamber with an ionized hydrogen source. Fig. C-3 displays the normalized angular response for modulator voltages between 400 and 970 and a beam energy of 600 ev.

C. The Electronics

A block diagram of the complete experiment is shown in Fig. C-4. The high voltage modulator (a "Cockcroft-Walton" chain) provides the square wave potential to the modulator grid #2. The plasma incident upon the two semi-circular collecting plates is modulated by this potential. The outputs of the two sensitive preamplifiers are alternately added, and subtracted prior to passing through the time shared narrow band filter and compression amplifier. The compression amplifier was a quasi-logarithmic device which compressed the 4 decade input range to within the 0-5 volt output range for the telemetry.

During the times when the "difference" signal was present at the output of the compression amplifier, a gate was opened to a peak reading circuit which would store the maximum difference signal obtained during a frame. Another circuit would determine which of the two semi-circular collectors was receiving the larger signal. This information was transmitted as "Peak Difference Signal" in channel 15, and "Polarity Marker" in the second half of channel 14, respectively (See Fig. C-2).

The "sum" signal was not processed via a peak reading device. Rather, at the end of each half channel, the output of the compression amplifier was sampled rectified and held for the telemetry during the succeeding half channel. The rectifier was a half wave diode rectifier and thus achieved amplitude demodulation, insensitive to the phase of the signal with respect to the modulator voltage. These data samples were read out by the telemetry in each half channel 1 through 13 inclusive.

The first half channel of channel 14 was devoted to instrumental status information. Four time each format, an internal calibration current would be gated into the input of the preamplifiers, processed by the measurement chain, and read out during this half channel. On the remaining two frames within the format, two separate temperature measurements were gated to the telemetry. This information was used to correct the instrument's measurements for temperature effects.

APPENDIX D

DATA PROCESSING

In order to analyze the nearly 5 months of satellite data in a reasonable fashion, an efficient method of presenting the measurements had to be devised. In this section, a brief description of the main processing computer program will be given.

The data is obtained from the Goodard Space Flight Center and is stored on magnetic tape. After editing and sorting in time sequence, the data is available for analysis. As mentioned in Appendix C, the information is in the form of a comb filter number which corresponds to the best estimate of the analog voltage presented to the telemetry system by the M.I.T. experiment. This voltage, in turn, corresponds to a measured current in a particular channel. Thus there are two major transformations required to convert from the comb filter numbers to the measured currents. Both transformations are temperature sensitive. The conversion from voltage to comb filter number fortunately was well compensated.

The temperature dependence of the current to voltage characteristics could not be ignored. This turned out to be especially important due to the higher and more widely varying temperatures encountered on IMP-2 due to the non-nominal orbital injection (See Chapter 2). These factors were taken into account by performing a parabolic interpolation for the current at the actual measured temperature. The information used was from preflight calibration data taken at 10, 26, and 44 °C.

The simplified flow diagram for the main processing program is shown in Fig. D-1 . The function of the eleven major subroutines are briefly:

1. TPSCAN: Scans the data tape for the beginning of the time period of interest.

2. SEQCON: Arranges the data according to increasing channel number.

3. SUNTIME: Computes the time within the frame when the angle between the cup normal and the sun satellite line is a minimum.

4. CONVRT: Converts the data in comb filter numbers to engineering units such as current, angles and temperature. The currents are adjusted for the actual temperature measured.

5. ROLL: Reorganizes the converted data within each channel according to azimuthal angle β measured from the suntime.

At this point in the program a decision is made concerning which of several ways the data is to be presented.

6. SMCOMP: Finds the maximum signal in each channel (insures that the maximum has a legitimate smaller signal on each side of it) and finds the arithmetic average current within the $\pm$ 60 angular sector centered about the anti solar direction.

7. SMPLOT: Plots the summary data as depicted in Figures 37-44 at a scale of one inch per hour.

8. DAPRNT: Prints the data in engineering units.

9. RLPLOT: Plots the detailed roll data at a scale of 1 revolution per inch (See Figures 8-10).

10. SUPLOT: Superimposes on a larger scale the detailed roll plots.

11. FINIS: Closes out all plotting and exists to the computer system.

These are the major subroutines of the main program. There are many additional peripheral subroutines not mentioned above which are required to perform the analysis.

LIST OF ILLUSTRATIONS

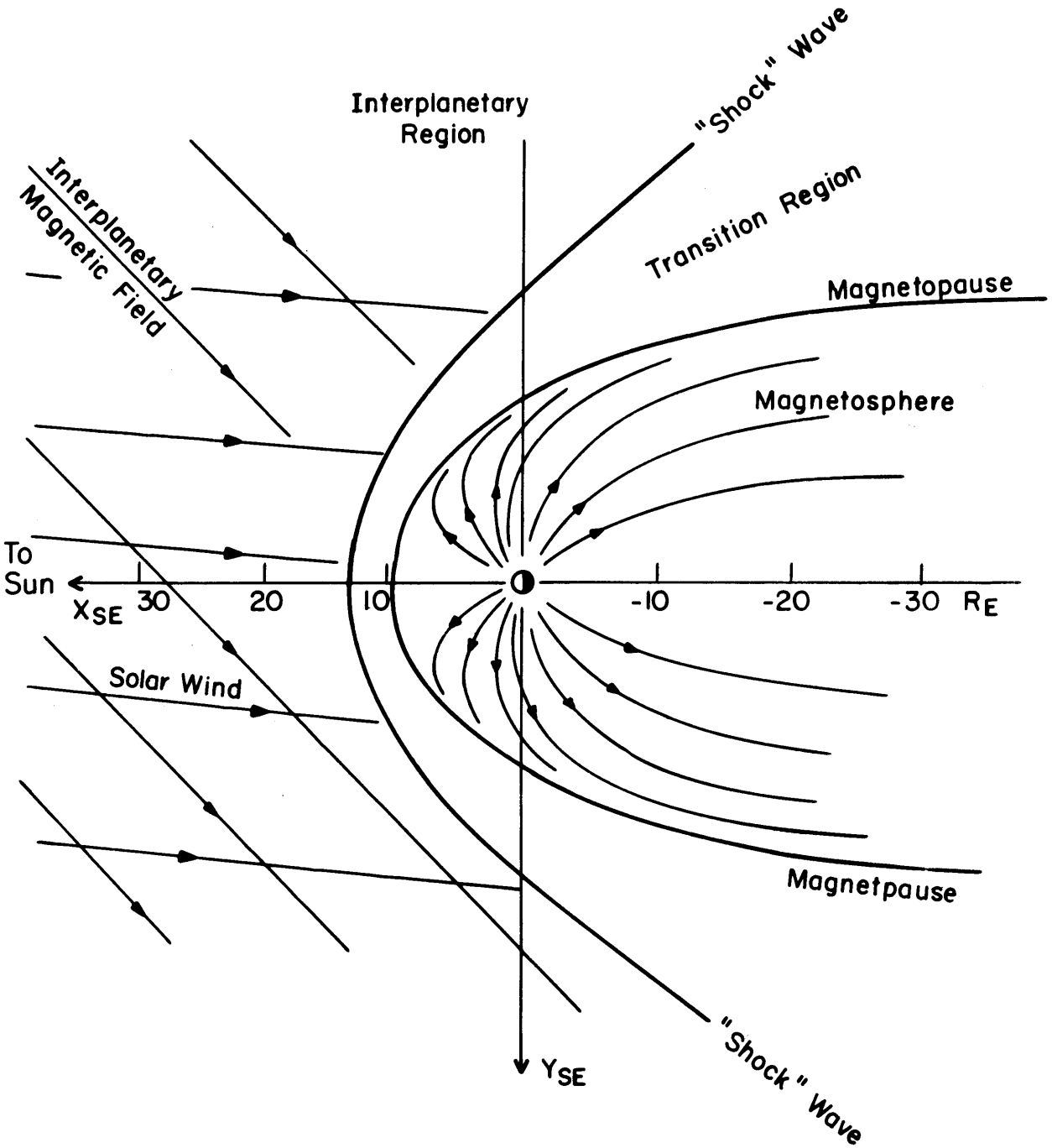
Interplanetary Region
"Shock" Wave
Interplanetary Magnetic Field
Transition Region
Magnetopause
Magnetosphere
To Sun
30
20
10
-10
-20
-30 RE
XSE
Solar Wind
Magnetpause
YSE
"Shock" Wave

Figure 1

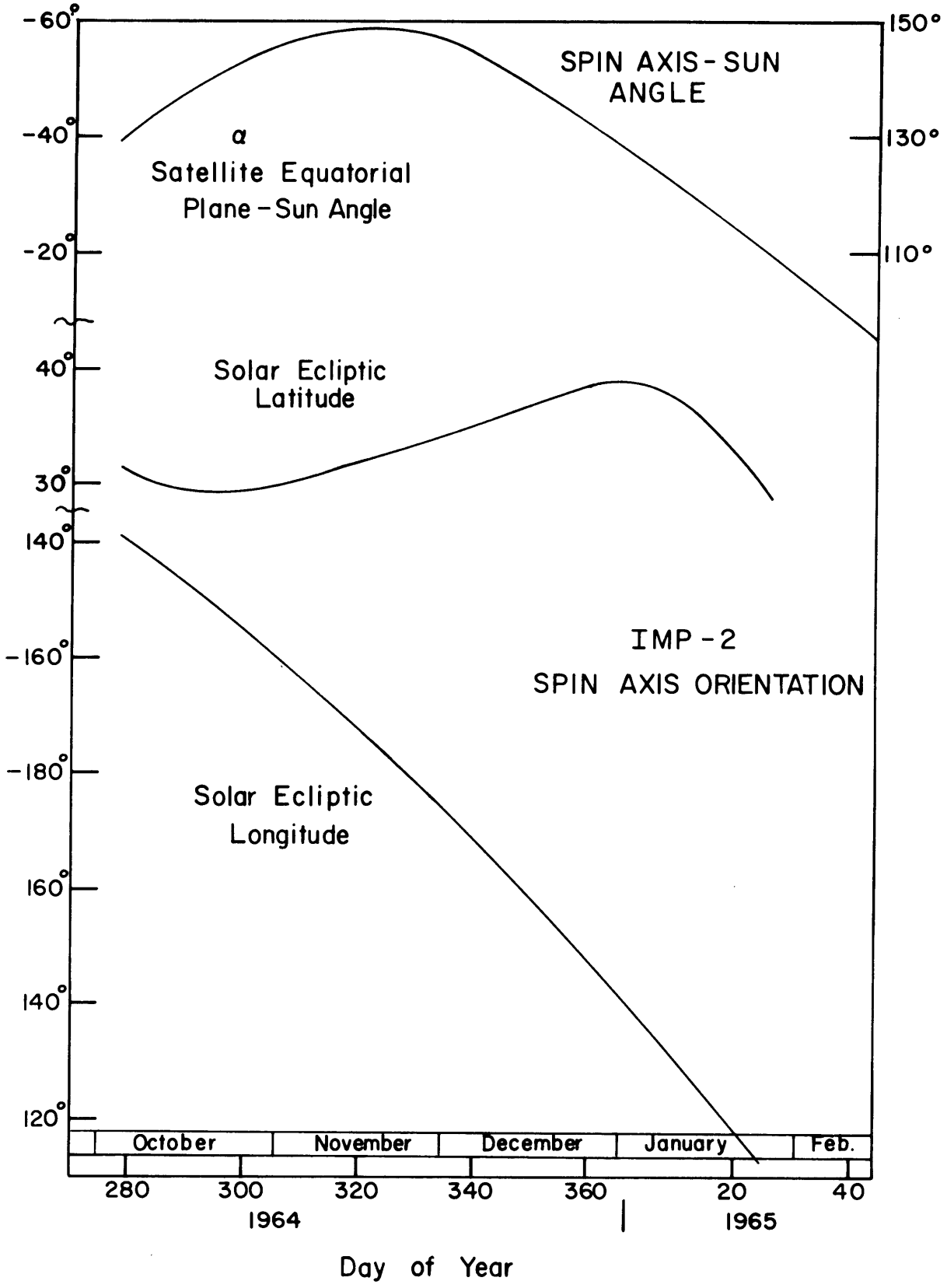
-60°
-40°
-20°
40°
30°
140°
-160°
-180°
160°
140°
120°
150°
130°
110°
SPIN AXIS - SUN ANGLE
α
Satellite Equatorial Plane - Sun Angle
Solar Ecliptic Latitude
Solar Ecliptic Longitude
IMP - 2
SPIN AXIS ORIENTATION
October
November
December
January
Feb.
280
300
320
340
360
20
40
1964
1965
Day of Year

Figure 2

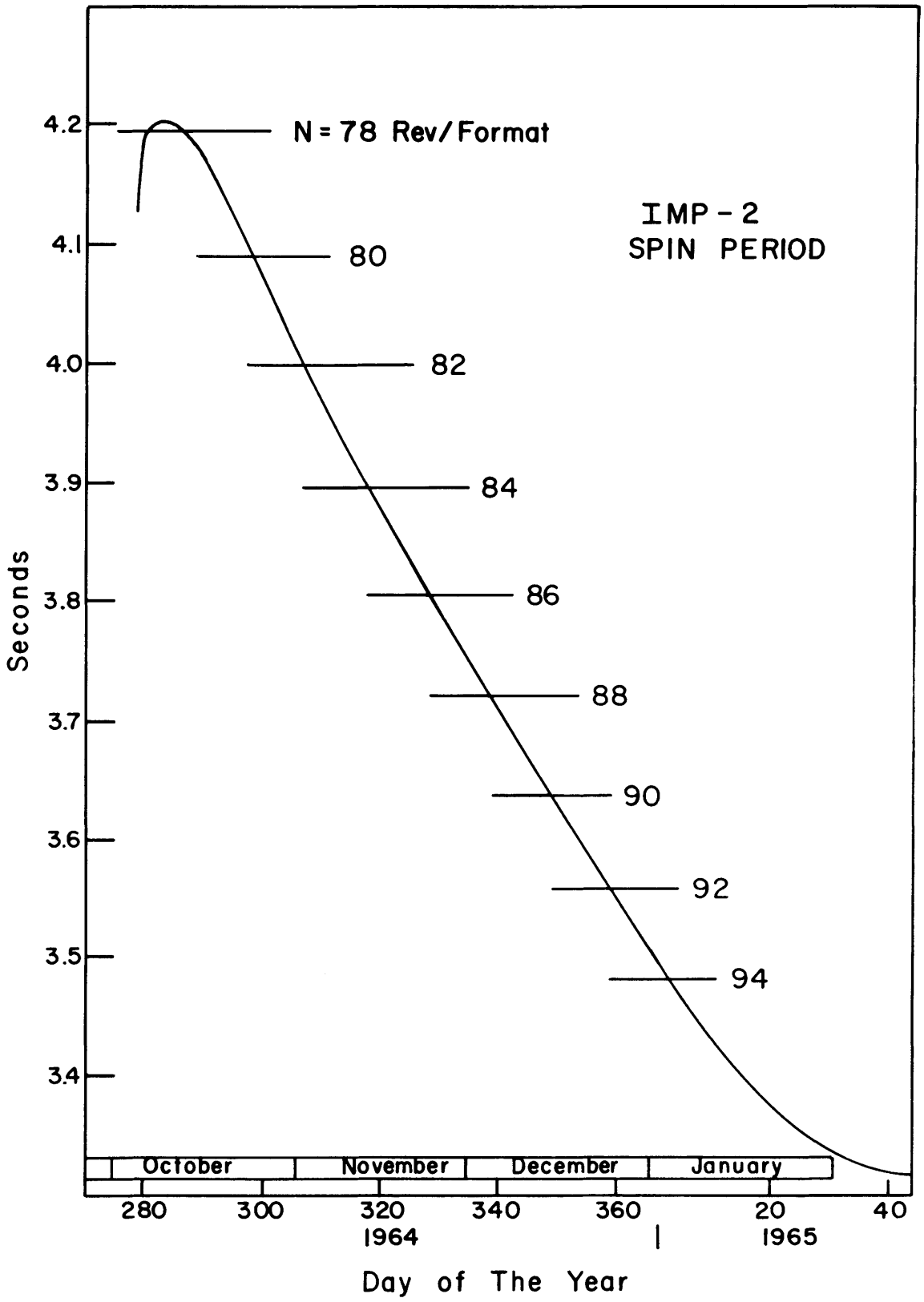
N = 78 Rev/Format
IMP - 2
SPIN PERIOD
80
82
84
86
88
90
92
94
4.2
4.1
4.0
3.9
3.8
3.7
3.6
3.5
3.4
Seconds
October
November
December
January
280
300
320
340
360
20
40
1964
1965
Day of The Year

Figure 3

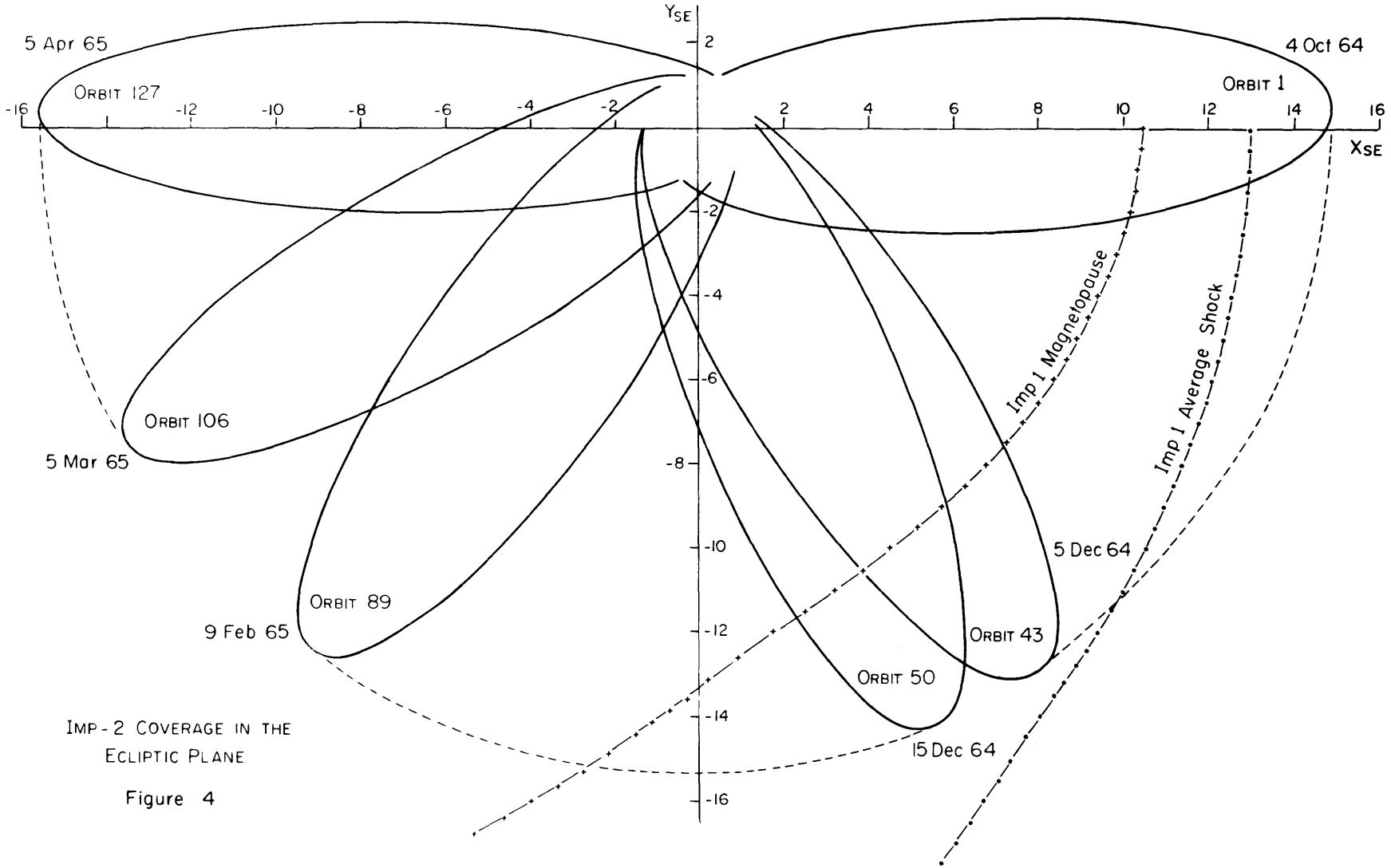

IMP-2 COVERAGE IN THE ECLIPTIC PLANE

Figure 4

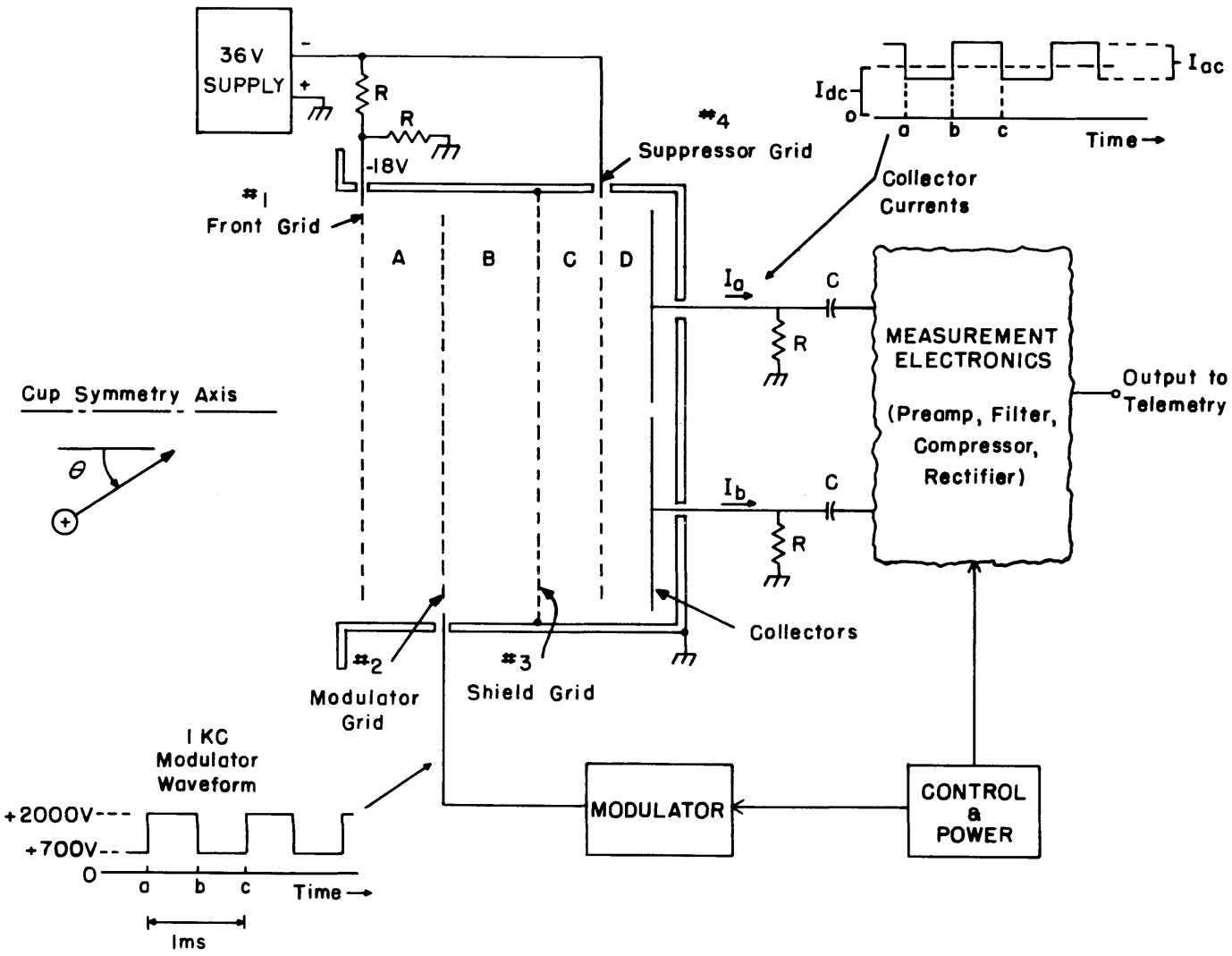

IMP CUP

Figure 5

IMP-2
M.I.T. TIMING AND DATA SEQUENCING

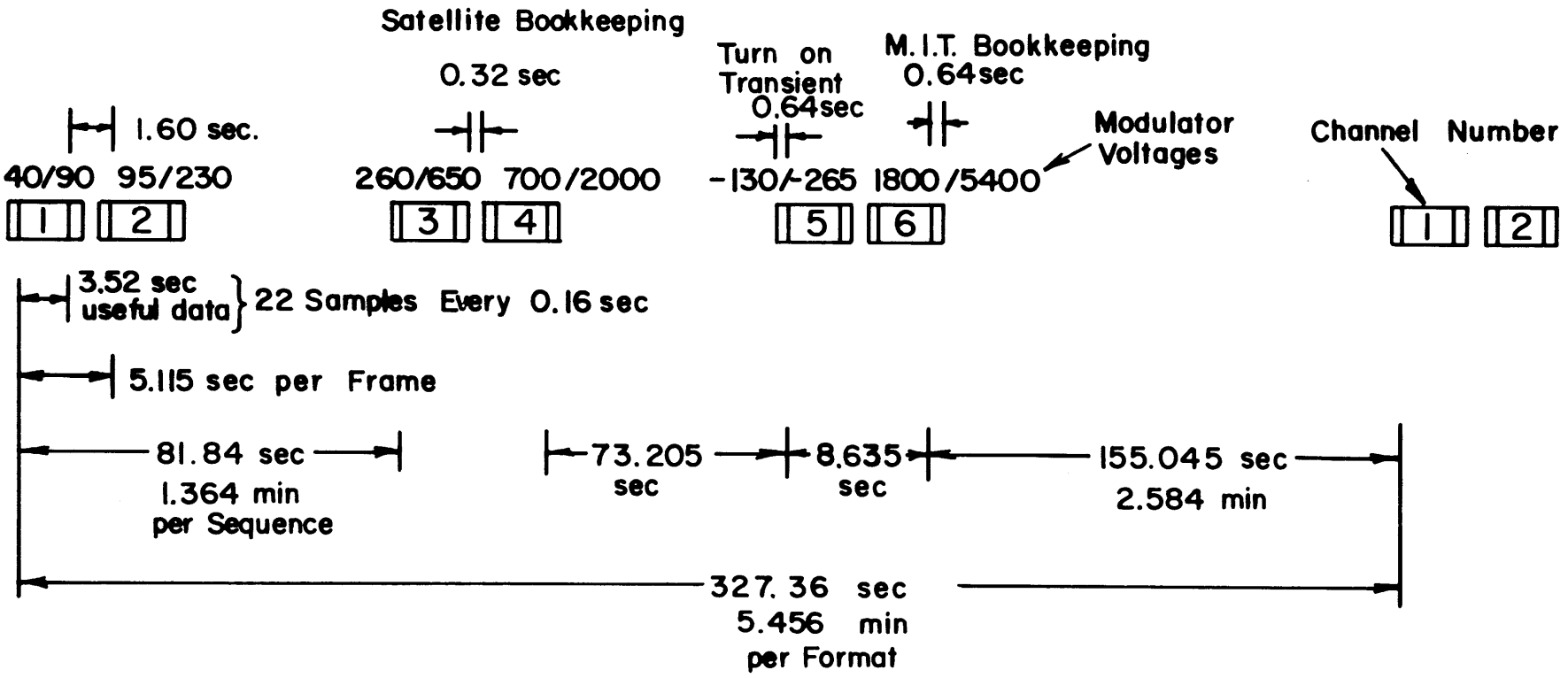

Figure 6

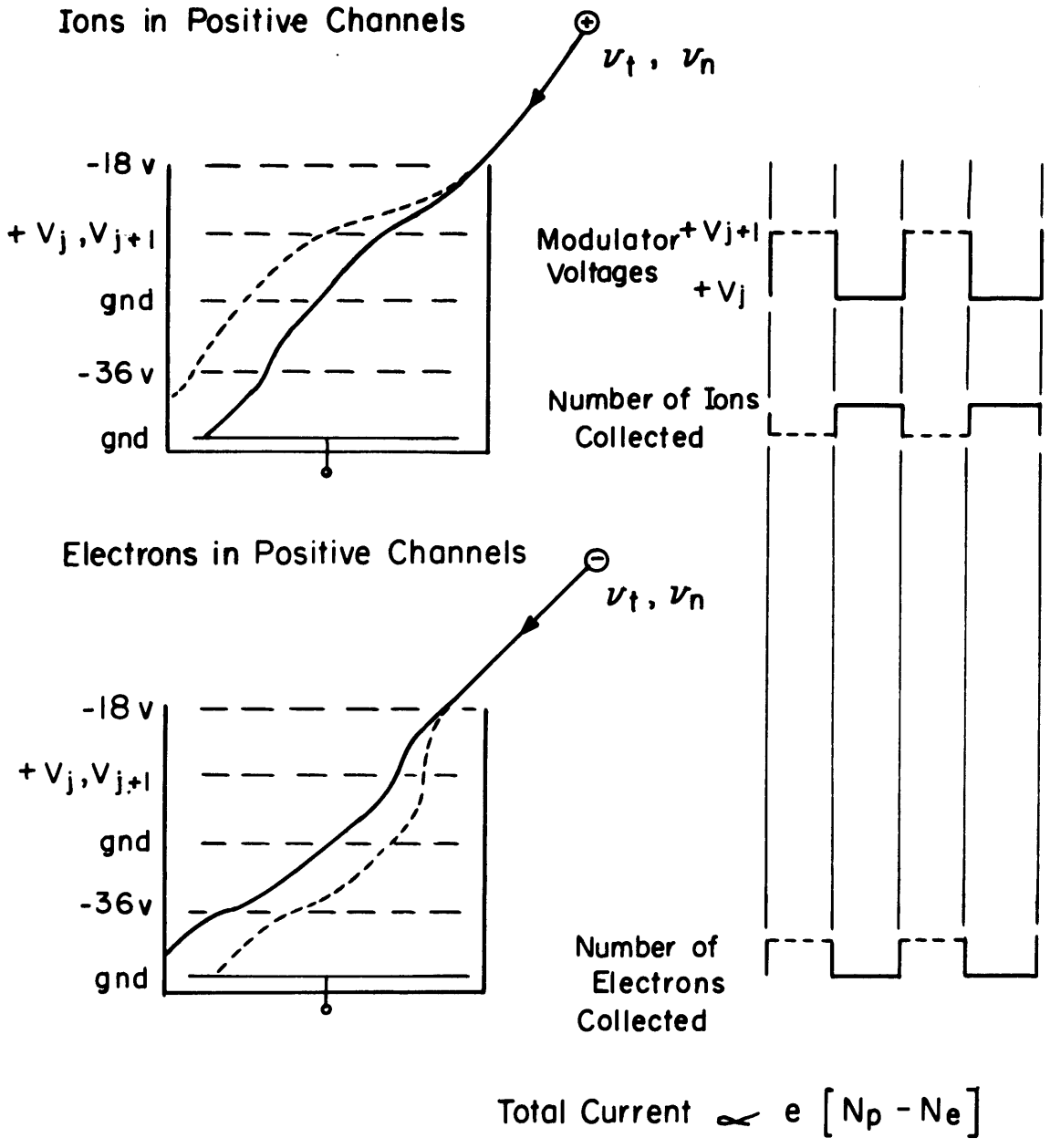

Fig. 7. REFRACTION OF CHARGED PARTICLES IN THE POSITIVE CHANNELS

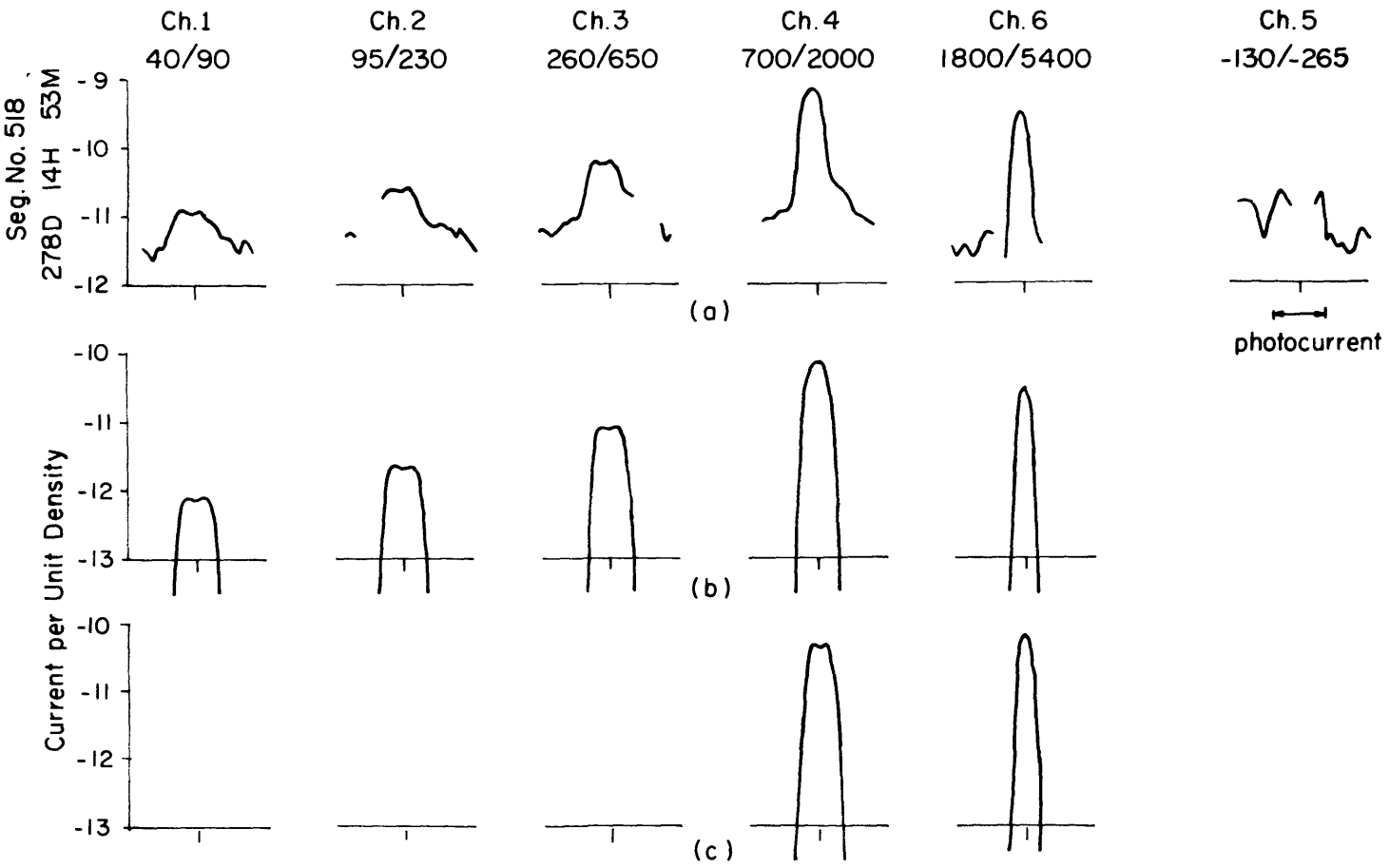

(a) Interplanetary Data , Orbit No. 1

(b) Refraction Model : $\alpha = 40°$, V = 800 Km/sec , ω_o = 50 Km/sec

(c) Same parameters but neglecting refraction

Figure 8

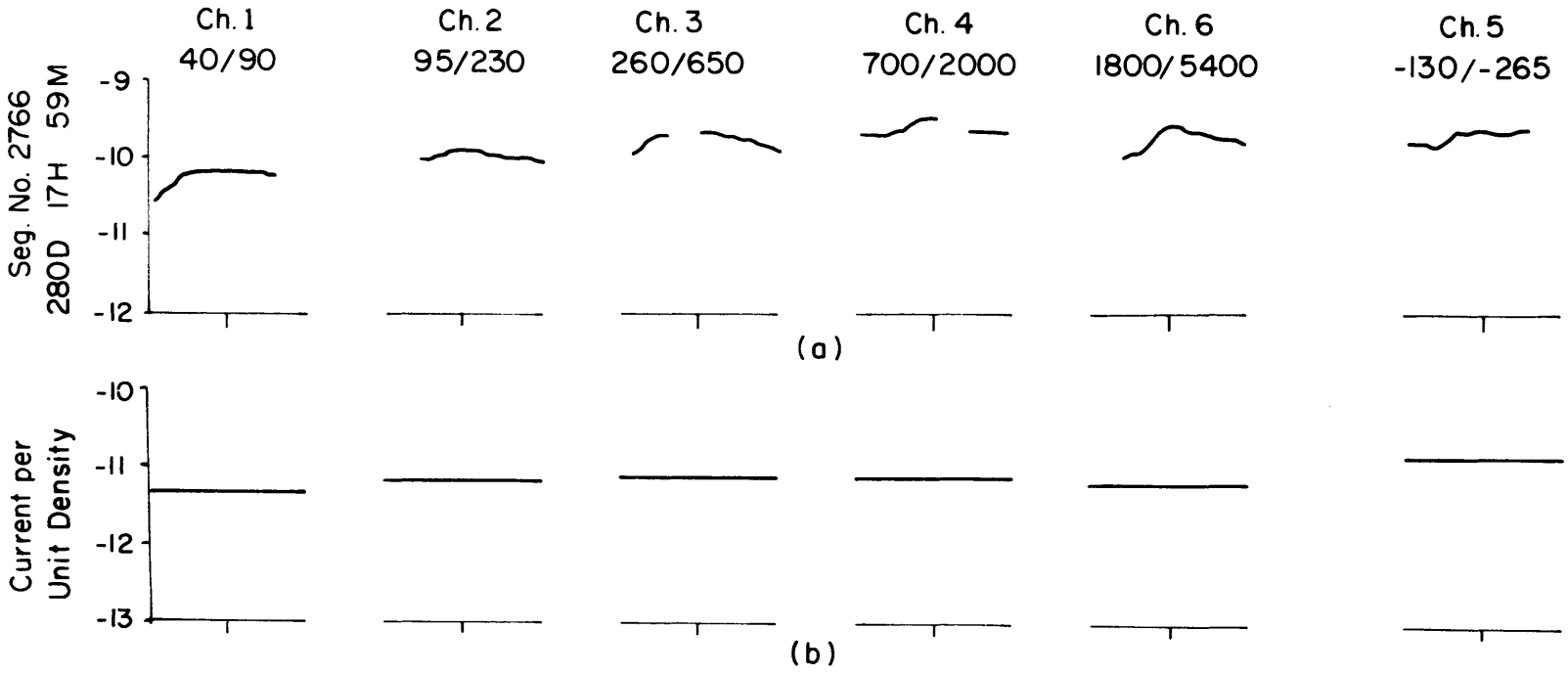

LOG INDIVIDUAL CHANNEL CURRENTS

(a) Transition Region Data, Orbit No. 2

(b) Refraction Model for Isotropic Electrons : $K = 4$, $\omega_o = 4000$ km/sec
$E_o = 40$ eV

Figure 9

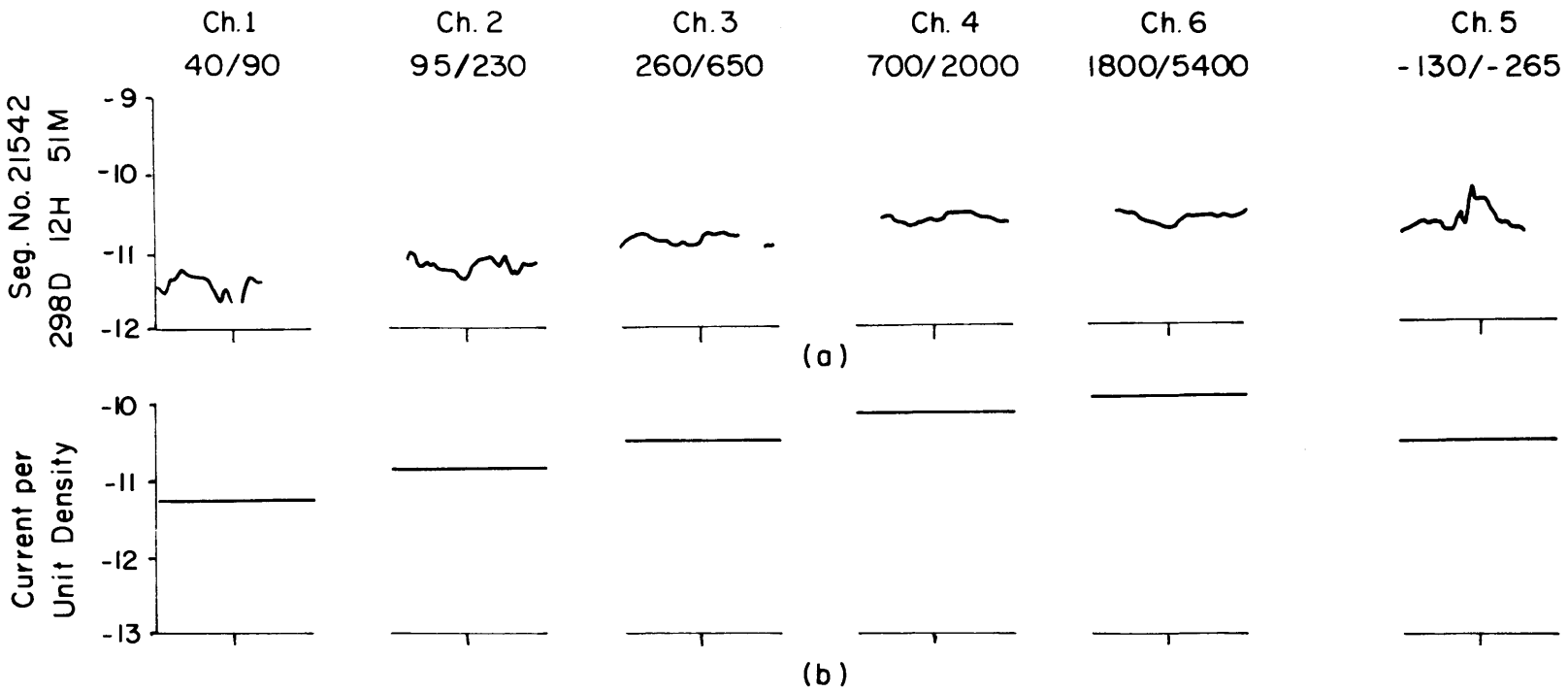

LOG INDIVIDUAL CHANNEL CURRENTS

(a) Magnetosphere Data , Orbit No. 15

(b) Refraction Model for Isotropic Electrons : $K = 5$, $\omega_o = 30{,}000$ km/sec
$E_o = 2.5$ keV

Figure 10

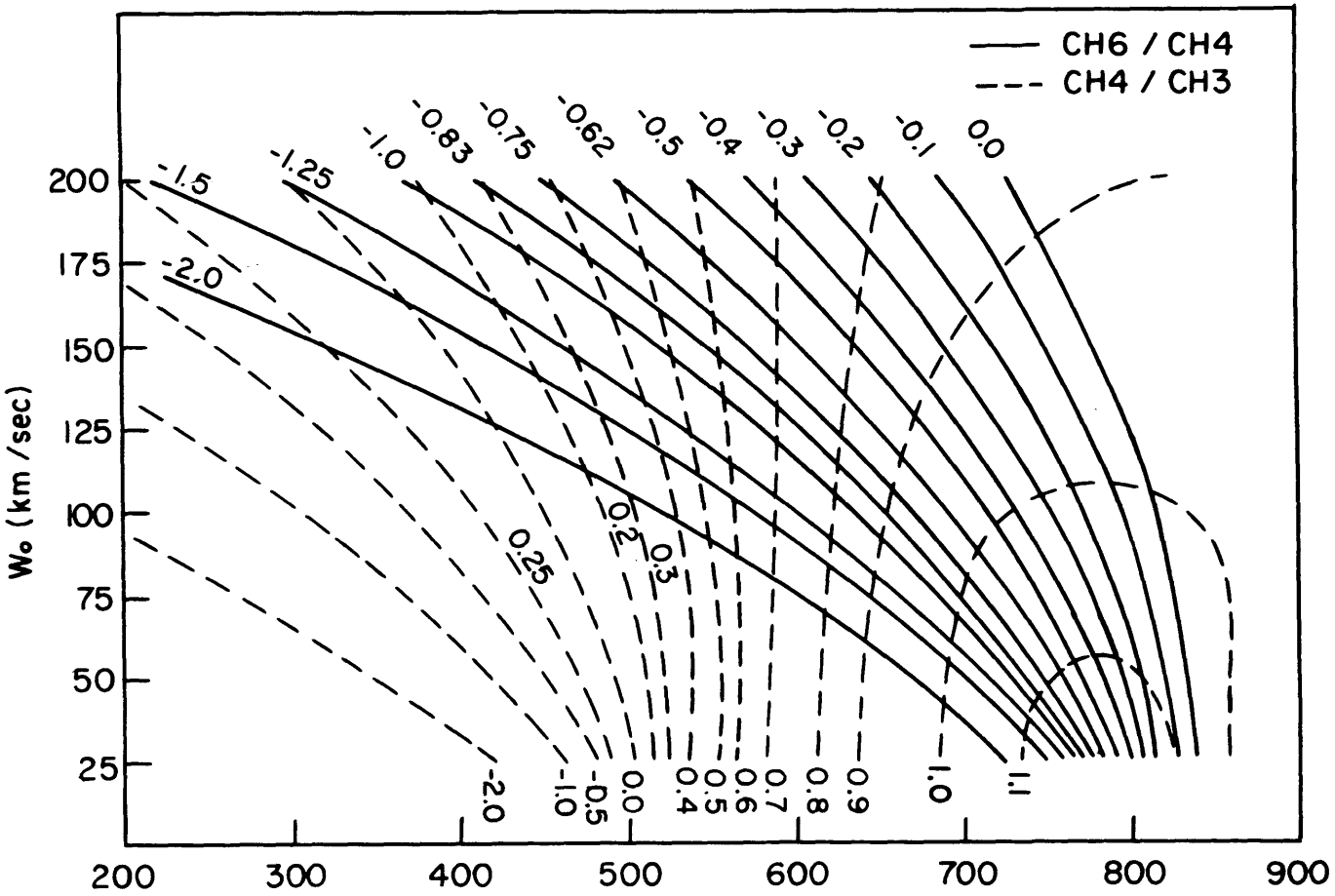

Log Peak Current Ratios
Maxwellian Protons in Positive Channels
$\alpha = 40°$

Figure 11

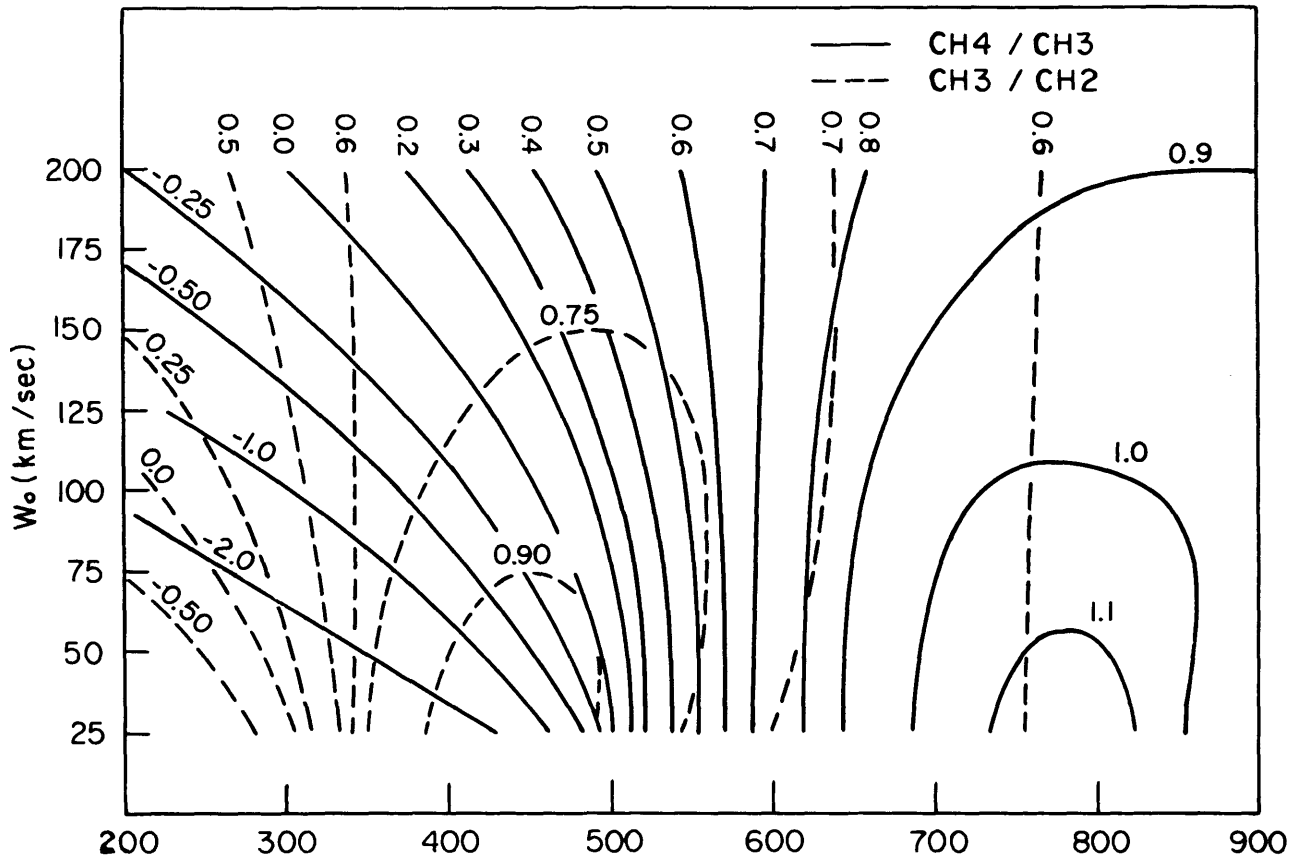

Log Peak Current Ratios
Maxwellian Protons in Positive Channels
$\alpha = 40°$

Figure 12

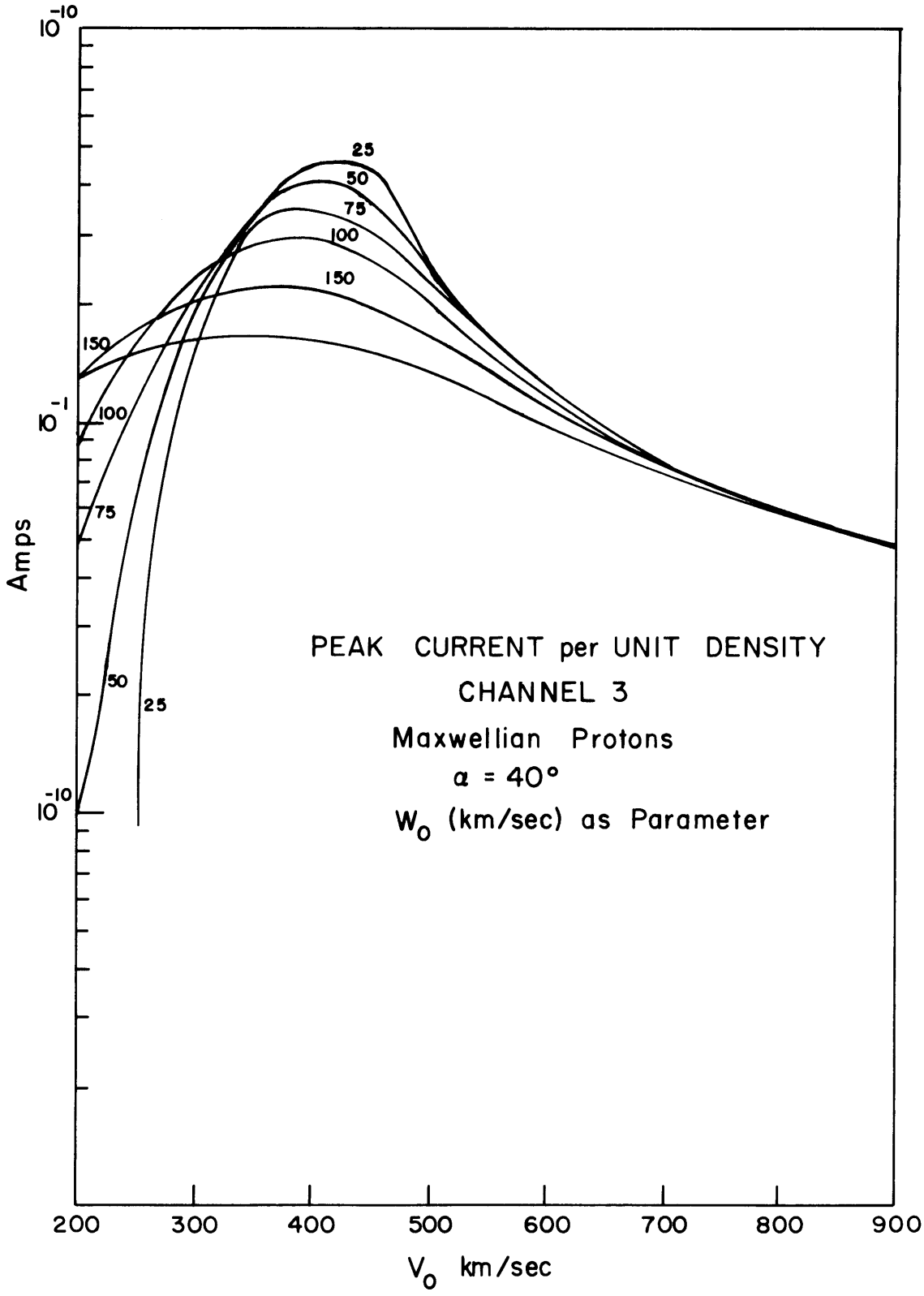
10^{-10}
10^{-1}
10^{-10}
Amps
25
50
75
100
150
150
100
75
50
25
PEAK CURRENT per UNIT DENSITY
CHANNEL 3
Maxwellian Protons
$\alpha = 40°$
W_0 (km/sec) as Parameter
200
300
400
500
600
700
800
900
V_0 km/sec

Figure 13

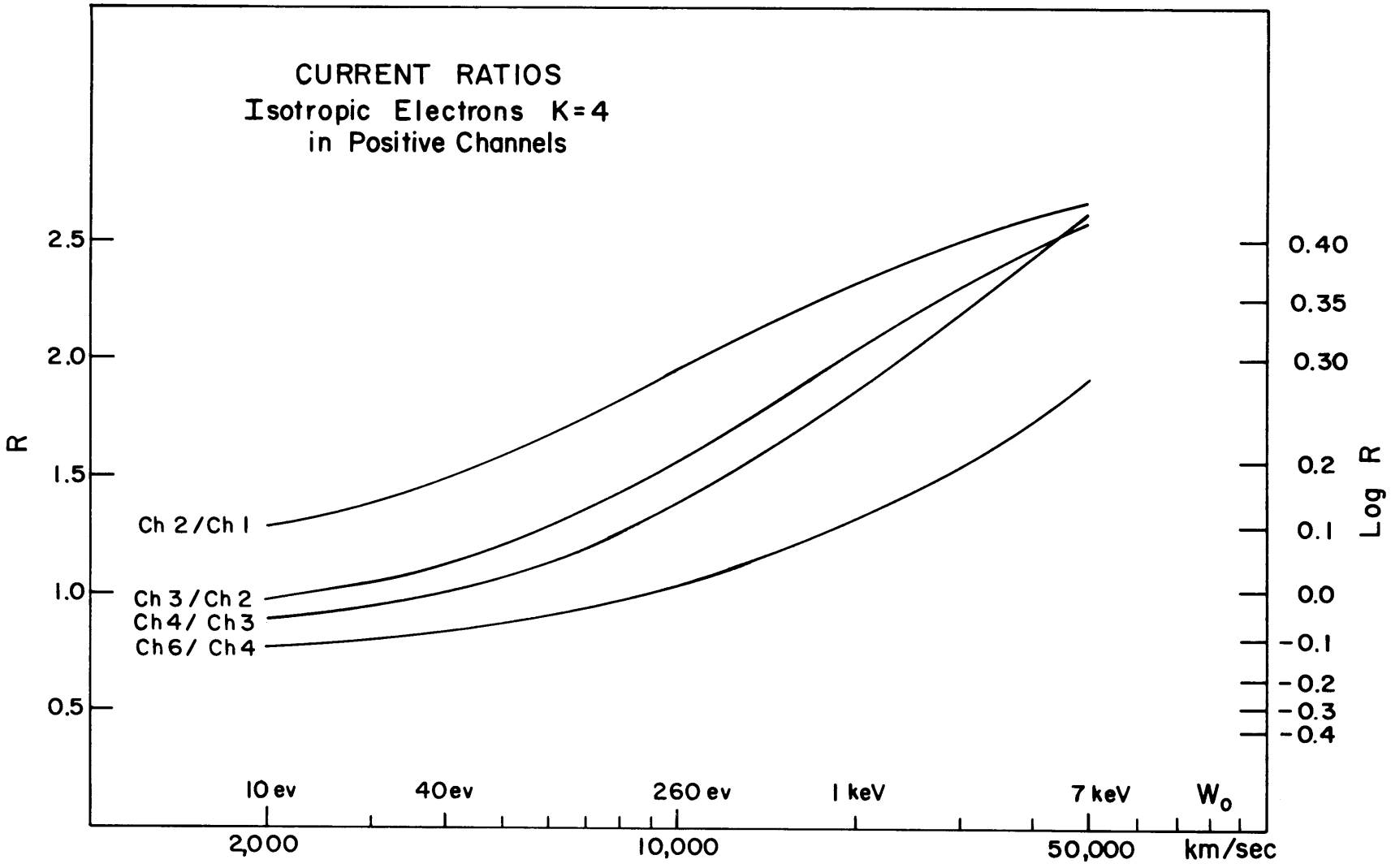
CURRENT RATIOS
Isotropic Electrons K=4
in Positive Channels
R
2.5
2.0
1.5
1.0
0.5
Ch 2/Ch 1
Ch 3/Ch 2
Ch4/ Ch3
Ch6/ Ch4
0.40
0.35
0.30
0.2
0.1
0.0
-0.1
-0.2
-0.3
-0.4
Log R
10 ev
40ev
260 ev
1 keV
7 keV
W_o
2,000
10,000
50,000
km/sec

Figure 14

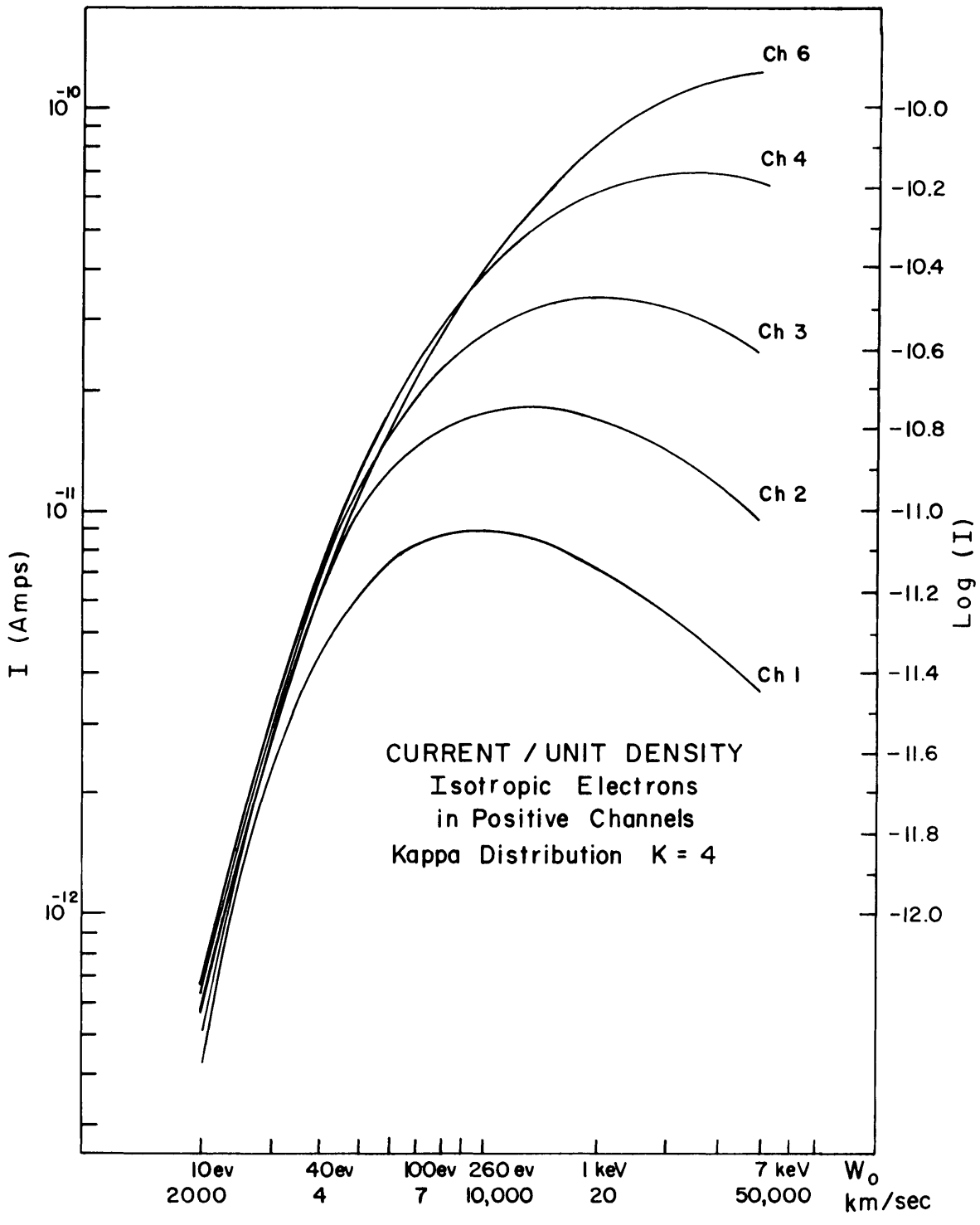
Ch 6
Ch 4
Ch 3
Ch 2
Ch 1
10^{-10}
10^{-11}
10^{-12}
I (Amps)
-10.0
-10.2
-10.4
-10.6
-10.8
-11.0
-11.2
-11.4
-11.6
-11.8
-12.0
Log (I)
CURRENT / UNIT DENSITY
Isotropic Electrons
in Positive Channels
Kappa Distribution K = 4
10ev
2000
40ev
4
100ev
7
260 ev
10,000
1 keV
20
7 keV
50,000
W_o
km/sec

Figure 15

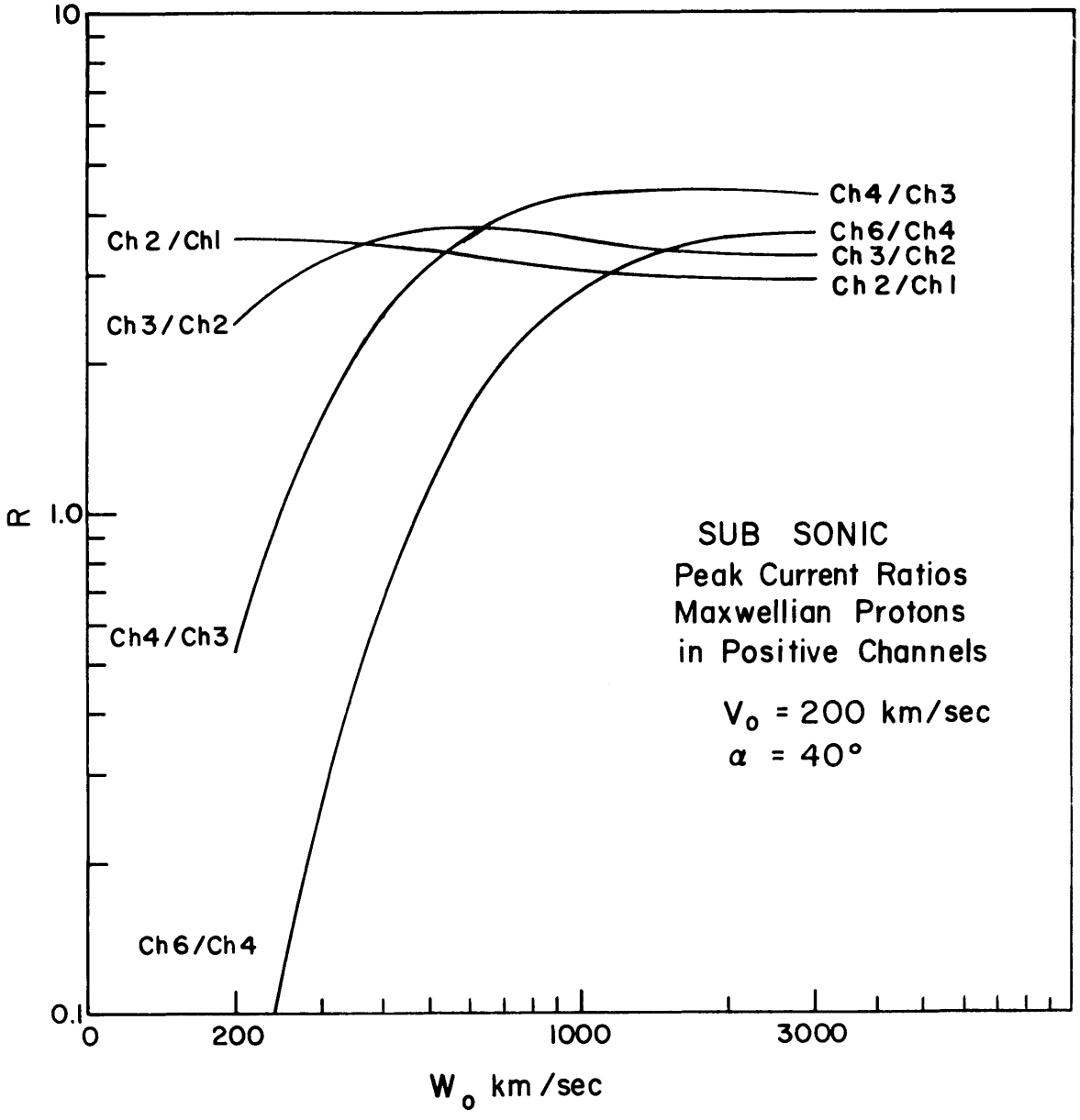
10
1.0
0.1
R
Ch4/Ch3
Ch6/Ch4
Ch3/Ch2
Ch2/Ch1
Ch2/Ch1
Ch3/Ch2
Ch4/Ch3
Ch6/Ch4
SUB SONIC
Peak Current Ratios
Maxwellian Protons
in Positive Channels
V_0 = 200 km/sec
α = 40°
0
200
1000
3000
W_0 km/sec

Figure 16

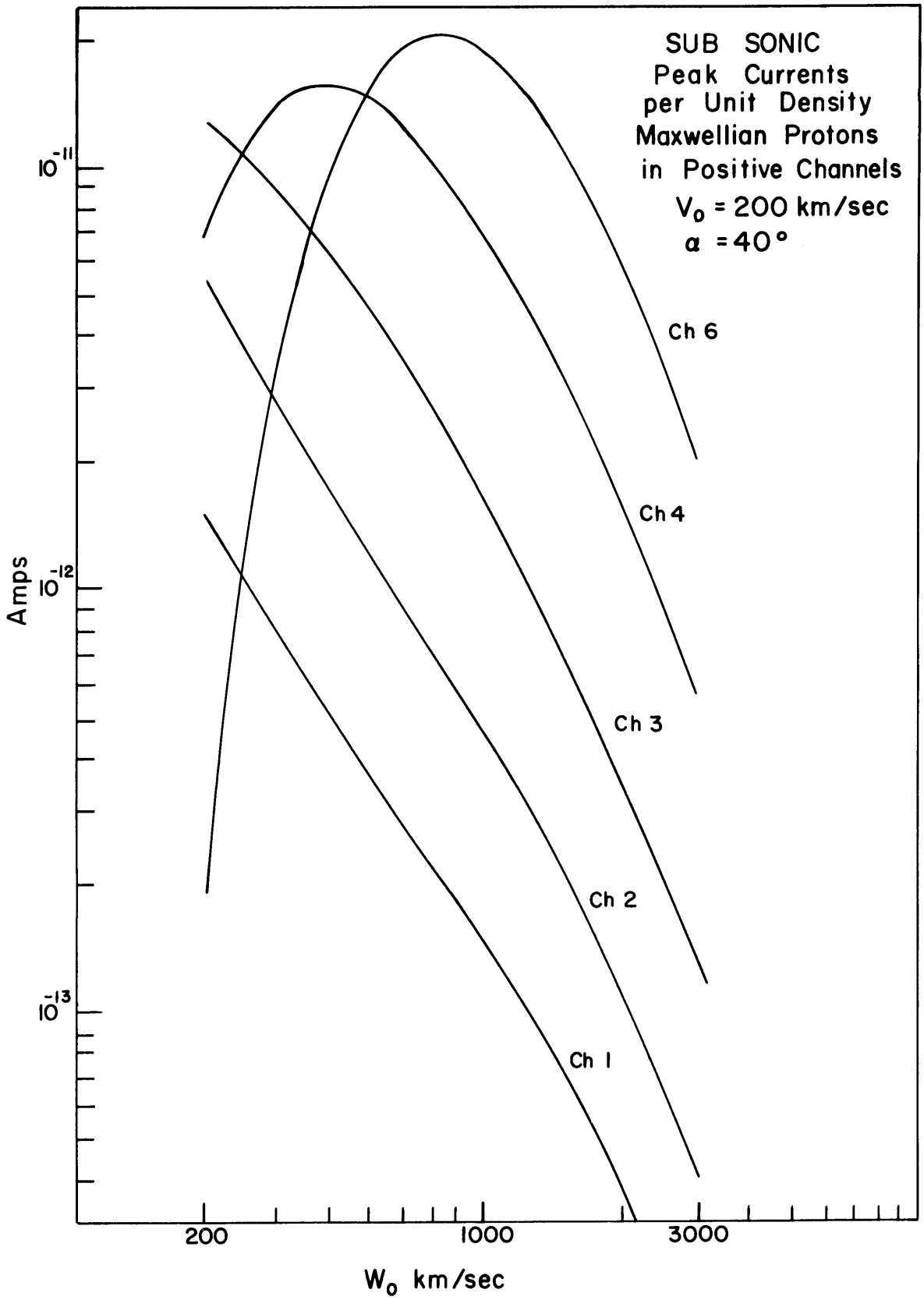
SUB SONIC
Peak Currents
per Unit Density
Maxwellian Protons
in Positive Channels
V_0 = 200 km/sec
α = 40°
Ch 6
Ch 4
Ch 3
Ch 2
Ch 1
Amps
10^{-11}
10^{-12}
10^{-13}
200
1000
3000
W_0 km/sec

Figure 17

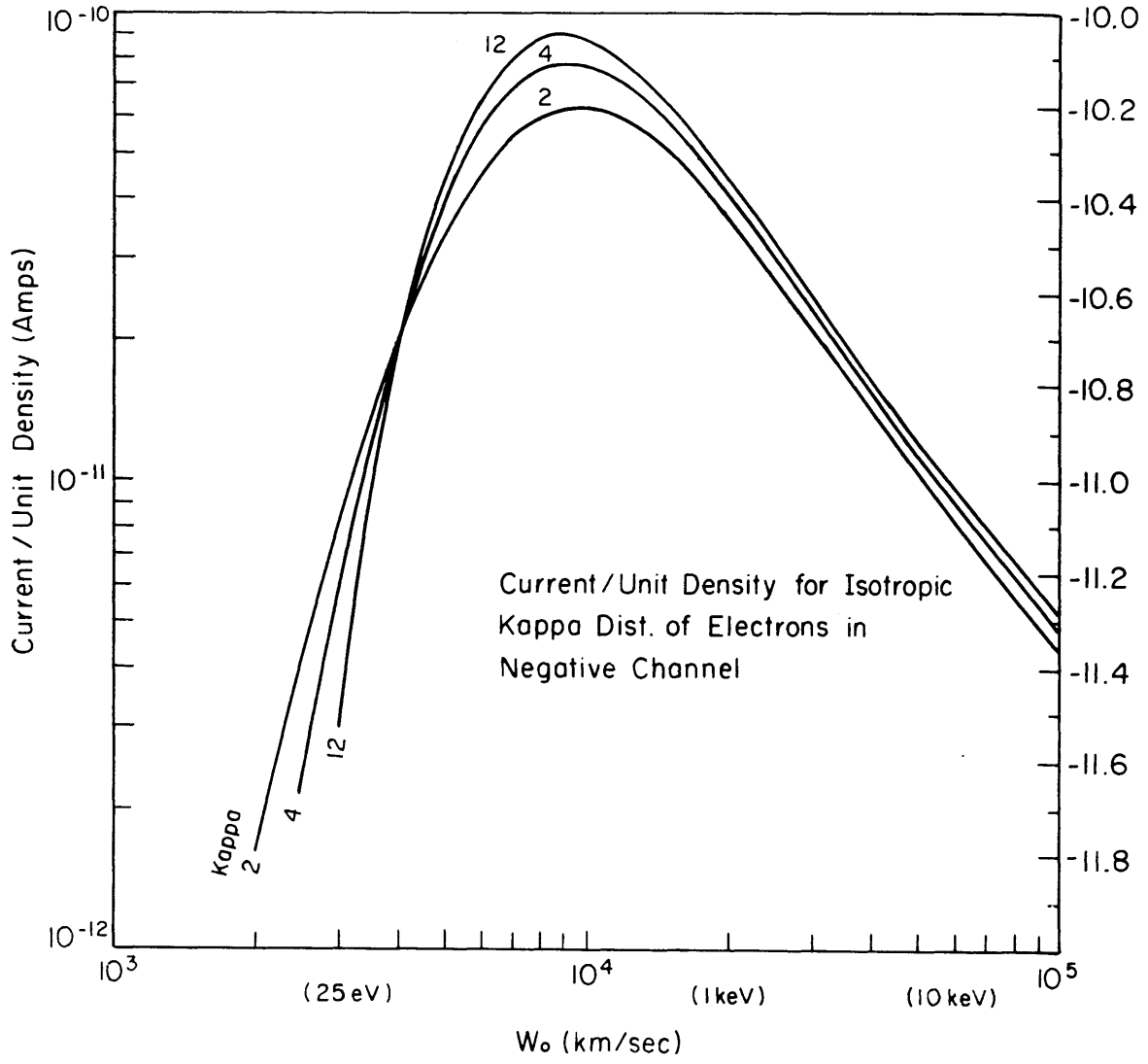
Current / Unit Density (Amps)
10^-10
10^-11
10^-12
-10.0
-10.2
-10.4
-10.6
-10.8
-11.0
-11.2
-11.4
-11.6
-11.8
12
4
2
Kappa
2
4
12
Current / Unit Density for Isotropic
Kappa Dist. of Electrons in
Negative Channel
10^3
(25 eV)
10^4
(1 keV)
(10 keV)
10^5
Wo (km/sec)

Figure 18

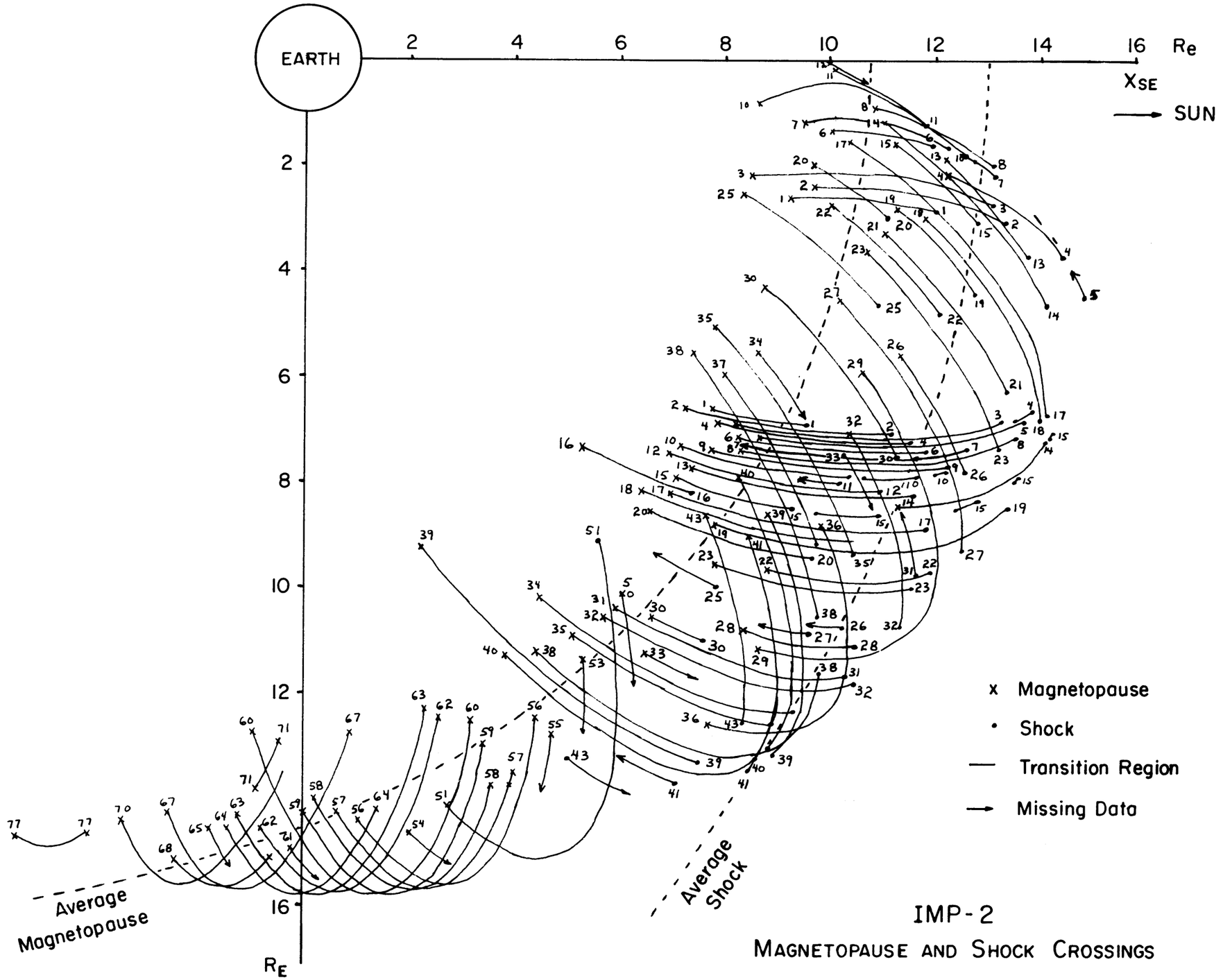

IMP-2

MAGNETOPAUSE AND SHOCK CROSSINGS

Figure 19

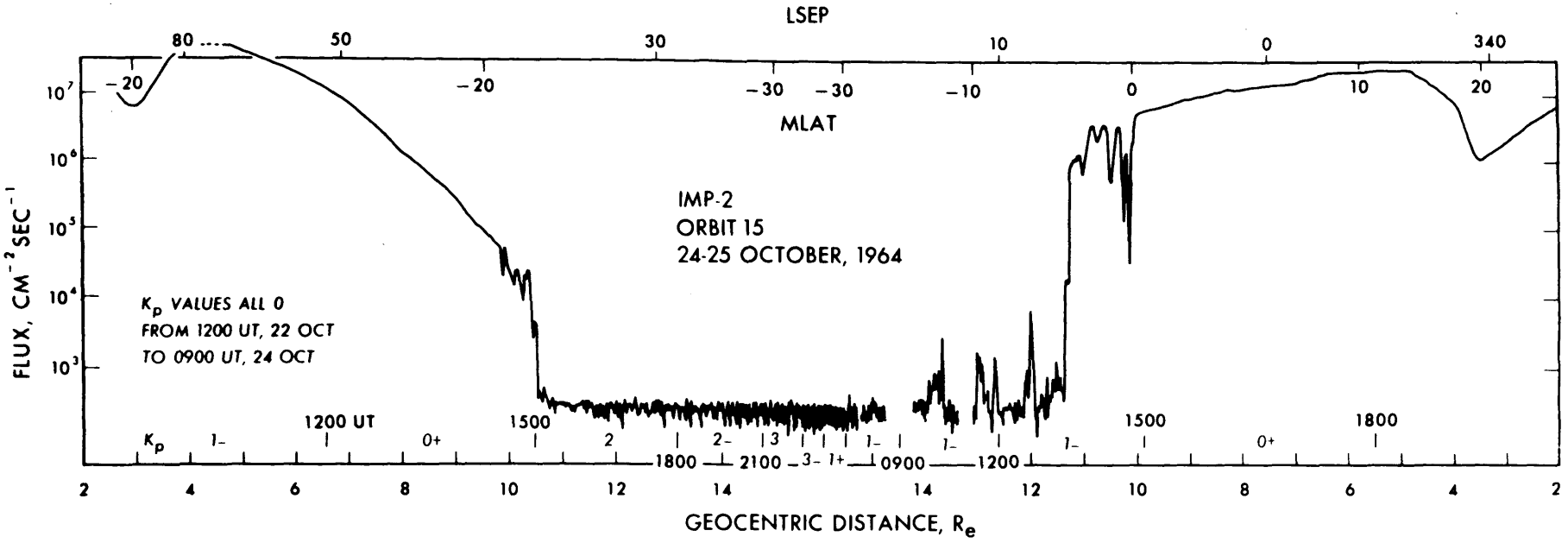
LSEP
80
50
30
10
0
340
-20
-20
-30
-30
-10
0
10
20
MLAT
10^7
10^6
10^5
10^4
10^3
FLUX, $CM^{-2}SEC^{-1}$
IMP-2
ORBIT 15
24-25 OCTOBER, 1964
K_p VALUES ALL 0
FROM 1200 UT, 22 OCT
TO 0900 UT, 24 OCT
1200 UT
1500
1500
1800
K_p
1-
0+
2
2-
3
1-
1-
1-
0+
1800
2100
3-
1+
0900
1200
2
4
6
8
10
12
14
14
12
10
8
6
4
2
GEOCENTRIC DISTANCE, R_e

FIGURE 20

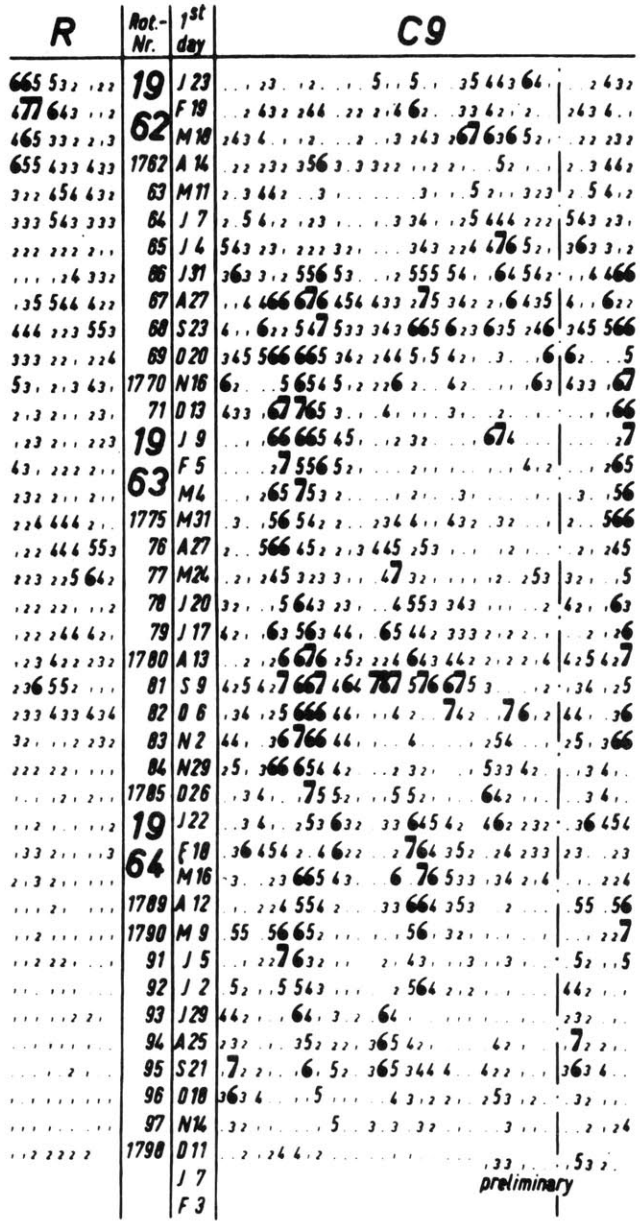

Symbol	.	,	2	3	4	5	6	7	8	9
R =	0	1 15	16 30	31 45	46 60	61 80	81 100	101 130	131 170	171
C9 =	0	1	2	3	4	5	6	7	8	9
Cp =	0.0 0.1	0.2 0.3	0.4 0.5	0.6 0.7	0.8 0.9	1.0 1.1	1.2 1.4	1.5 1.8	1.9	2.0 2.5
Ap =	0 4	5 7	8 10	11 13	14 17	18 24	25 40	41 91	92 140	141 400

DAILY GEOMAGNETIC CHARACTER FIGURES C9 AND SUNSPOT NUMBERS R

For explanation and previous years see J. Bartels:
„Abhandlungen der Akademie der Wissenschaften, Göttingen, Beiträge zum I.G.J., Heft 3 (1958)"
(may be requested from Geophysikalisches Institut, Herzberger Landstrasse 180, 34 Göttingen (Germany)

COMMERCE - STANDARDS - BOULDER

FIGURE 21

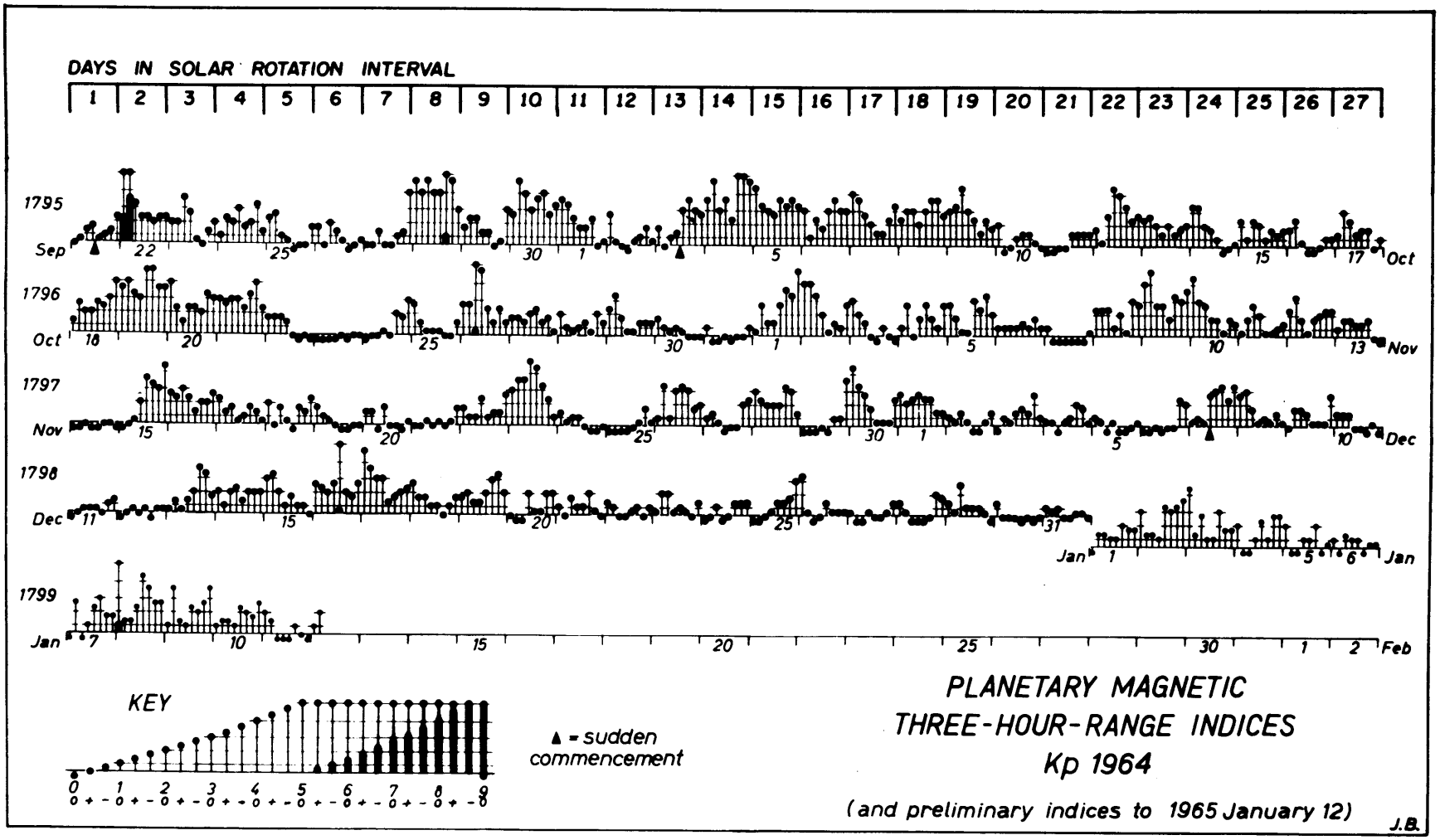
DAYS IN SOLAR ROTATION INTERVAL
1 2 3 4 5 6 7 8 9 10 11 12 13 14 15 16 17 18 19 20 21 22 23 24 25 26 27
1795
Sep 22 25 30 1 5 10 15 17 Oct
1796
Oct 18 20 25 30 1 5 10 13 Nov
1797
Nov 15 20 25 30 1 5 10 Dec
1798
Dec 11 15 20 25 31 Jan 1 5 6 Jan
1799
Jan 7 10 15 20 25 30 1 2 Feb
KEY
0 1 2 3 4 5 6 7 8 9
▲ = sudden commencement
PLANETARY MAGNETIC
THREE-HOUR-RANGE INDICES
Kp 1964
(and preliminary indices to 1965 January 12)
J.B.
COMMERCE - STANDARDS - BOULDER

FIGURE 22

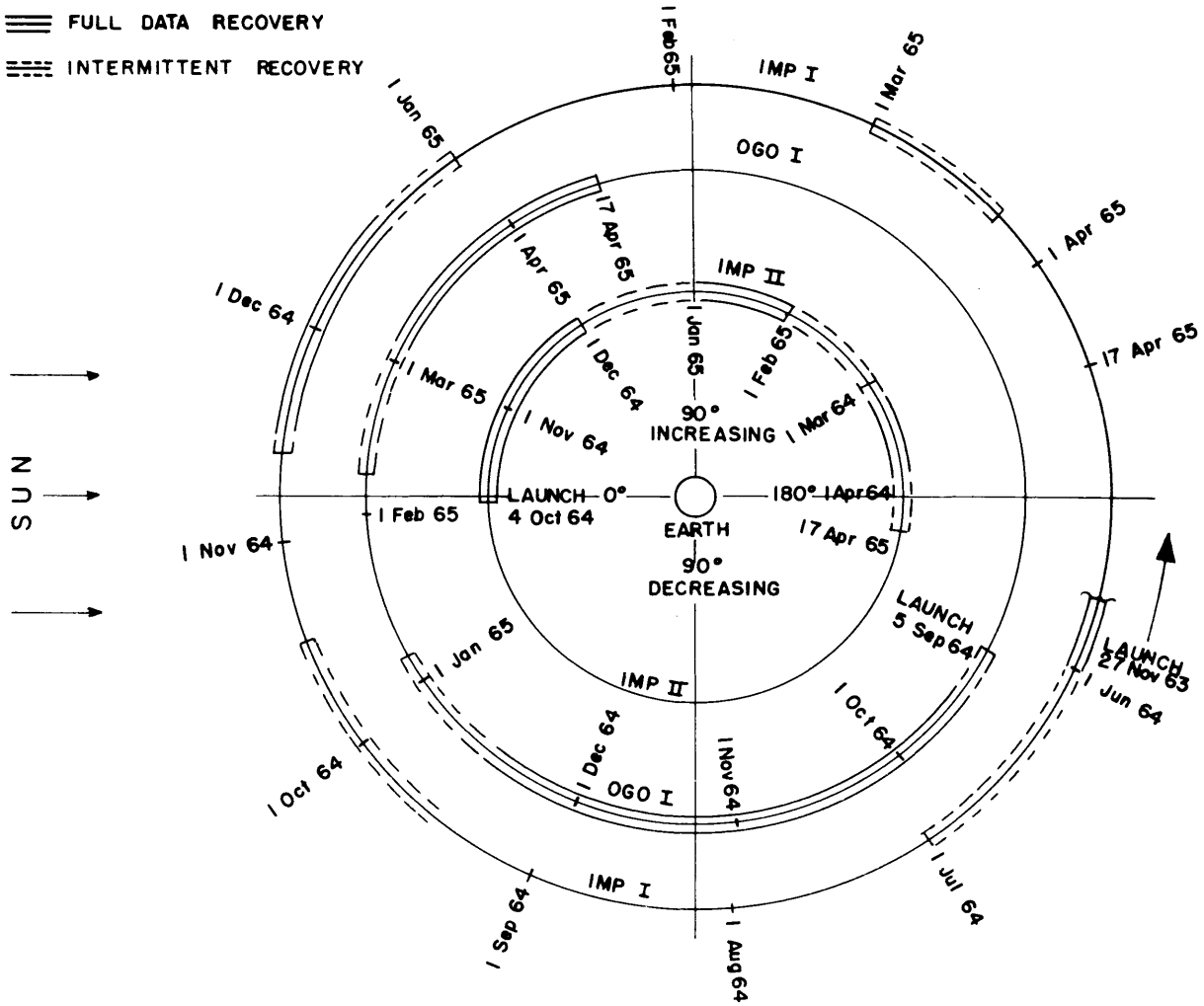

PROJECTION OF APOGEE POSITIONS ON ECLIPTIC PLANE

Figure 23

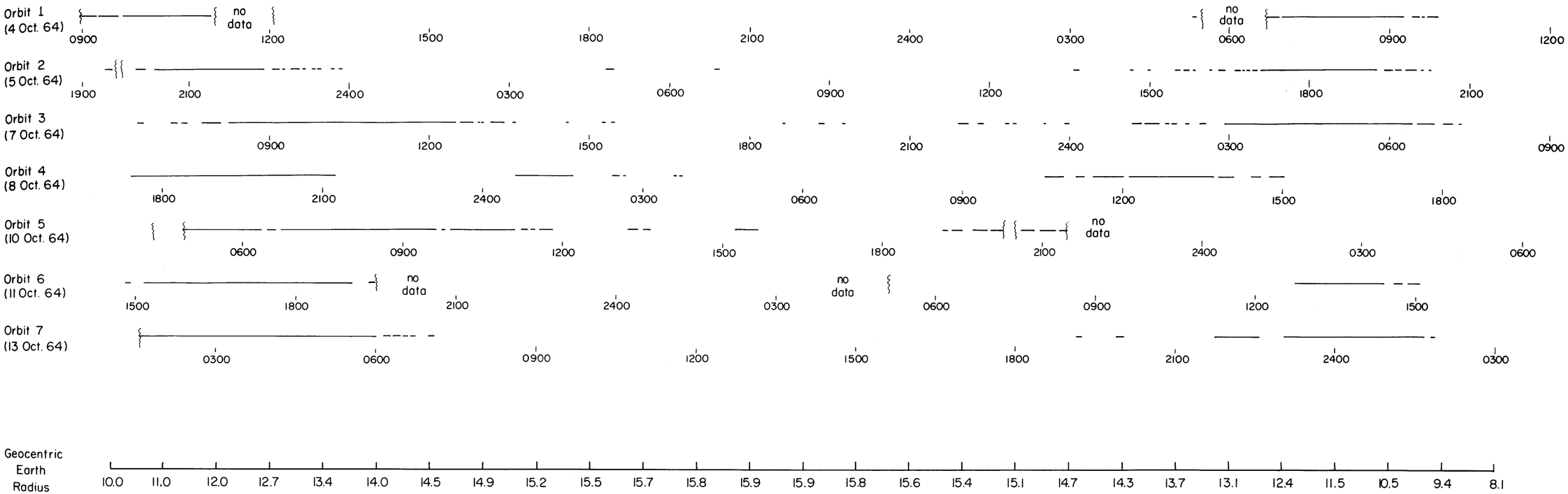

DETAILED SPACE-TIME POSITIONS OF TRANSITION-LIKE PLASMA FOR IMP-2 ORBITS 1-7

Figure 24

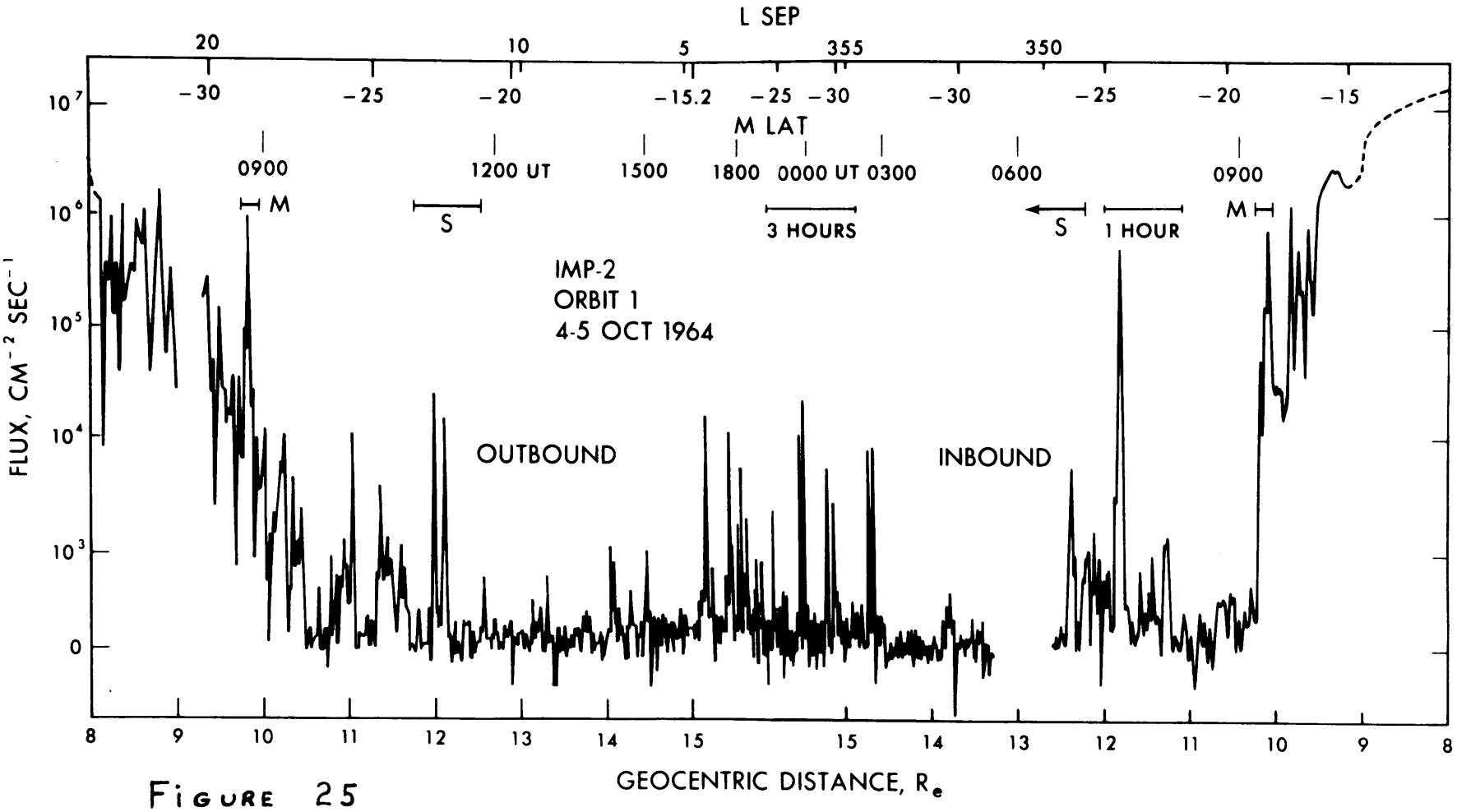
L SEP
20
10
5
355
350
-30
-25
-20
-15.2
-25
-30
-30
-25
-20
-15
M LAT
0900
1200 UT
1500
1800
0000 UT
0300
0600
0900
M
S
3 HOURS
S
1 HOUR
M
IMP-2
ORBIT 1
4-5 OCT 1964
OUTBOUND
INBOUND
FLUX, CM^{-2} SEC^{-1}
10^7
10^6
10^5
10^4
10^3
0
8
9
10
11
12
13
14
15
15
14
13
12
11
10
9
8
GEOCENTRIC DISTANCE, R_e

FIGURE 25

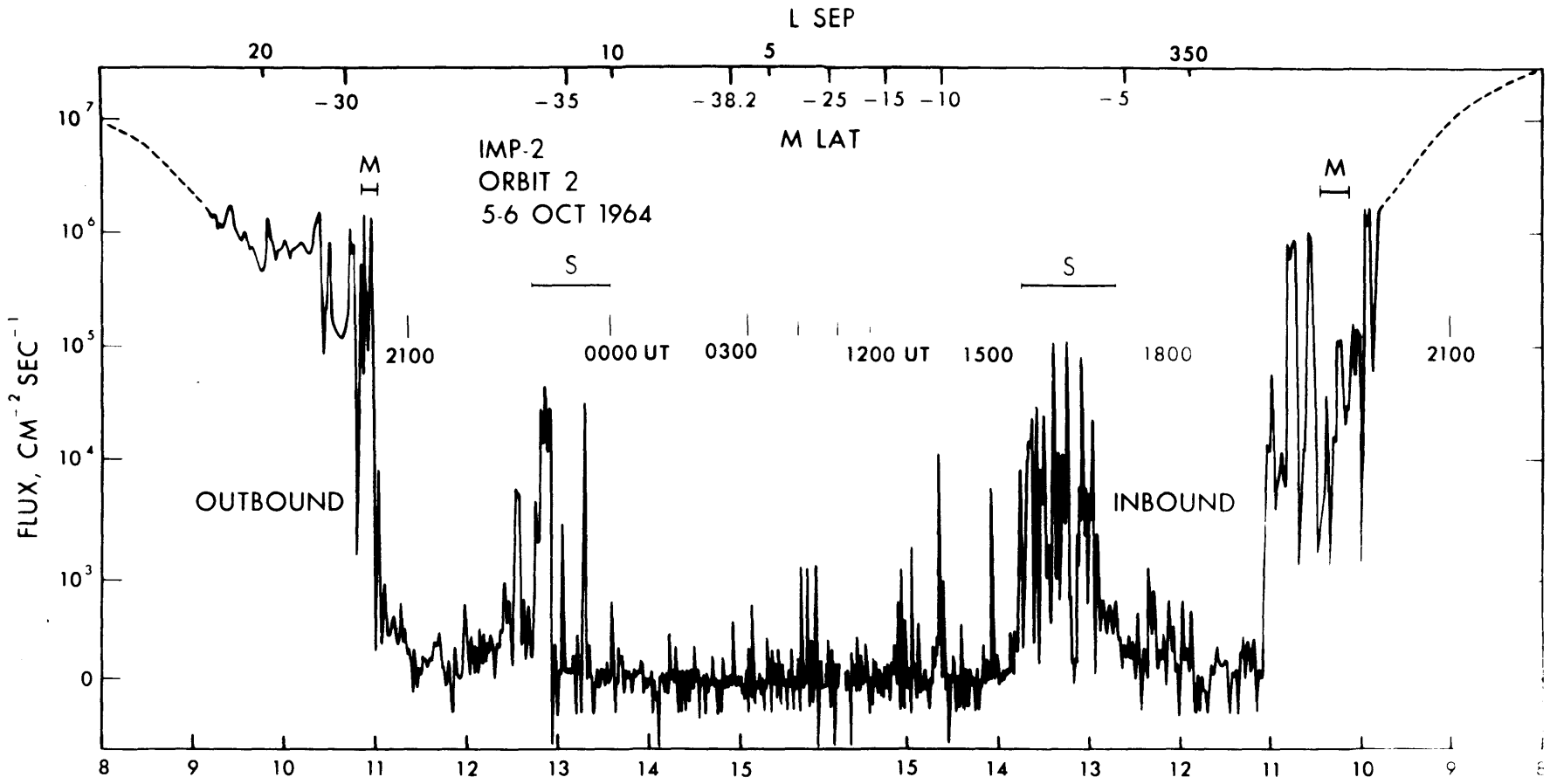
L SEP
20
10
5
350
-30
-35
-38.2
-25
-15
-10
-5
M LAT
IMP-2
ORBIT 2
5-6 OCT 1964
M
M
S
S
2100
0000 UT
0300
1200 UT
1500
1800
2100
OUTBOUND
INBOUND
FLUX, CM⁻² SEC⁻¹
10⁷
10⁶
10⁵
10⁴
10³
0
8
9
10
11
12
13
14
15
15
14
13
12
11
10
9
GEOCENTRIC DISTANCE, Re

FIGURE 26

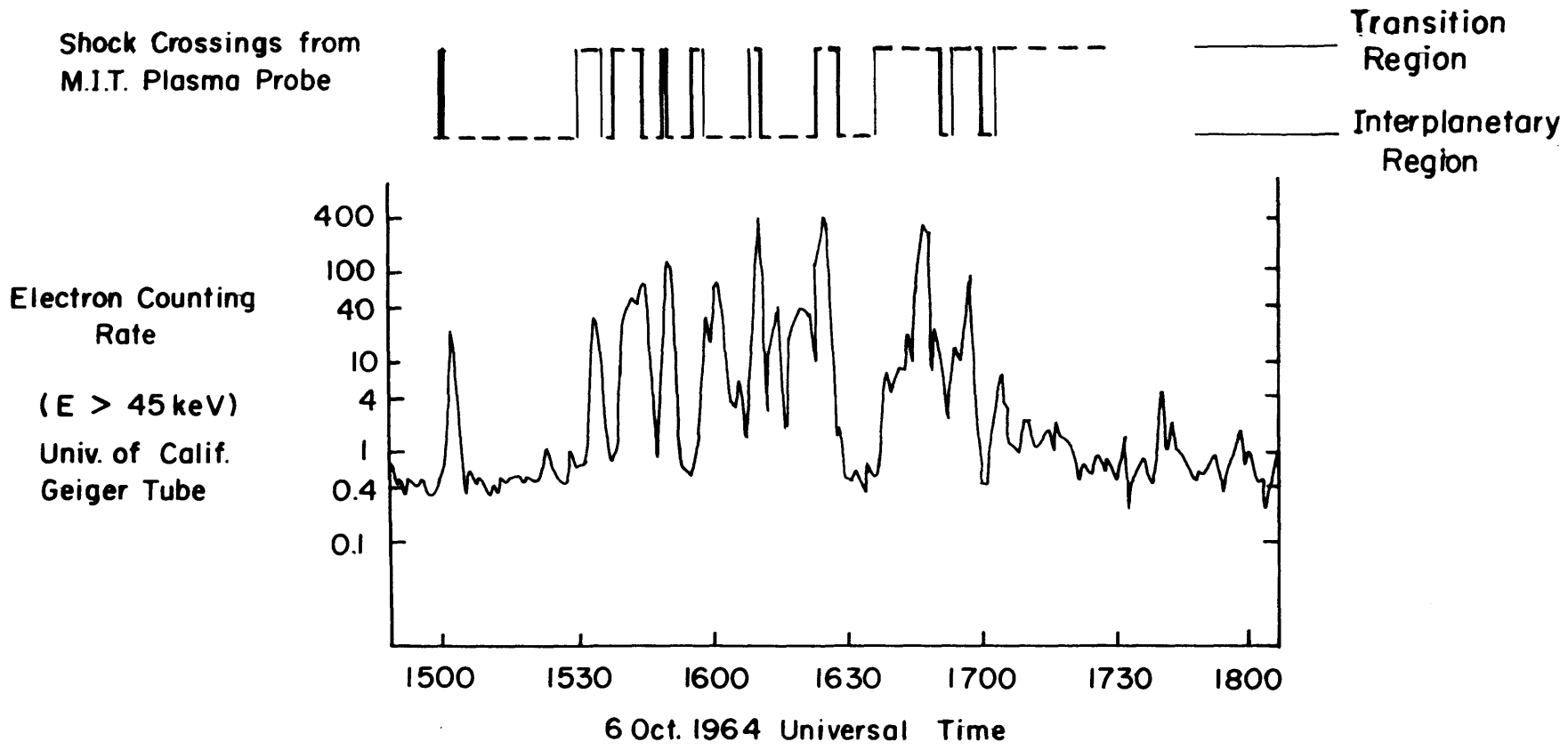

IMP - 2 ORBIT 2 INBOUND

Figure 27

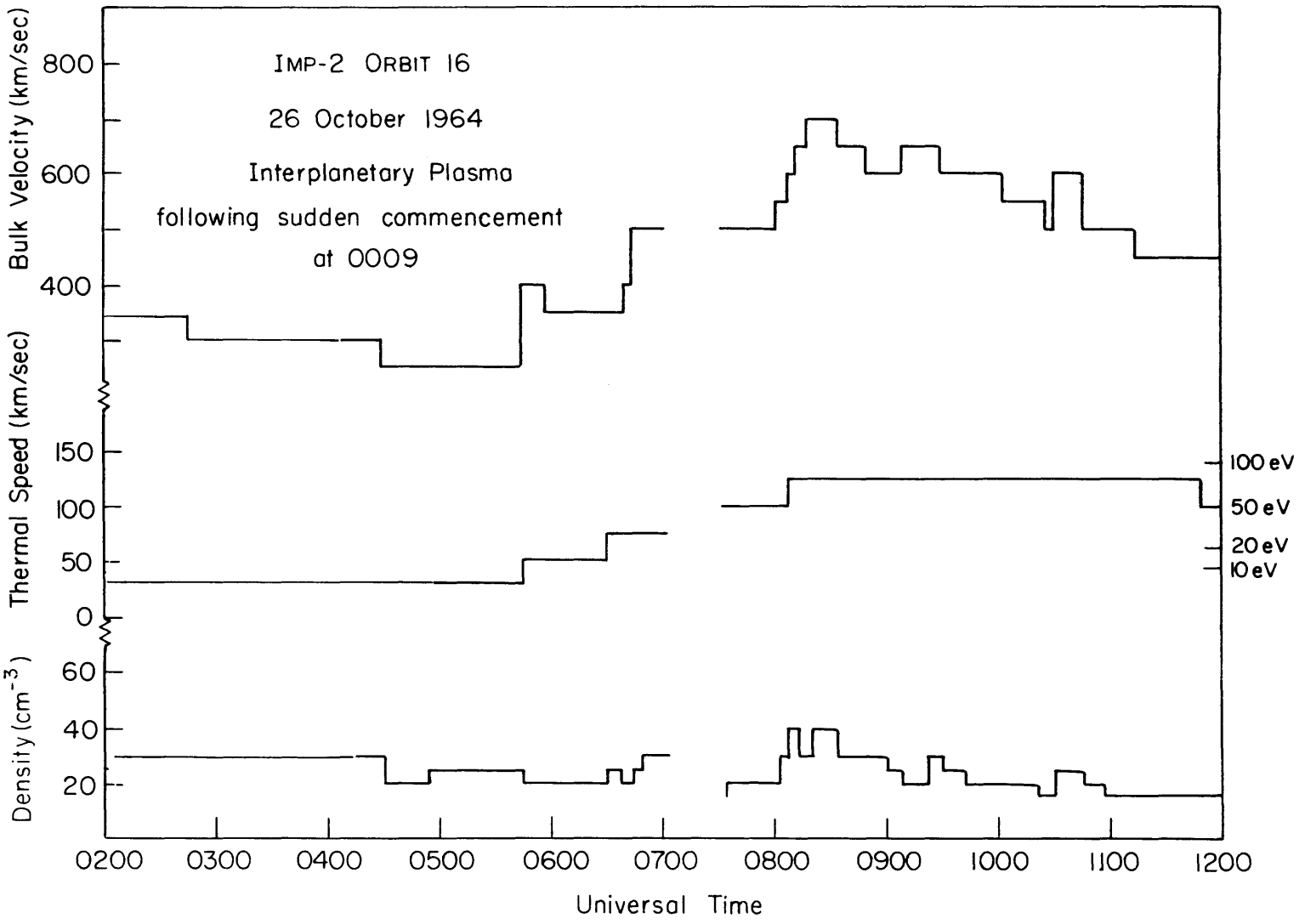
IMP-2 ORBIT 16
26 October 1964
Interplanetary Plasma
following sudden commencement
at 0009
Bulk Velocity (km/sec)
800
600
400
Thermal Speed (km/sec)
150
100
50
0
100 eV
50 eV
20 eV
10 eV
Density (cm⁻³)
60
40
20
0200
0300
0400
0500
0600
0700
0800
0900
1000
1100
1200
Universal Time

Figure 28

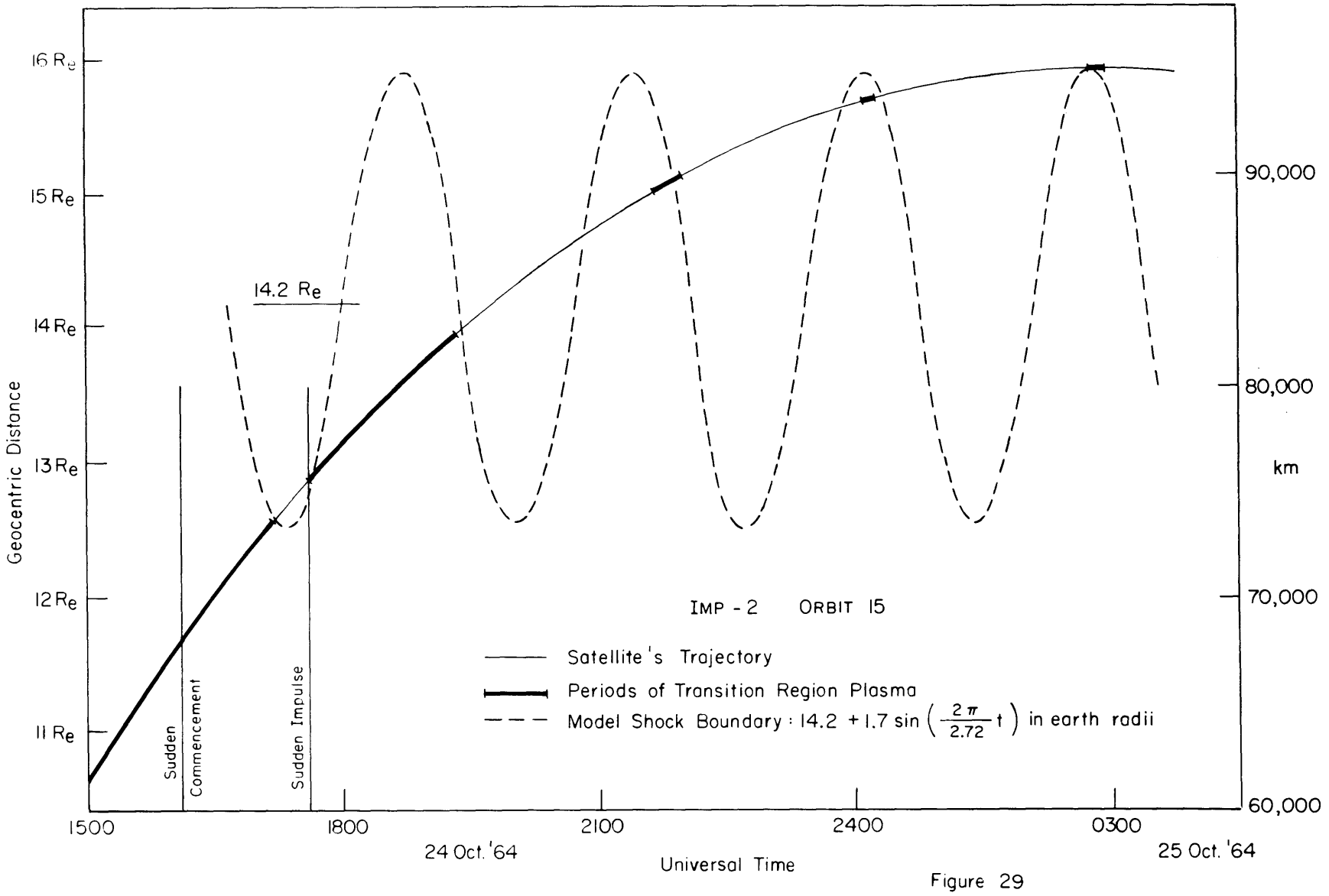
16 Re
15 Re
14 Re
13 Re
12 Re
11 Re
Geocentric Distance
90,000
80,000
km
70,000
60,000
14.2 Re
Sudden Commencement
Sudden Impulse
IMP - 2 ORBIT 15
Satellite's Trajectory
Periods of Transition Region Plasma
Model Shock Boundary : 14.2 + 1.7 sin (2π/2.72 t) in earth radii
1500
1800
2100
2400
0300
24 Oct. '64
25 Oct. '64
Universal Time

Figure 29

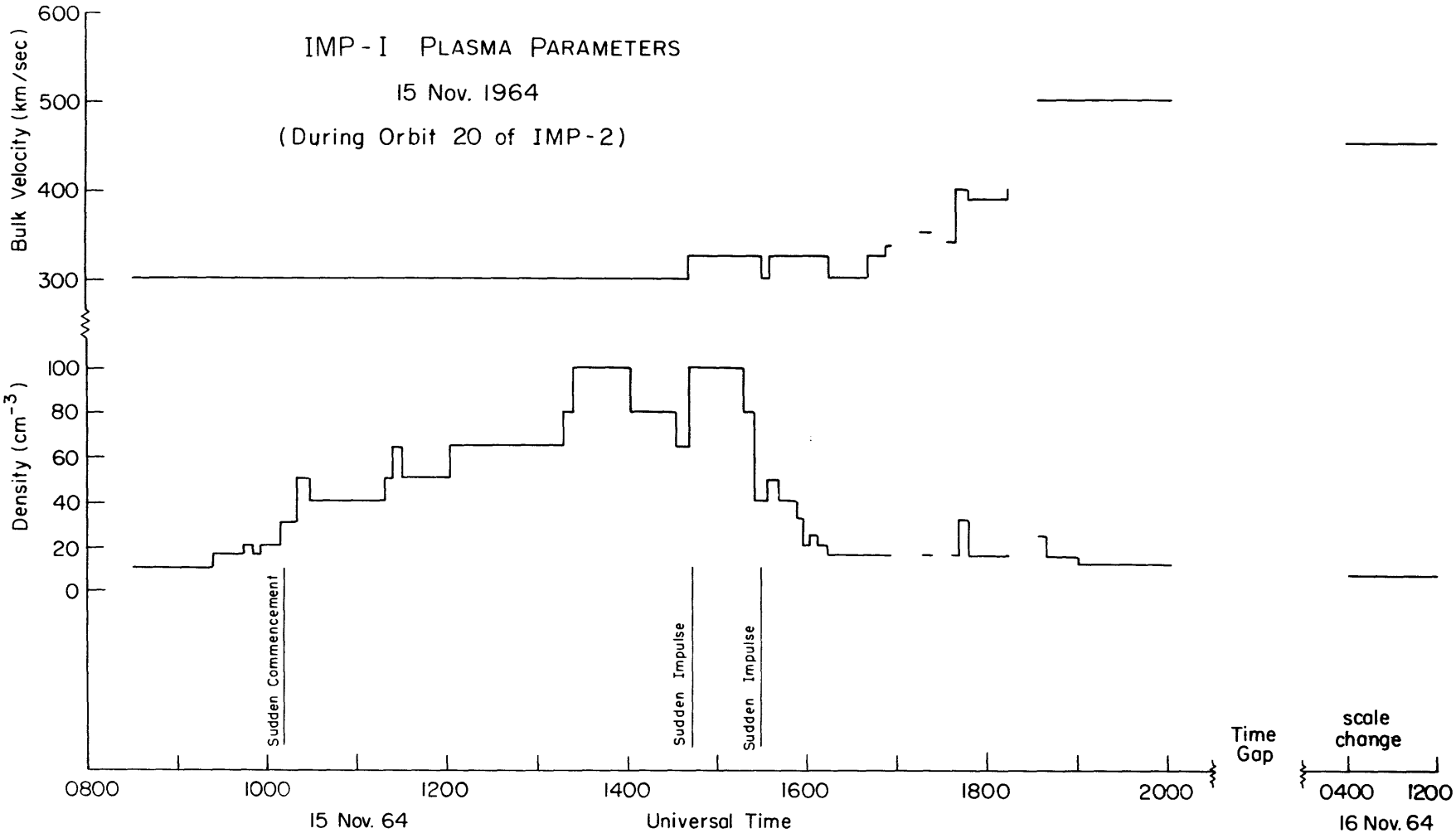
IMP - I PLASMA PARAMETERS
15 Nov. 1964
(During Orbit 20 of IMP - 2)
Bulk Velocity (km/sec)
600
500
400
300
Density (cm⁻³)
100
80
60
40
20
0
Sudden Commencement
Sudden Impulse
Sudden Impulse
0800
1000
1200
1400
1600
1800
2000
15 Nov. 64
Universal Time
Time Gap
scale change
0400
1200
16 Nov. 64

Figure 30

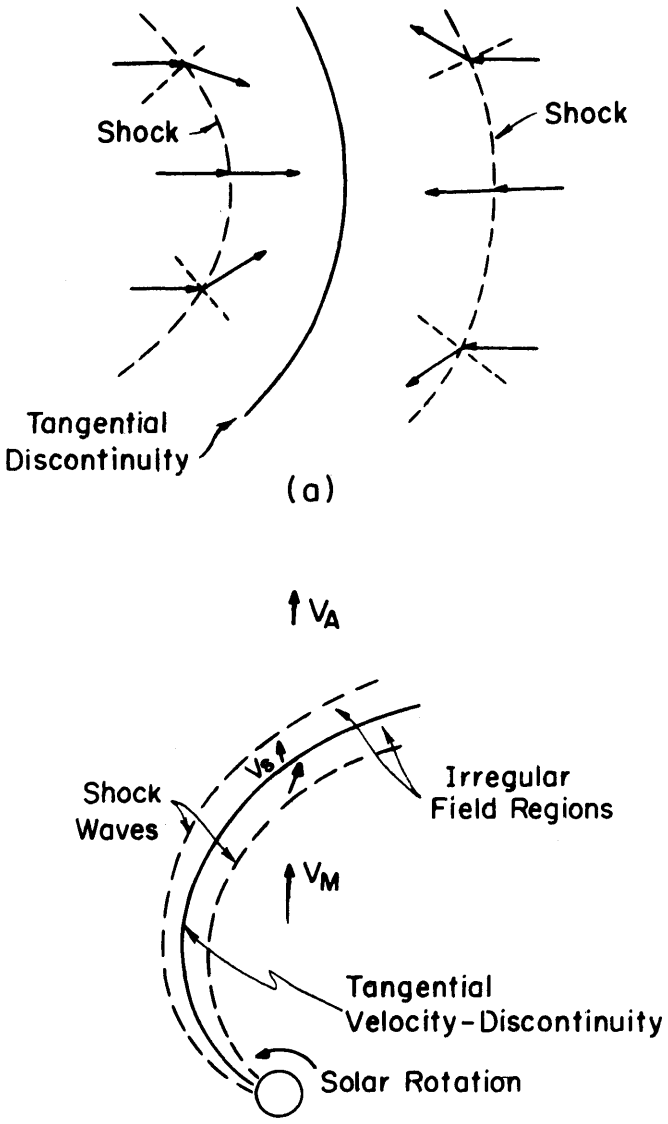
Shock
Shock
Tangential
Discontinuity
(a)
V_A
Shock
Waves
V_S
Irregular
Field Regions
V_M
Tangential
Velocity-Discontinuity
Solar Rotation
(b)
V_S Velocity in Standoff
Region, km/sec
700
500
300
500km/sec
400
300
500
800
1000
1200
V_M Velocity in M Stream, km/sec
(c)

Figure 31

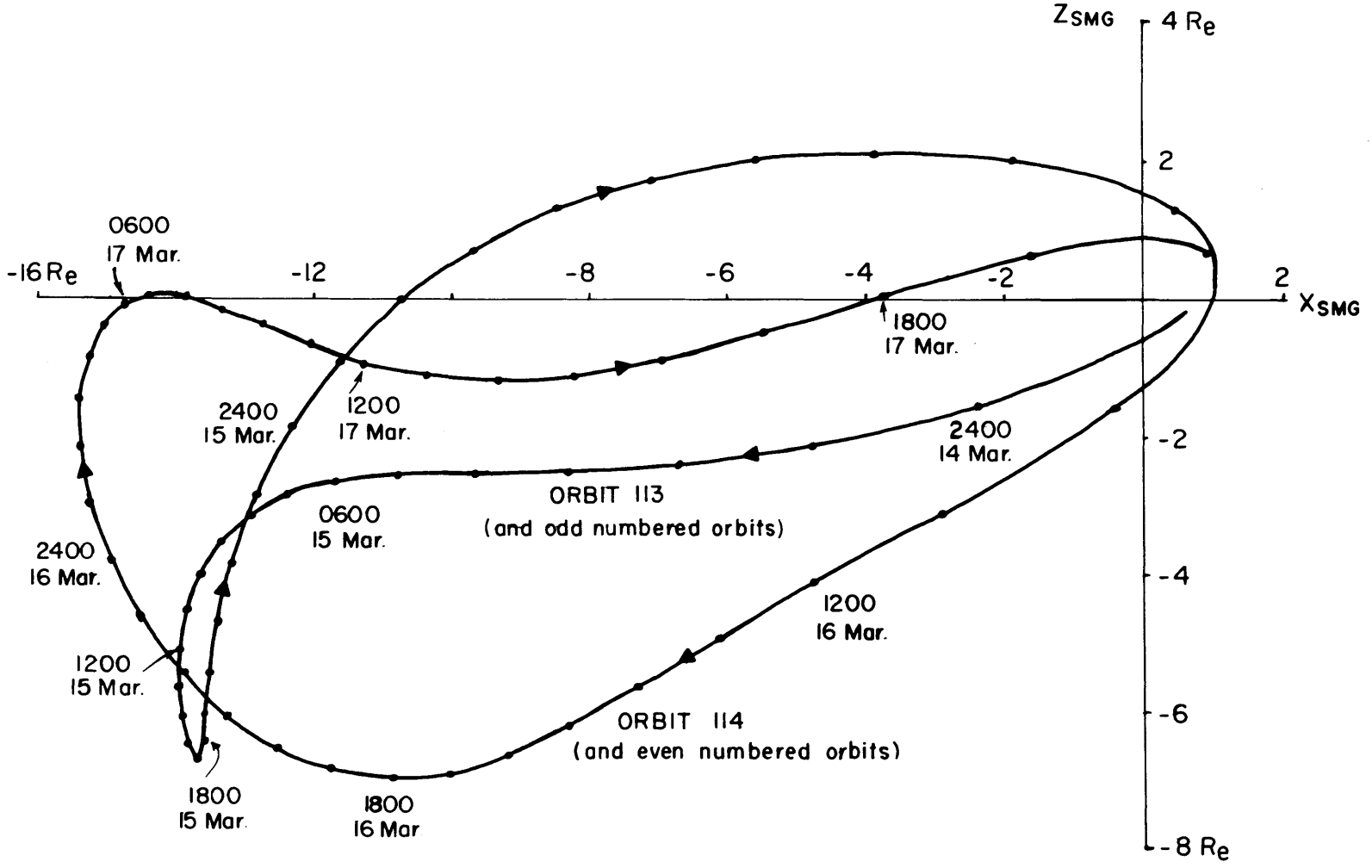

SAMPLE ORBITS IN THE DIPOLE MERIDIAN PLANE OF SOLAR MAGNETIC COORDINATES

Figure 32

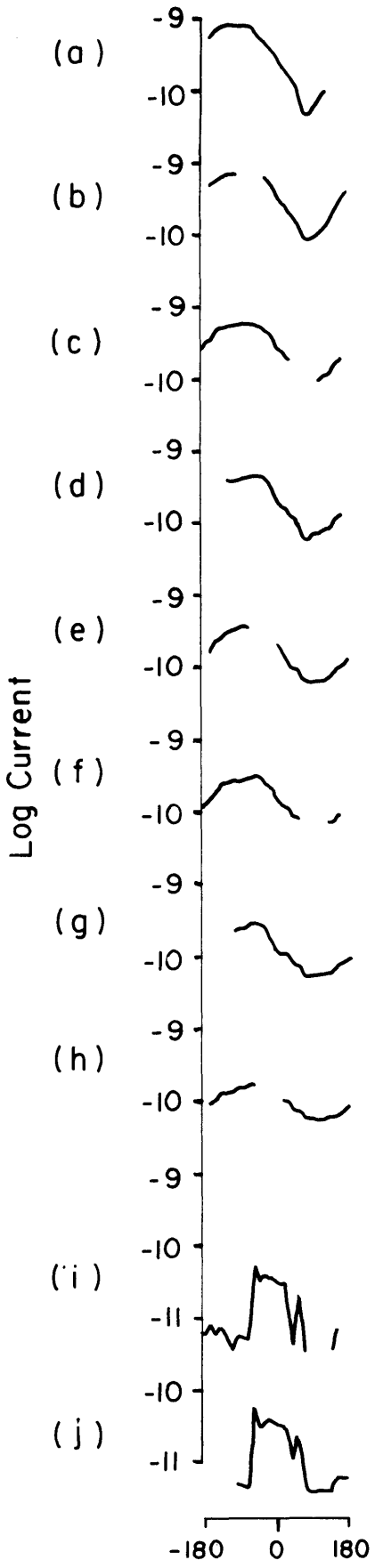

IMP-2

14 Oct. 1964

Orbit 8 Outbound

Negative Channel Currents in the Magnetosphere

(a)-(h.) Secondary electrons from dense positive ions.

(i)-(j.) Photoelectrons from modulator grid.

Figure 33

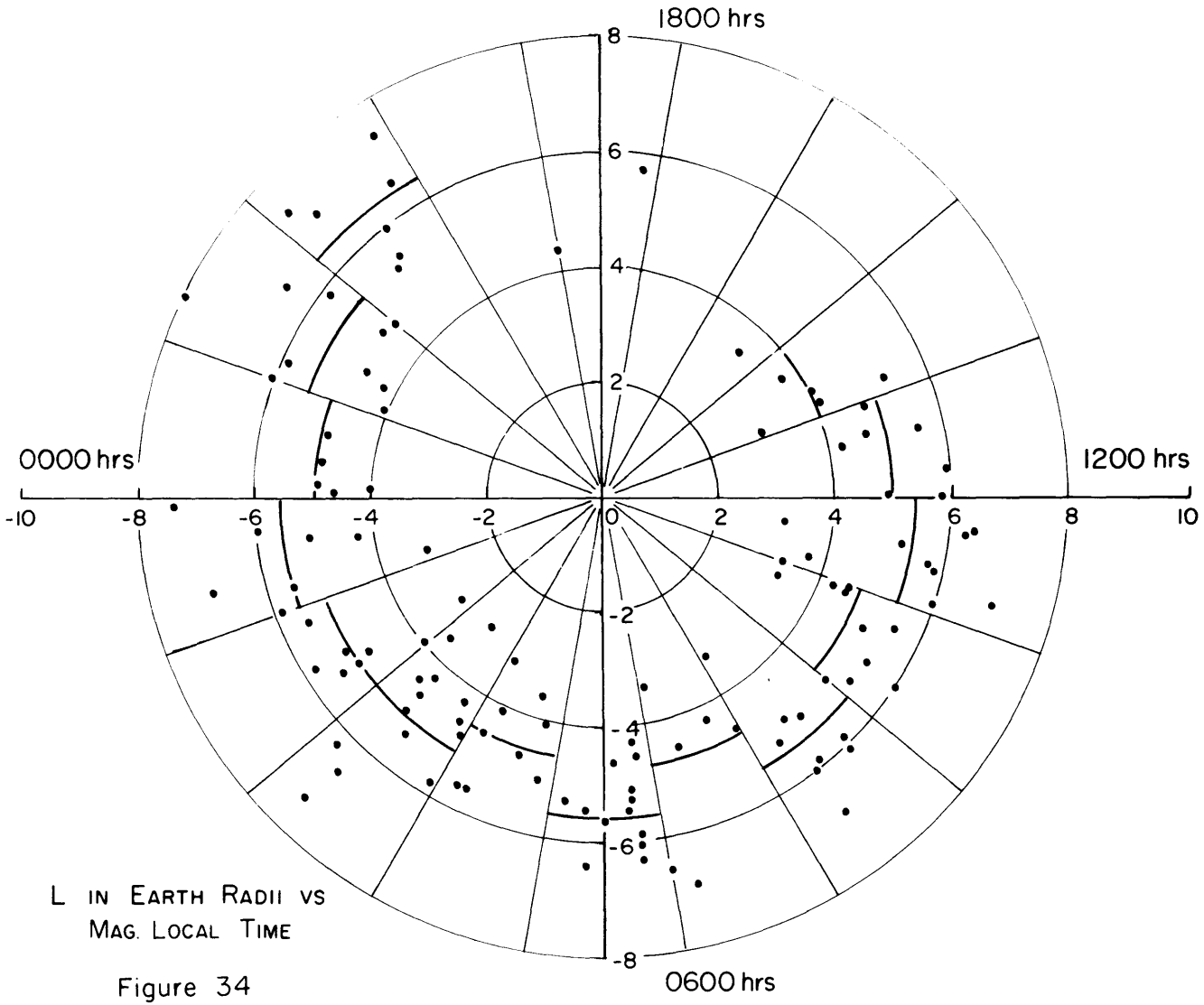

L IN EARTH RADII VS
MAG. LOCAL TIME

Figure 34

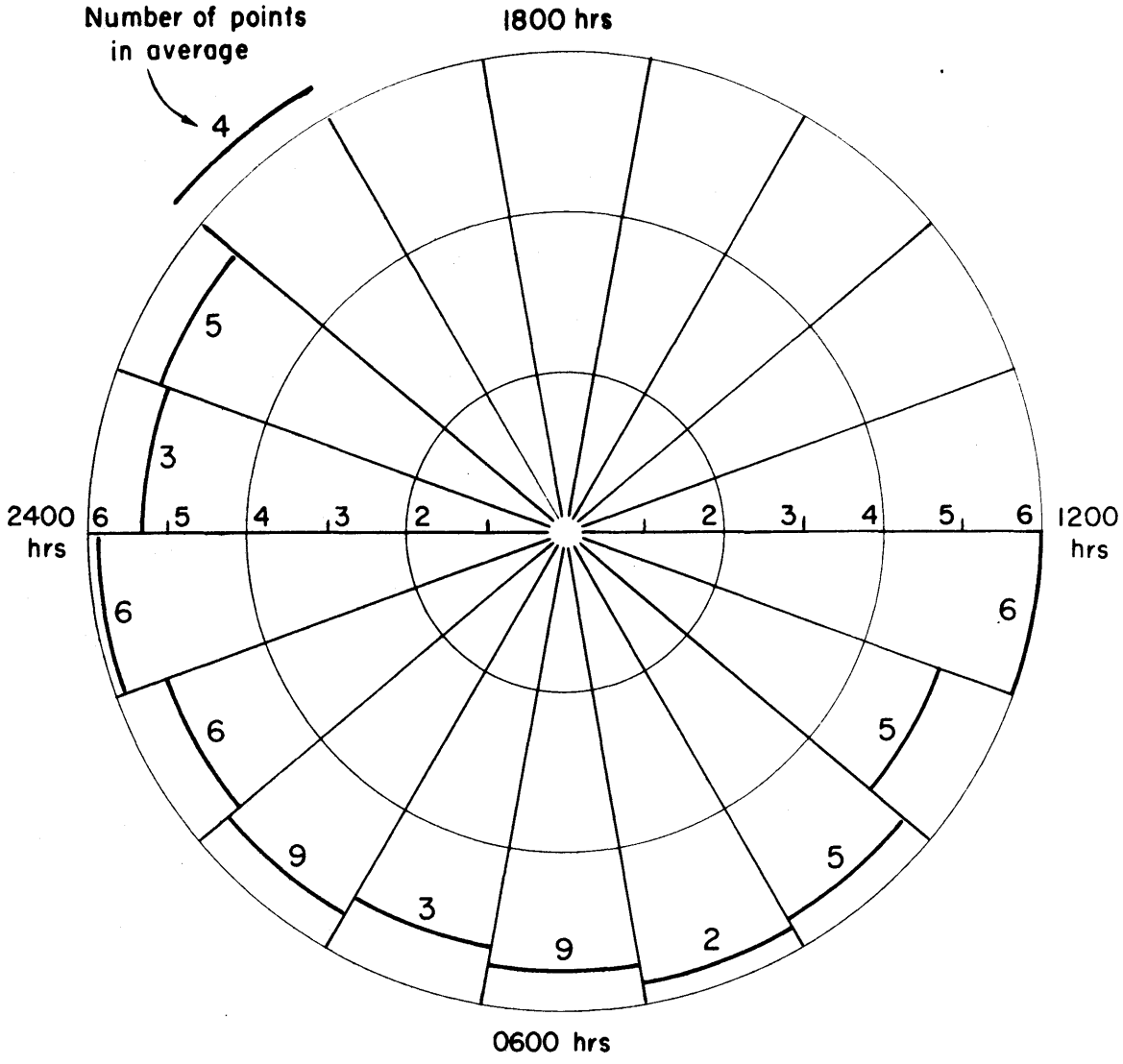

AVERAGE L FOR $K_p \leq 1$

L IN EARTH RADII VS. MAG. LOCAL TIME

Figure 35

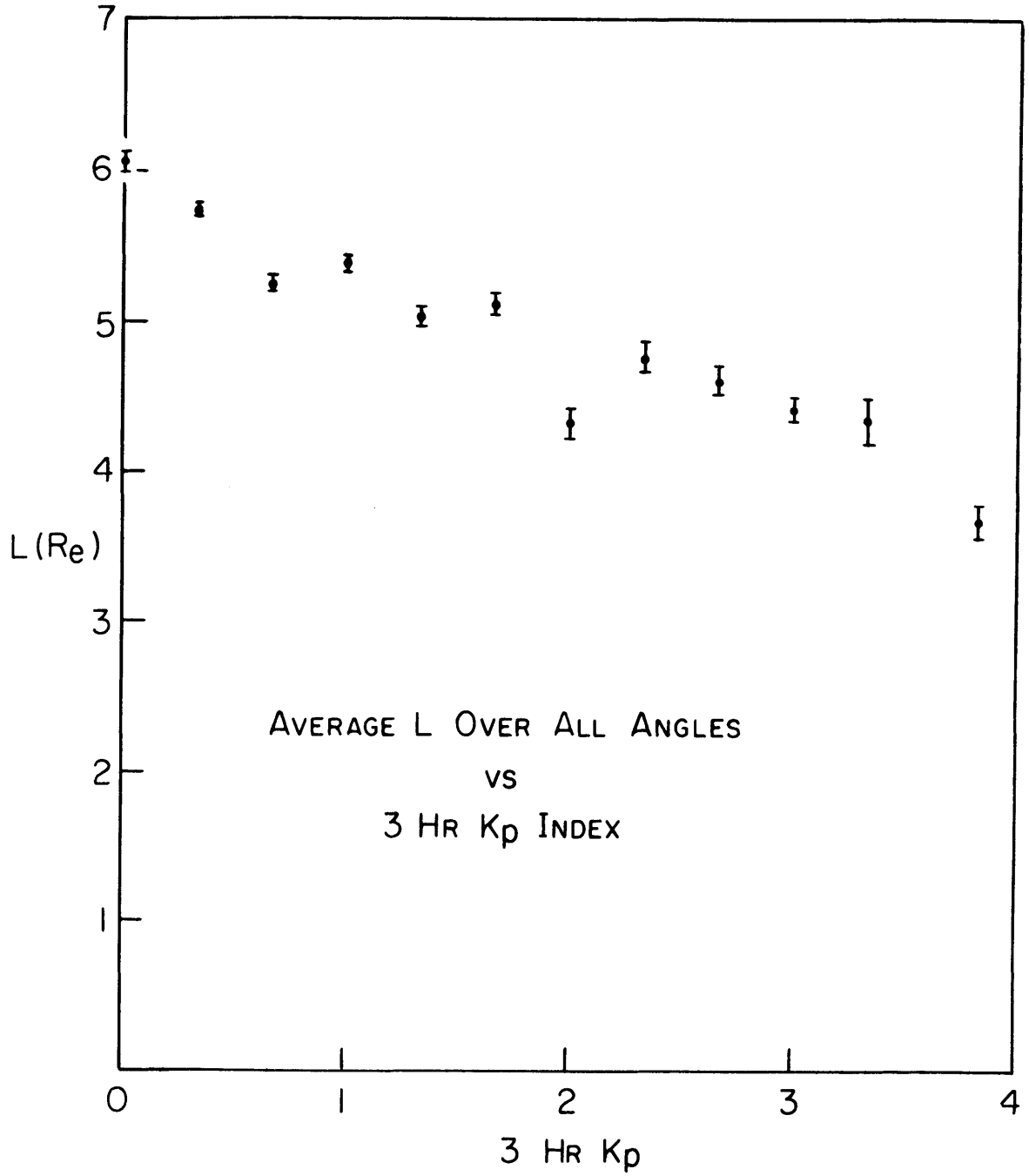
7
6
5
4
3
2
1
L(Re)
AVERAGE L OVER ALL ANGLES
VS
3 HR Kp INDEX
0
1
2
3
4
3 HR Kp

Figure 36

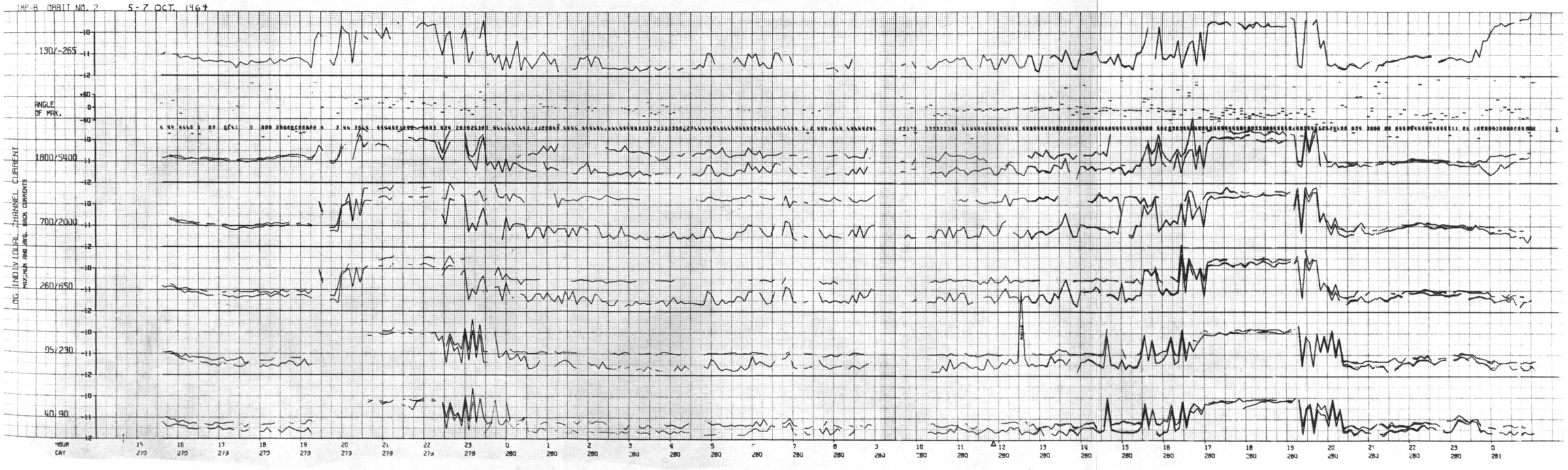

FIGURE 37
ORBIT 2

FIGURE 38
ORBIT 3

FIGURE 39

ORBIT 12

FIGURE 40
ORBIT 15

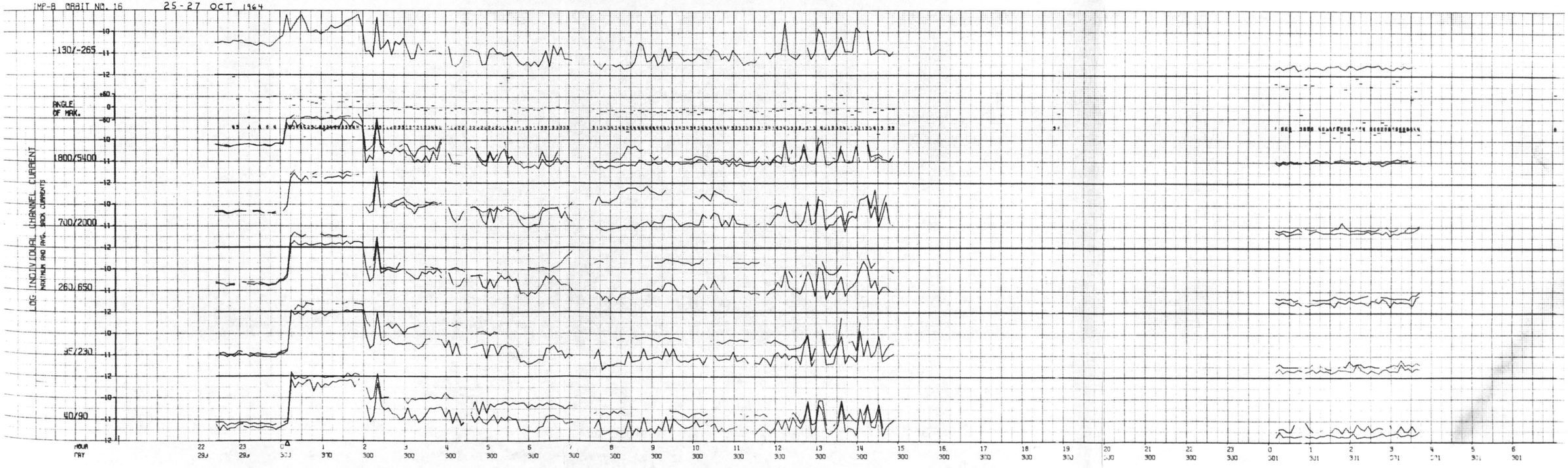

FIGURE 41
ORBIT 16

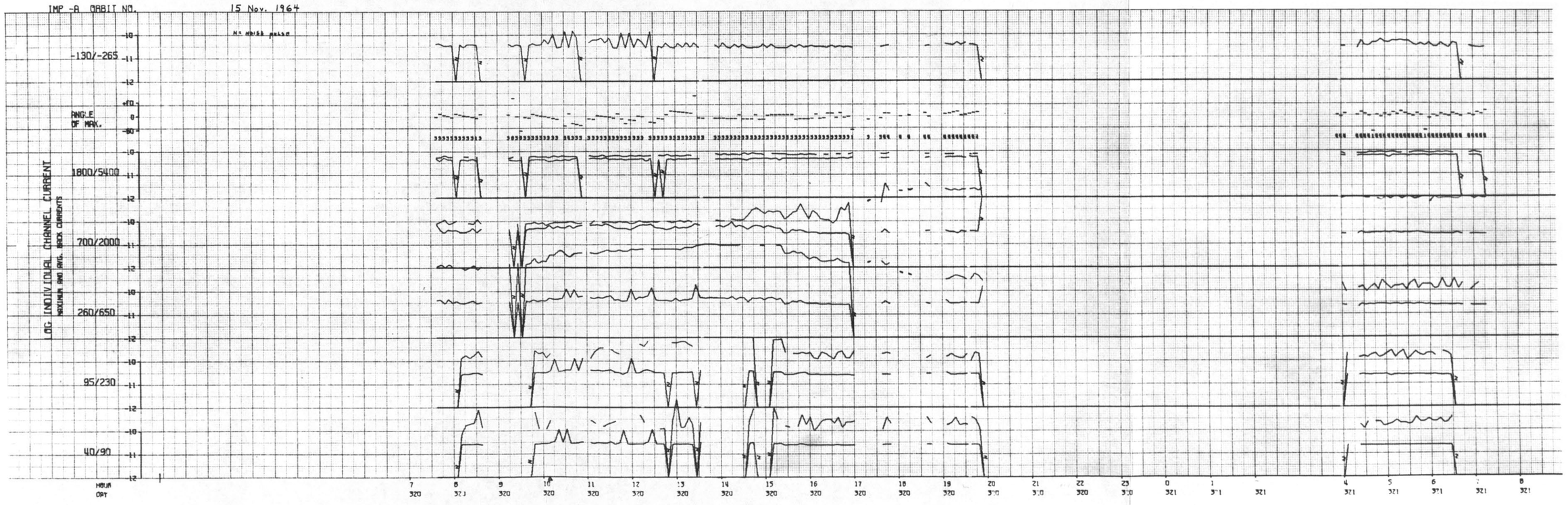

FIGURE 42

IMP - 1

FIGURE 43
ORBIT 63

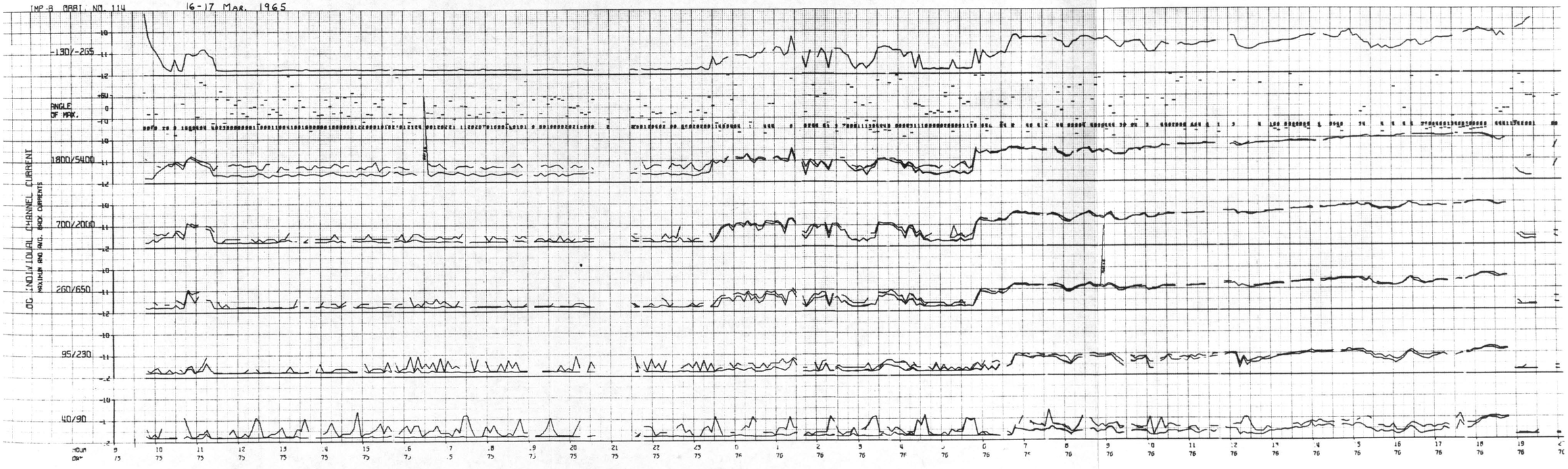

FIGURE 44
ORBIT 114

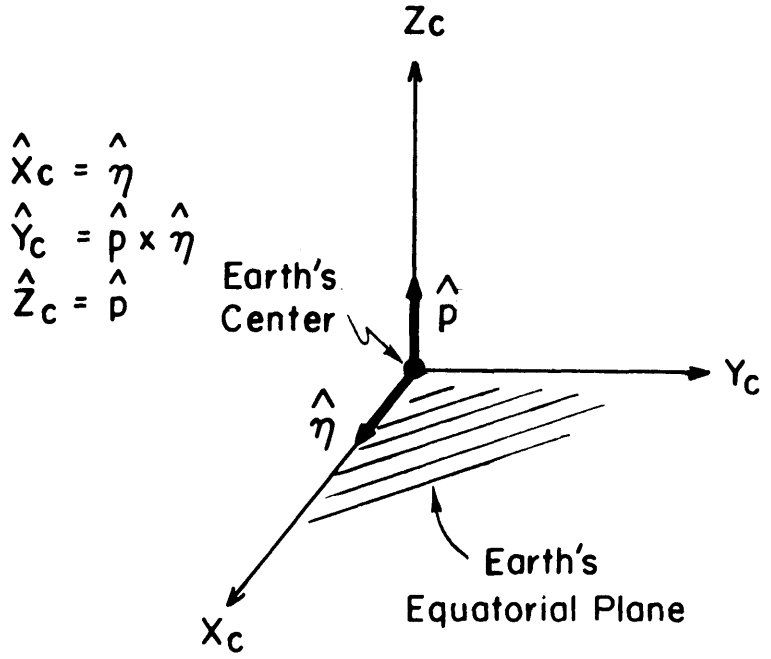

Fig. A-1 CELESTIAL COORDINATE SYSTEM

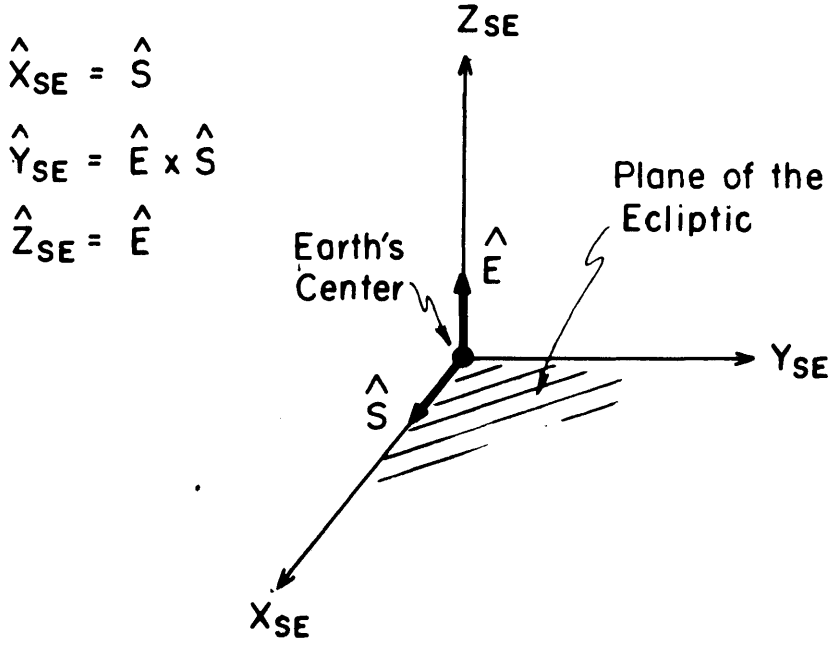

Fig. A-2 SOLAR ECLIPTIC COORDINATE SYSTEM

$$\hat{X}_{SMG} = \left[\frac{\hat{d} \times \hat{s}}{\sqrt{1-(\hat{d}\cdot\hat{s})^2}}\right] \times \hat{d}$$

$$\hat{Y}_{SMG} = \frac{\hat{d} \times \hat{s}}{\sqrt{1-(\hat{d}\cdot\hat{s})^2}}$$

$$\hat{Z}_{SMG} = \hat{d}$$

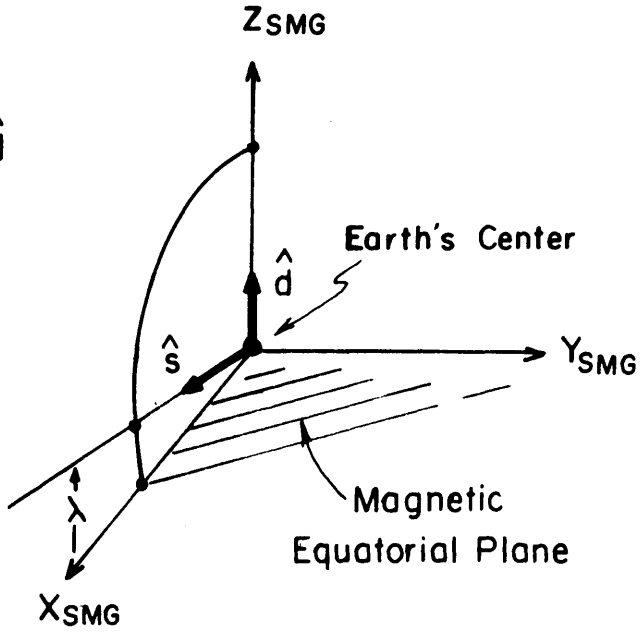

Fig. A-3 SOLAR MAGNETIC COORDINATE SYSTEM

$$\hat{X}_{SMS} = \hat{s}$$

$$\hat{Y}_{SMS} = \frac{\hat{d} \times \hat{s}}{\sqrt{1-(\hat{d}\cdot\hat{s})^2}}$$

$$\hat{X}_{SMS} = \hat{s} \times \left[\frac{\hat{d} \times \hat{s}}{\sqrt{1-(\hat{d}\cdot\hat{s})^2}}\right]$$

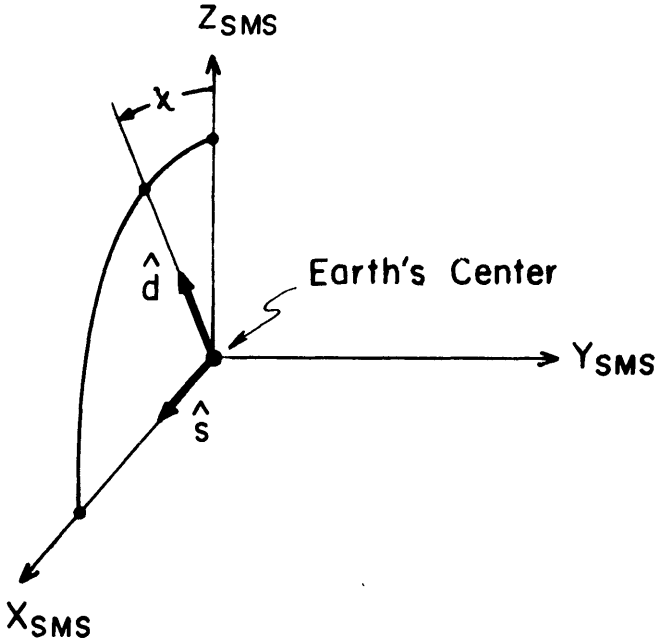

Fig. A-4 SOLAR MAGNETOSPHERIC COORDINATE SYSTEM

$$\hat{X}_{CUP} = \hat{\ell}$$

$$\hat{Y}_{CUP} = \hat{n} + \hat{\ell}$$

$$\hat{X}_{CUP} = \hat{n}$$

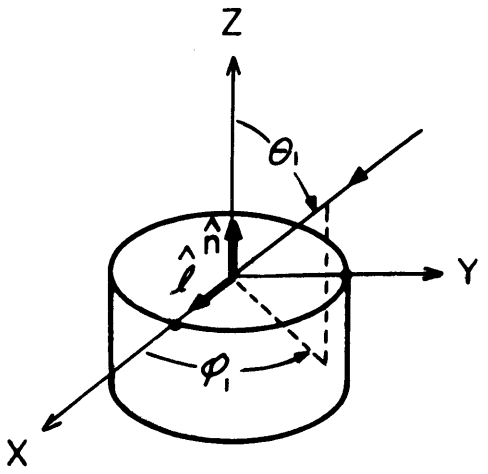

Fig. A-5 CUP COORDINATE SYSTEM

$$\hat{X}_{SS} = \left[\frac{\hat{\ell} \times \hat{q}}{\sqrt{1-(\hat{\ell}\cdot\hat{q})^2}} \right] \times \hat{\ell}$$

$$\hat{Y}_{SS} = \frac{\hat{\ell} \times \hat{q}}{\sqrt{1-(\hat{\ell}\cdot\hat{q})^2}}$$

$$\hat{Z}_{SS} = \hat{\ell}$$

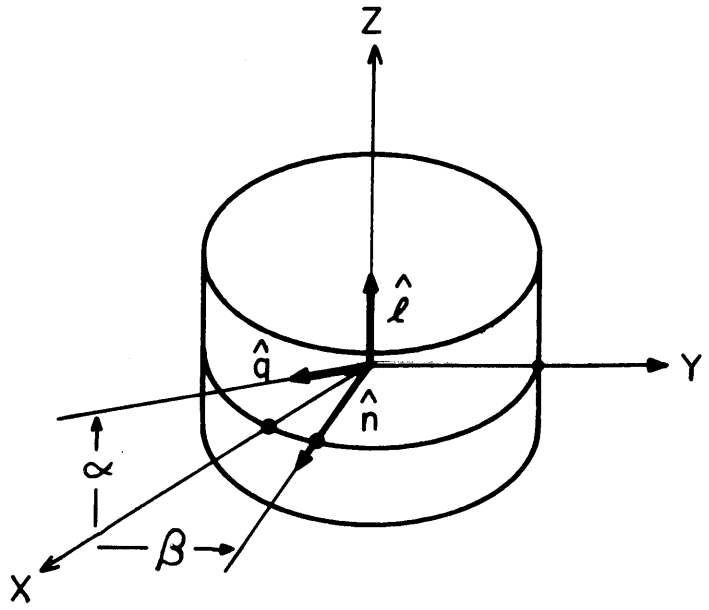

Fig. A-6 SATELLITE SUN COORDINATE SYSTEM

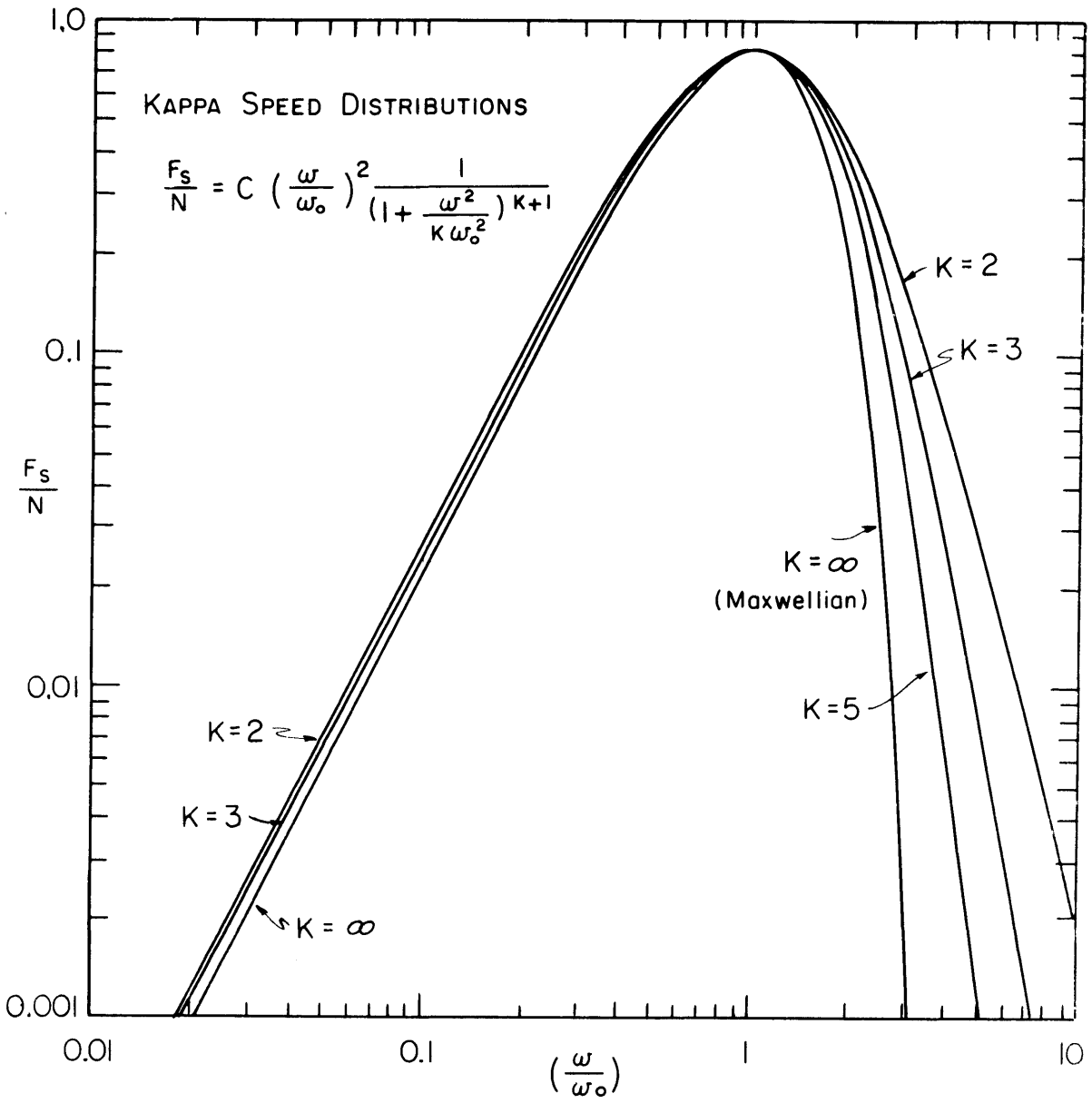
KAPPA SPEED DISTRIBUTIONS
$\frac{F_s}{N} = C \left(\frac{\omega}{\omega_o}\right)^2 \frac{1}{\left(1+\frac{\omega^2}{K\omega_o^2}\right)^{K+1}}$
1.0
0.1
0.01
0.001
$\frac{F_s}{N}$
0.01
0.1
1
10
$\left(\frac{\omega}{\omega_o}\right)$
K = 2
K = 3
K = ∞
(Maxwellian)
K = 5
K = 2
K = 3
K = ∞

Figure B-1

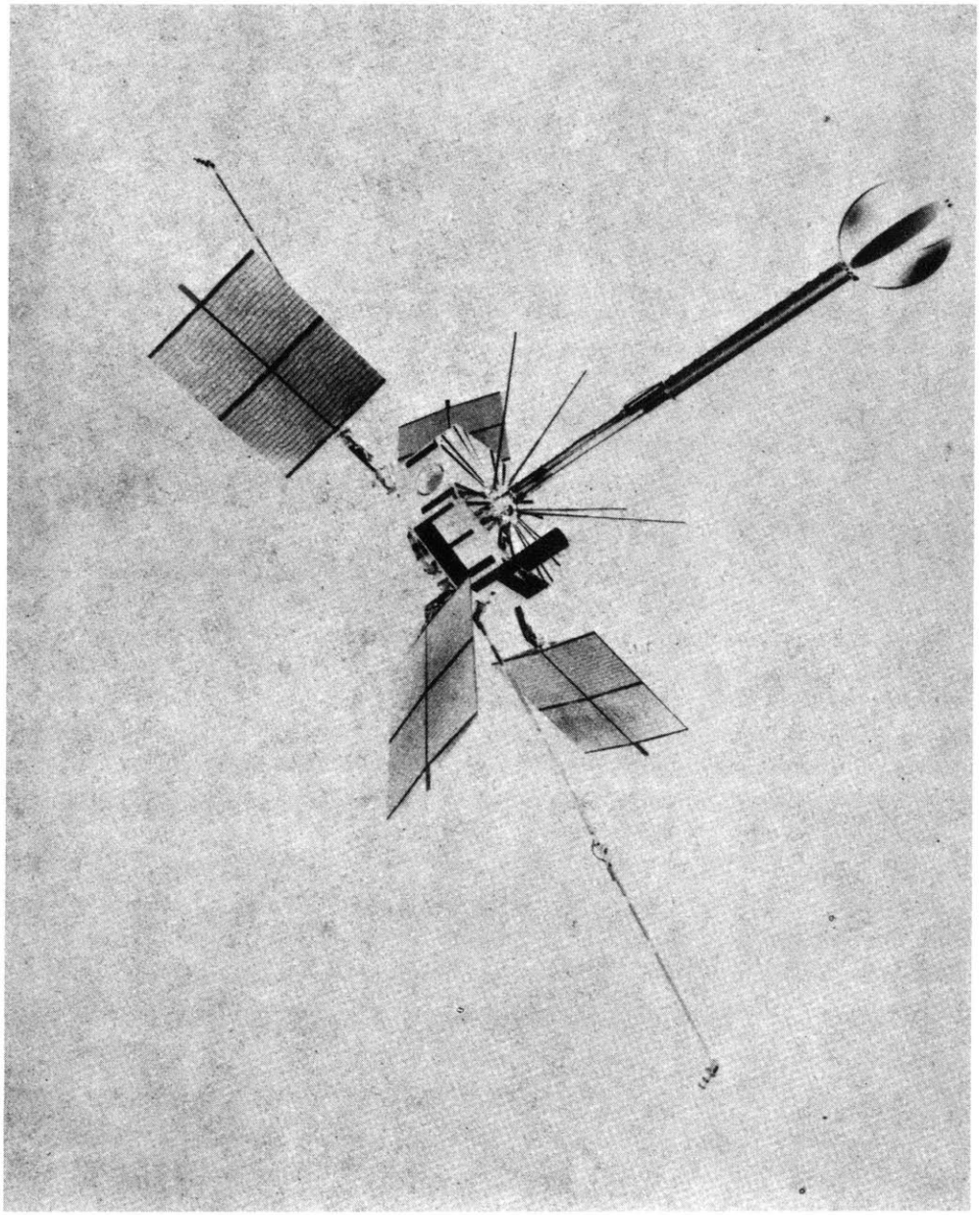

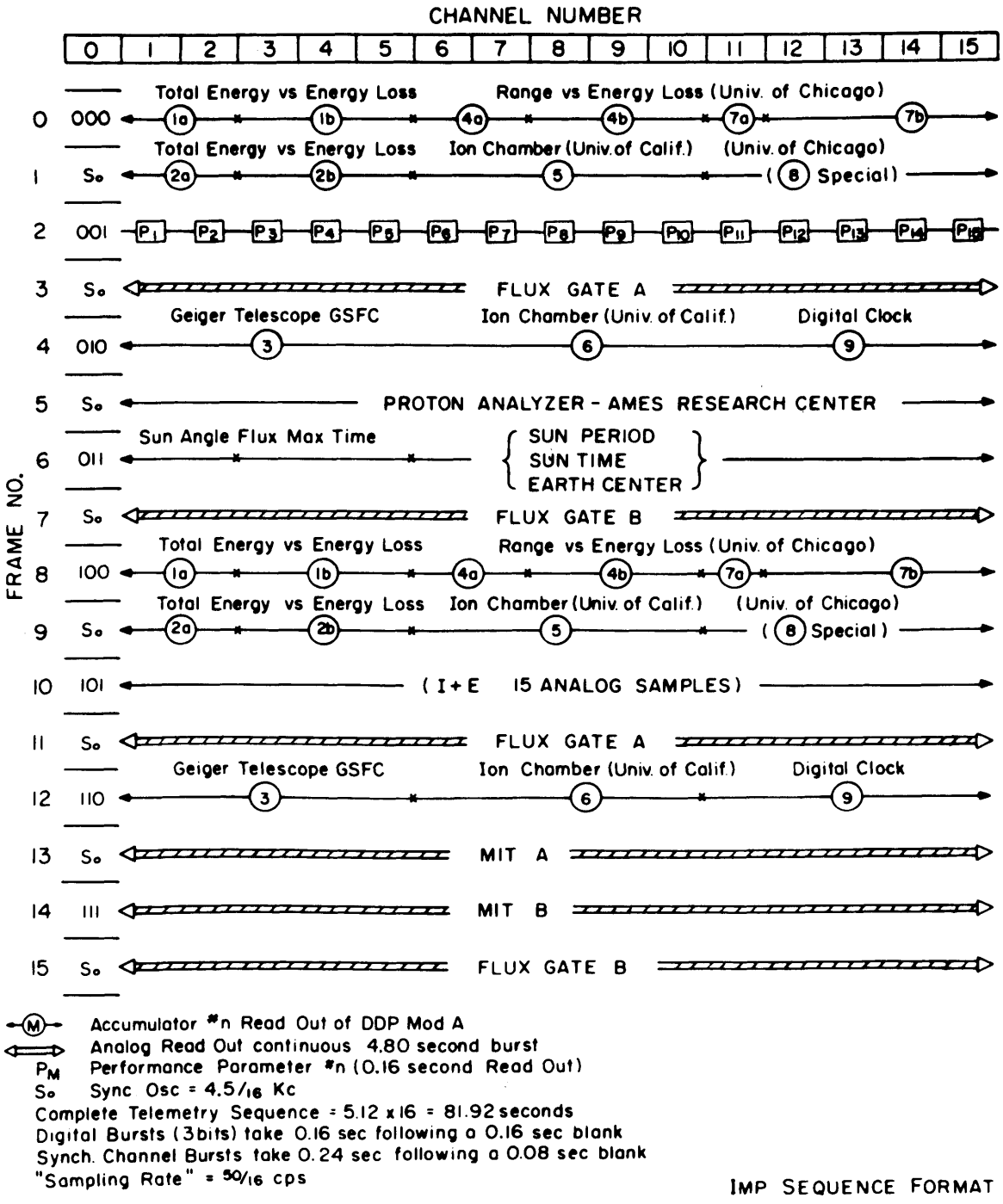

(M) Accumulator #n Read Out of DDP Mod A
Analog Read Out continuous 4.80 second burst
P_M Performance Parameter #n (0.16 second Read Out)
So Sync Osc = 4.5/16 Kc
Complete Telemetry Sequence = 5.12 x 16 = 81.92 seconds
Digital Bursts (3 bits) take 0.16 sec following a 0.16 sec blank
Synch. Channel Bursts take 0.24 sec following a 0.08 sec blank
"Sampling Rate" = 50/16 cps

IMP SEQUENCE FORMAT

FIGURE C-1

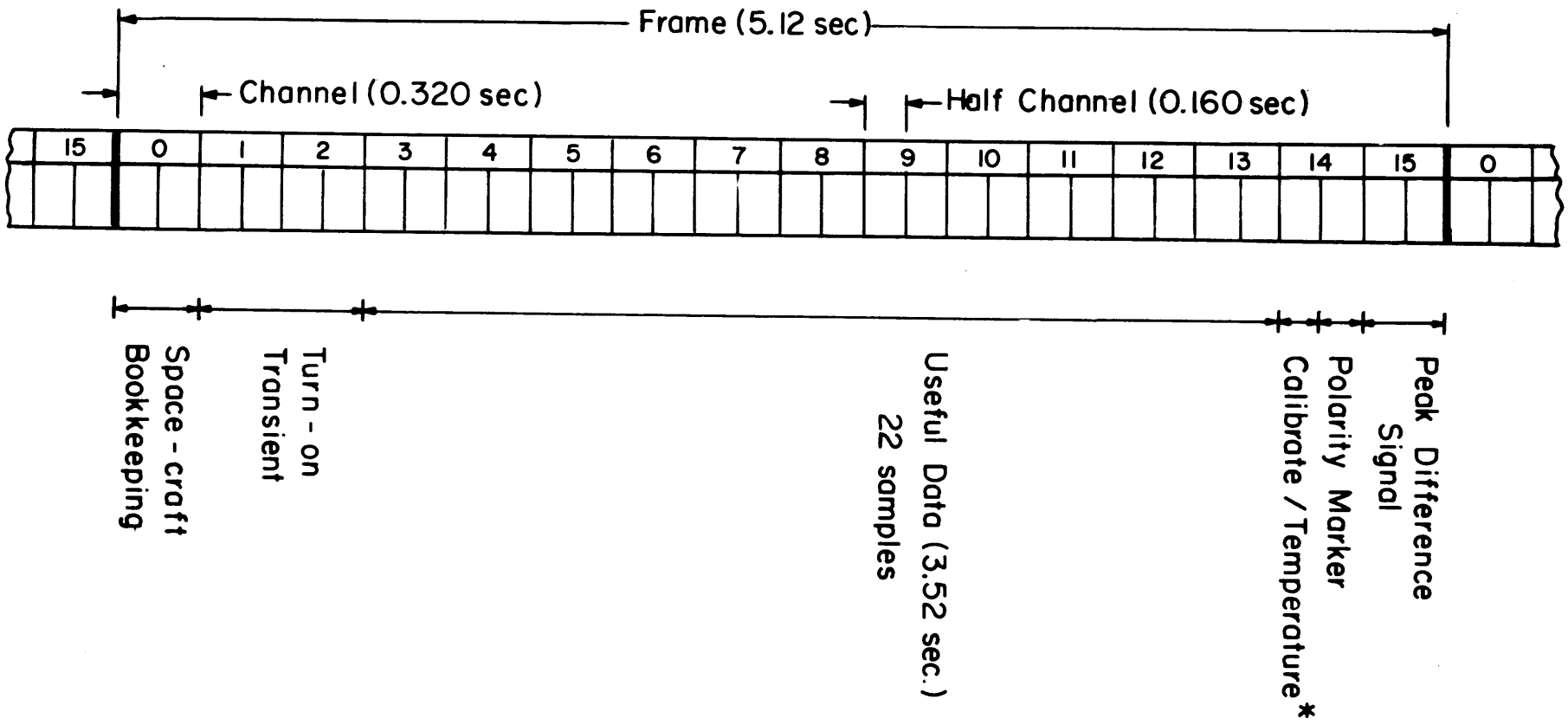

* Temperature for only Frame 14 of Sequences 2 and 3

Fig.C-2. FRAME STRUCTURE

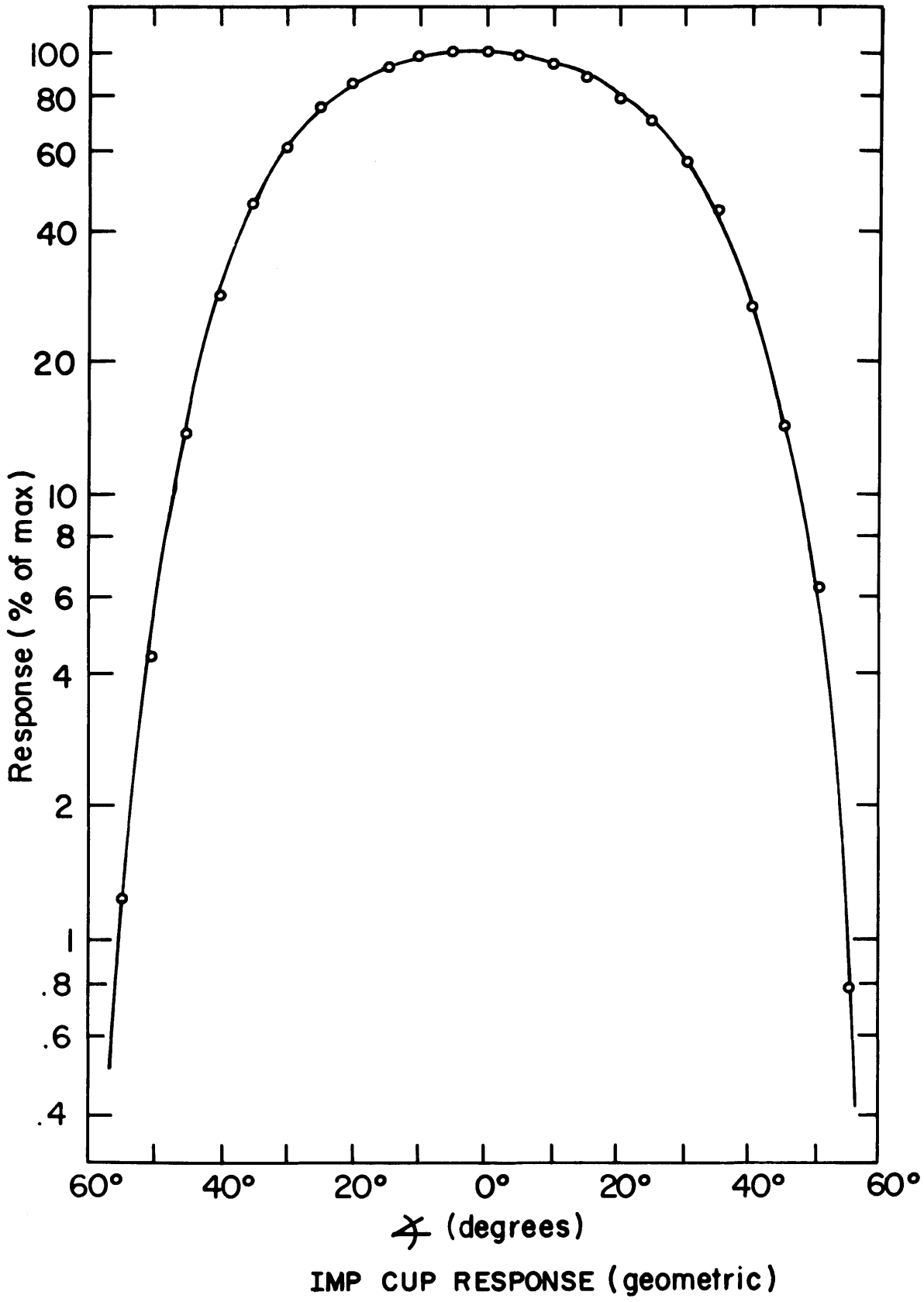
100
80
60
40
20
10
8
6
4
2
1
.8
.6
.4
Response (% of max)
60°
40°
20°
0°
20°
40°
60°
(degrees)
IMP CUP RESPONSE (geometric)

Figure C-3

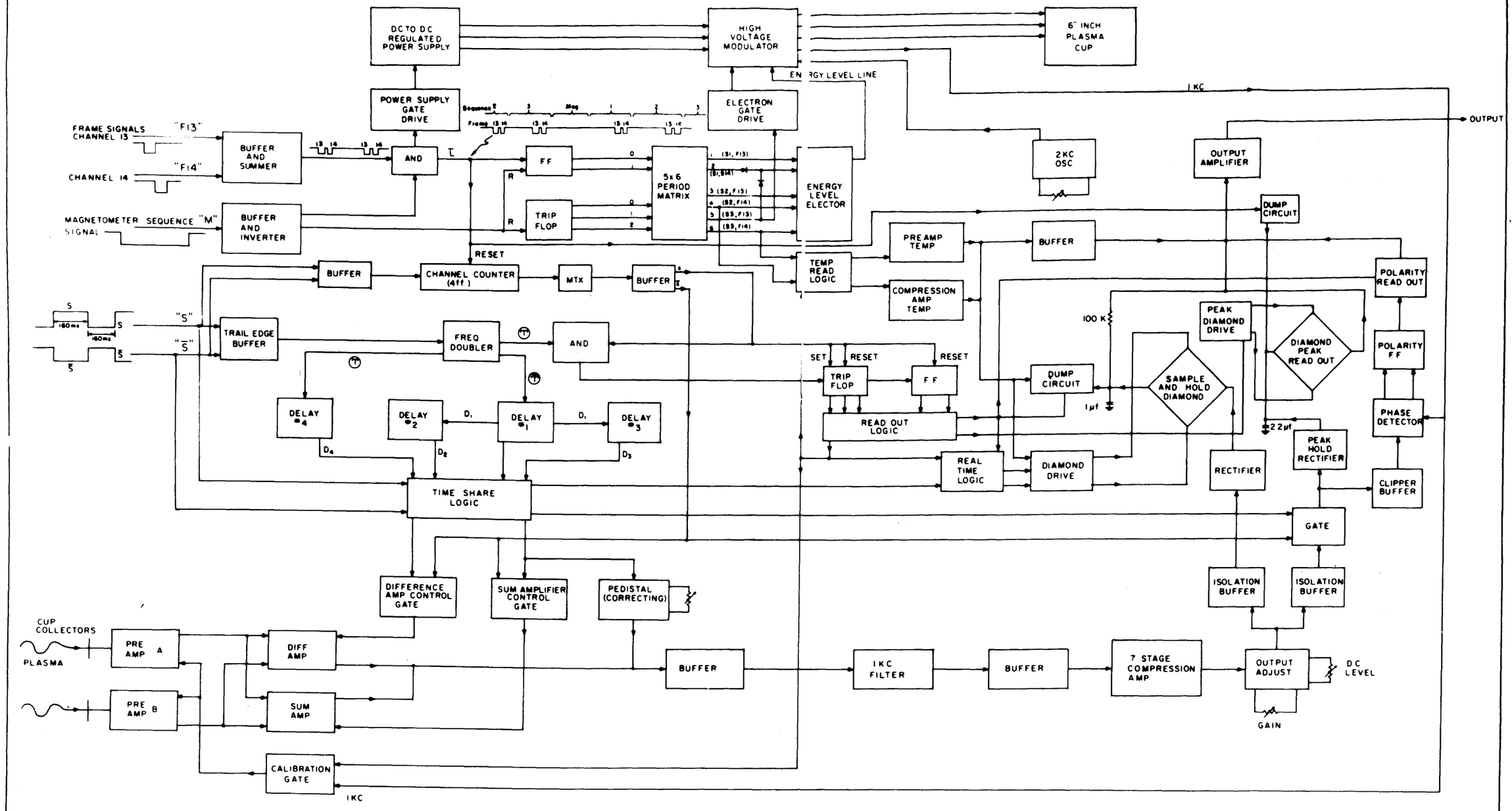

FIGURE C-4

Ref Linc Lab Dwg No D-14104-6

LABORATORY FOR NUCLEAR SCIENCE
MASSACHUSETTS INSTITUTE OF TECHNOLOGY
CAMBRIDGE MASS

DRAWN BY LYON
DESIGNED BY E.W.G.
CHECKED BY
DATE DEC. 28, 65.

TITLE
IMP BLOCK DIAGRAM (A,B,C)

DWG NO D- 5026-A
PROJ 9375

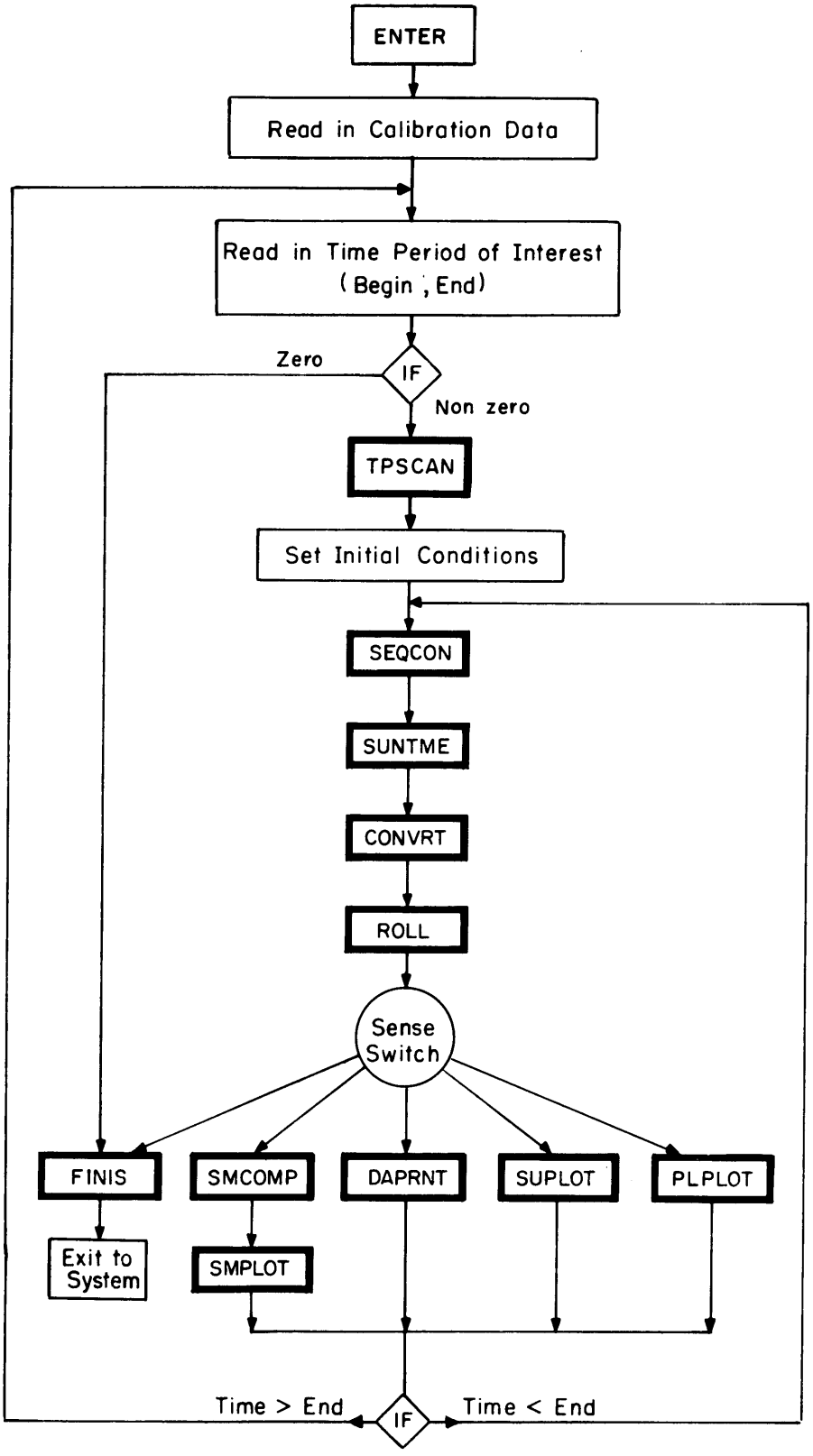

SIMPLIFIED FLOW DIAGRAM FOR MAIN PROCESSING PROGRAM

Figure D-1

BIBLIOGRAPHY

Akasofu, S.-I. and C.E. McIlwain, Energetic neutral hydrogen atoms as a source of the ring current particles, Trans. Am. Geophys. Union, 44, 883, 1963.

Akasofu, S.-I., The neutral hydrogen flux in the solar wind flow - I, Planet. Space Sci., 12, 905-913, 1964.

Alfven, H., Granulation, Magneto-hydrodynamic waves, and the heating of the solar corona, Mon. Not. Roy. Astron. Soc., 107, 211-219, 1947.

Alfven, H., Cosmical Electrodynamics, Oxford Press, London, 1950.

Alfven, H. and Carl-Gunne Falthammar, Cosmical Electrodynamics, Second Edition, Ocford Press, London, 1963.

Anderson, K.A., Energetic Electron Spikes in and beyond the transition region, Proc. Int. Conf. on Cosmic Rays, London, 1965a.

Anderson, K.A., H.K. Harris and R.J. Paoli, Energetic Electron Fluxes in and Beyond the Earth's Outer Magnetosphere, J. Geophys. Res., 70, 1039-1050, 1965b.

Anderson, K.A., Energetic Electron Fluxes in the Tail of the Geomagnetic Field, J. Geophys. Res., 70, 4741-4764, 1965c.

Anderson, K.A., and N.F. Ness, Correlation of Magnetic Fields and Energetic Electrons on the IMP-1 Satellite, J. Geophys. Res., 71, 3705-3728, 1966.

Angerami, J.J. and D.L. Carpenter, Whistler Studies of the Plasmapause in the Magnetosphere, 2, Electron Density and Total Tube Electron Content Near the Knee in Magnetospheric Ionization, J. Geophys. Res., 71, 711-726, 1966.

Auer, P.L., H. Hurwitz and R.W. Kilb, Low Mach Number Magnetic Compression Waves in a Collision-Free Plasma, Phys. Fluids, 4, 1105-1121, 1961.

Auer, P.L., H. Hurwitz, Jr. and R.W. Kilb, Large Amplitude Magnetic Compression of a Collision-Free Plasma, 2, Development of a Thermalized Plasma, Phys. Fluids, 5, 298-316, 1962.

Axford, W.I. and C.O. Hines, A Unifying Theory of High Latitude Geophysical Phenomena and Geomagnetic Storms, Can. Journ. Phys., 39, 1433-1464, 1961.

Axford, W.I., The Interaction Between the Solar Wind and the Earth's Magnetosphere, J. Geophys. Res., 67, 3791-3796, 1962.

Axford, W.I., A.J. Dessler and B. Gottlieb, Termination of Solar Wind and Solar Magnetic Field, Astrophys. J., 137, 1268-1278, 1963.

Axford, W.I., The Interaction of the Solar Wind with Comets, Planet Space Sci., 12, 719-720, 1964.

Axford, W.I., The Modulation of Galactic Cosmic-Rays in the Inter-Planetary Medium, Planet. and Space Sci., 13, 115-130, 1965a.

Axford, W.I., Anisotropic Diffusion of Solar Cosmic Rays, Planet. Space Sci., 13, 1301-1309, 1965b.

Babcock, H.W. and H.D. Babcock, The Sun's Magnetic Field, Astrophys. J., 121, 349-366, 1955.

Bartels, J., Geomagnetic and Solar Data, J. Geophys. Res.,54, 296-297, 1949.

Beard, D.B., The Interaction of the Terrestrial Magnetic Field with the Solar Corpuscular Radiation, J. Geophys. Res., 65, 3559-3568, 1960.

Beard, D.B., The Effect of an Interplanetary Magnetic Field on the Solar Wind, J. Geophys. Res., 69, 1159-1168, 1964.

Bernstein, W., R.W. Fredericks and F.L. Scarf, A Model for a Broad Disordered Transition Between the Solar Wind and the Magnetosphere, J. Geophys. Res., 69, 1201-1210, 1964.

Biermann, L., Kometenschweife und solare Korpuskularstrahlung, Zeit. F. Astrophys., 29, 274-286, 1951.

Biermann, L. and Rh. Lüst, Comets: Structure and Dynamics of Tails, in The Solar System, IV, Edited by B. Middlehurst and G.P. Kuiper, Chapt 18, Univ. of Chicago Press, Chicago, 1963.

Birkeland, Kr., The Norwegian Aurora Polaris Expedition 1902-3, Vol. 1, On the Cause of Magnetic Storms and the Origin of Terrestrial Magnetism, First Section, H. Aschehoug and Co., Christiania, 1908.

Birkeland, Kr., The Norwegian Aurora Polaris Expedition 1902-3, Vol. 1, On the Cause of Magnetic Storms and the Origin of Terrestrial Magnetism, Second Section, H. Aschehoug and Co., Christiania, 1913.

Bloom, A.L., Principles of Operation of the Rubidium Vapor Magnetometer, Applied Optics, 1, 61-68, 1962.

Bonetti, A., H.S. Bridge, A.J. Lazarus, E.F. Lyon, R. Rossi, and F. Scherb, Explorer 10 Plasma Measurements, in Space Research III, Edited by W. Priester, Interscience Publishers, a Division of John Wiley and Sons, Inc., New York, 1963a.

Bonetti, A., H.S. Bridge, A.J. Lazarus, B. Rossi and F. Scherb, Explorer 10 Plasma Measurements, J. Geophys. Res., 68, 4017-4063, 1963b.

Bridge, H.A., Plasmas in Space, Physics Today, 16, 31-37, 1963.

Bridge, H.S. Private Communication, Cambridge, Mass., 1966.

Bryant, D.A., T.L. Cline, U.D. Desai, and F.B. McDonald, Studies of Solar Protons with Explorers 12 and 14, Astrophys. J., 141, 478-499, 1965.

Bumba, V. and R. Howard, Large Scale Distribution of Solar Magnetic Fields, Astrophys. J., 141, 1502-1512, 1965.

Cahill, L.J. and P.G. Amazeen, The Boundary of the Geomagnetic Field, J. Geophys. Res., 68, 1835-1844, 1963.

Carpenter, D.L., Whistler Evidence of a "Knee" in the Magnetospheric Ionization Density Profile, J. Geophys. Res., 68, 1675-1682, 1963.

Carpenter, D.L., Whistler Studies of the Plasmapause in the Magneto-Sphere, 1, Temporal Variations in the Position of the Knee and Some Evidence on Plasma Motions near the Knee, J. Geophys. Res., 71, 693-710, 1966.

Carr, F.A., Flight Report IMP-II (Explorer XXI), NASA Technical Note, NASA TN D-3353, June, 1966.

Chamberlain, J.W., Interplanetary Gas II; Expansion of a Model Solar Corona, Astrophys. J., 131, 47-56, 1960.

Chamberlain, J.W., Interplanetary Gas. III; A Hydrodynamic Model of the Corona, Astrophys. J., 133, 675-687, 1961.

Chamberlain, J.W., On the Existence of Slow Solutions in Coronal Hydrodynamics, Astrophys. J., 141, 320-322, 1965.

Chandrasekhar, S., Hydrodynamic and Hydromagnetic Stability, Oxford Press, London, 1961.

Chapman, S., The Energy of Magnetic Storms, Monthly Not. Roy. Astron. Soc., 79, 70-83, 1918.

Chapman, S., An Outline of a Theory of Magnetic Storms, Proc. Roy. Soc. London (A), 95, 61-83, 1919.

Chapman, S., Solar Streams of Corpuscles: Their Geometry, Absorption of Light, and Penetration, Monthly Not. Roy. Astronom. Soc. London, 89, 456-70, 1929.

Chapman, S. and V.C.A. Ferraro, Nature, 126, 129, 1930.

Chapman, S. and Ferraro, V.C.A., A New Theory on Magnetic Storms, Terr. Mag. and Atmos. Elec., 36, 77-97, 171-186, 1931: 37, 147-156, 421-429, 1932; 38, 79-96, 1933.

Chapman, S., and J. Bartels, Geomagnetism, Oxford Press, London, 1940.

Chapman, S., Interplanetary Space and the Earth's Outermost Atmosphere, Proc. Roy. Soc. London, A253, 462-481, 1959.

Chapman, S., Idealized Problems of Plasma Dynamics Relating to Geomagnetic Storms, Revs. Mod. Phys., 32, 919-933, 1960.

Chapman, S., Solar Plasma Geomagnetism and Aurora in Geophysics: The Earth's Environment, Les Houches 1962 Lectures, edited by C. DeWitt et al., 371-502, Gordon and Breach, New York, 1963.

Clauser, F.H., The Aerodynamics of Mass Loss and Mass Gain of Stars, Laboratory Report, AFOSR TN 60-1386, The Johns Hopkins University, Nov., 1960.

Colburn, D.S. and C.P. Sonett, Discontinuities in the Solar Wind, Space Science Reviews, 5, 439-506, 1966.

Coleman, P.J., Jr., L. Davis and C.P. Sonett, Steady Component of the Interplanetary Magnetic Field: Pioneer V, Phys. Rev. Letters, 5, 43-46, 1960.

Coleman, P.J., C.P. Sonett and L. Davis, On The Interplanetary Magnetic Storm, Pioneer V, J. Geophys. Res., 66, 2043-2046, 1961.

Coleman, P.J., L. Davis, E.J. Smith and C.P. Sonett, The Mission of Mariner II: Preliminary Observations, Science, 138, 1095-1100, 1962.

Coleman, P.J., Jr., E.J. Smith, L. Davis, Jr., and D.E. Jones, Measurements of Magnetic Fields in the Vicinity of the Magnetosphere and in Interplanetary Space: Preliminary Results from Mariner 4, in Space Research VI, Interscience Publishers, a Division of John Wiley and Sons, New York, 1966a.

Coleman, P.J., L. Davis, Jr., E.J. Smith, and D.E. Jones, Variations in the Polarity Distribution of the Interplanetary Magnetic Field, J. Geophys. Res., 71, 2831-2839, 1966b.

Davis, L., Interplanetary Magnetic Fields and Cosmic Rays, Phys. Rev., 100, 1440-1444, 1955.

Davis, L., The Effect of Solar Disturbances and the Galactic Magnetic Field on the Interplanetary Gas, in Proceedings of the International Conference on Cosmic Rays and the Earth Storm, Kyoto, Journal of the Phys. Soc. of Japan, 17, Supplement A-II, 543-544, 1962.

Davis, L., Models of the Interplanetary Fields and Plasma Flow, in The Solar Wind, Edited by R.L. Mackin, Jr. and M. Neugabauer, pp. 147-157, Pergamon Press, New York, 1966a.

Davis, Leverett, Jr., E.J. Smith, P.J. Coleman, Jr., and C.P. Sonett, Interplanetary Magnetic Measurements, in The Solar Wind, Edited by R.L. Mackin, Jr., and M. Neugabauer, pp. 35-50, Pergamon Press, New York, 1966b.

De Hoffman, F. and E. Teller, Magnetohydrodynamic Shocks, Phys. Rev. 80, 692-703, 1950.

Dept. of Commerce, Compilations of Solar-Geophysical Data, National Dureau of Standards, CRPL, Boulder, Colo., 1965.

Dessler, A.J., The Stability of the Interface between the Solar Wind and the Geomagnetic Field, J. Geophys. Res., 66, 3587-3590, 1961.

Dessler, A.J., Further Comments on the Stability of the Interface Between the Solar Wind and the Geomagnetic Field, J. Geophys. Res., 67, 4892-4894, 1962.

Dessler, A.J. and J.A. Fejer, Interpretation of K_p index and M-region Geomagnetic Storms, Planet. Space Sci., 11, 505-511, 1963.

Dessler, A.J. and G.K. Walters, Hydromagnetic Coupling Between the Solar Wind and the Magnetosphere, Planet. Space Sci., 12, 1964.

Dessler, A.J. and F.C. Michel, Magnetospheric Models, Proceedings of Symposium on Radiation Trapped in the Earth's Magnetic Field, Bergen Norway, August 1965.

Dessler, A.J., The Solar Wind and Interplanetary Magnetic Field, to appear in Reviews of Geophysics, 1966.

Dungey, J.W., Electrodynamics of the Outer Atmosphere, Proc. Ionosphere Conf., The Physical Society of London, pp. 229-236, 1955.

Dungey, J.W., Cosmical Electrodynamics, Cambridge U. Press, 1958.

Dungey, J.W., Geophysics, the Earth's Environment, Ed. by C. DeWitt, J. Hieblot, and A. Lebeau, Gordon and Breach, N.Y., 1963.

Dungey, J.W., Effects of Electromagnetic Perturbations on Particles Trapped in the Radiation Belts, Space Science Reviews, 4, 199-222, 1964.

Egidi, A., H. Bridge, E. Lyon, and B. Rossi, Spatial Properties of the Interplanetary Plasma and Its Interaction with the Earth's Field as Observed by IMP-1, Am. Geophys. Union, 45, 605 (Abstract), 1964.

Egidi, A., Unpublished Notes, Cambridge, Mass., 1965.

Fairfield, D., Private Communication, NASA, Goddard Space Flight Center, Greenbelt, Md., 1966.

Fan, C.Y., G. Gloeckler, and J. A. Simpson, Acceleration of Electrons Near the Earth's Bow Shock and Beyond, J. Geophys. Res., 71, 1837-1856, 1966.

Fejer, J.A., Hydromagnetic Stability at a Fluid Velocity-Discontinuity Between Compressible Fluids, Phys. Fluids, 7, 499-503, 1964.

Ferraro, V.C.A., On the Theory of the First Phase of a Geomagnetic Storm, J. Geophys. Res., 57, 15-49, 1952.

Ferraro, V.C.A., An Approximate Method of Estimating the Size and Shape of the Stationary Hollow Carved Out in a Neutral Ionized Stream of Corpuscles Impinging on the Geomagnetic Field, J. Geophys. Res., 65, 3951-3953, 1960a.

Ferraro, V.C.A., Theory of Sudden Commencement and of the First Phase of a Magnetic Storm, Revs. Modern Phys., 32, 934-938, 1960b.

Fermi, E., Galactic Magnetic Fields and the Origin of Cosmic Radiation, Astrophys. J., 119, 1, 1954.

Finch, H.F. and B.R. Leaton, The Earth's Main Magnetic Field-Epoch 1955, MNRAS, GS, 4, 314-317, 1957.

Fishman, F.J., A.R. Kantrowitz and H.E. Petschek, Magnetohydrodynamic Shock Wave in a Collision-Free Plasma, Rev. Mod. Phys., 32, 959-966, 1960.

Frank, L., and J. Van Allen, Measurements of Energetic Electrons in the Vicinity of the Sunward Magnetospheric Boundary with Explorer 14, J. Geophys. Res., 69, 4923-4932, 1964.

Frank, L., Inward Radial Diffusion of Electrons E>1.6 Mev, in the Outer Radiation Zone, J. Geophys. Res., 70, 3533-3540, 1965.

Fredricks, R.W., and F.L. Scarf, Effects of Solar Wind Composition on the Threshold for Plasma Instability in the Transition Region, J. Geophys. Res., 70, 4765-4776, 1965.

Freeman, J.W., J.A. Van Allen and L.J. Cahill, Explorer XII Observations of the Magnetosphere Boundary and the Associated Solar Plasma on September 13, 1961, J. Geophys. Res., 68, 2121-2130, 1963.

Gold, T., Magnetic Fields in the Solar System, Nuovo Cimento, Suppl., (10) 13, 318-323, 1959.

Gold, T., Magnetic Storms, Space Sci. Rev., 1, 100-114, 1962.

Gold, T., Magnetic Field Configurations Near the Sun and in Interplanetary Space, Proc. Pontifical Academy, 431-457, 1963.

Gosling, J.T., J.R. Asbridge, S.J. Bame, and I.B. Strong, Vela 2 Measurements of the Magnetopause and Bow Shock Positions, Preprint LA-DC-8000 from Los Alamos Scientific Laboratory, Los Alamos, New Mexico, 1966.

Grad, H., Boundary Layer Between a Plasma and a Magnetic Field, Physics Fluids, 4, 1366-1375, 1961.

Greenstadt, E.W., Interplanetary Magnetic Effects of Solar Flares: Explorer 18 and Pioneer 5, J. Geophys. Res., 70, 5451-5452, 1965.

Gringauz, K.I., V.V. Bezrukikh, V.D. Ozerov, and R. Ye Rybchinskiy, Study of the Interplanetary Ionized Gas, High Energy Electrons, and Solar Corpscular Radiation by Means of Three Electrode Traps for Charged Particles on the Second Soviet Cosmic Rocket, Soviet Physics Dokl., 5, 361-364, 1960 (or, Doklady Akad. Nauk. SSSR, 131, 1301-1304, 1960).

Gringauz, K.I., Some Results of Experiments in Interplanetary Space by Means of Charged Particle Traps on Soviet Space Probes, in Space Research II, Edited by H.C. Van de Hulst, C. de Jager, and A.F. Moore, pp. 539-553, Interscience Publishers, Inc., New York, 1961.

Harrison, E.R., The Earth's Distant Geomagnetic Field, Geophys. J., 6, 479-491, 1962.

Heppner, J.P., N.F. Ness, T.L. Skillman and C.S. Scearce, Explorer X Magnetic Field Measurements, J. Geophys. Res., 68, 1-46, 1963.

Hess, W.N. and G.P. Mead, The Boundary of the Magnetosphere, in Introduction to Space Science, ed. by W. Hess, Gordon & Breach, N.Y., 1965.

Hida, K., An Approximate Study on the Detached Shock Wave in Front of A circular Cylinder and a Sphere, J. Phys. Sco., Japan, 8, 740-745, 1953.

Hines, C.O., The Magnetopause: A New Frontier in Space, Science, 141, 130-136, 1963.

Hines, C.O. And G.C. Reid, Theory of Geomagnetic and Auroral Storms, in Physics of the Earth's Upper Atmosphere, Edited by C.O. Hines, I. Paghis, T.R. Hartz, and J.A. Fejer, pp. 334-362, Prentice Hall, Inc. Englewood Cliffs, New Jersey, 1965.

Hinteregger, H.E., K.R. Damon, and L.A. Hall, J. Geophys. Res., 64, 961, 1959.

Hirshberg, J., Recurrent Geomagnetic Storms and the Solar Wind, J. Geophys. Res., 70, 5353-5360, 1965.

Hirshberg, J., The Relationship Between Solar Wind Velocities and Surface Magnetic Disturbances During Sudden Commencement Storms, J. Geophys. Res., 70, 4159-4164, 1965.

Hones, E.W., Motions of Charged Particles Trapped in the Earth's Magnetosphere, J. Geophys. Res., 68, 1209-1219, 1963.

Hurley, J.D., Interaction Between the Solar Wind and the Geomagnetic Field, Phys. Fluids, 4, 854-859, 1961.

Jaynes, E.T., Information Theory and Statistical Mechanics, Phys. Rev., 106, 620-630, 108, 171-190, 1957.

Jokipii, J.R. and L. Davis, Acceleration of Electrons Near the Earth's Bow Shock, Phys. Rev. Letters, 13, 739, 1964.

Jokipii, J.R., Diffusion and Convection of Energetic Electrons Behind the Earth's Bow Shock, J. Geophys. Res., 71, 3173-3176, 1966.

Johnson, F.S., The Gross Character of the Geomagnetic Field in the Solar Wind, J. Geophys. Res., 65, 3049-3052, 1960.

Kaufman, R.L., Conservation of the First and Second Adiabatic Invariants, J. Gephys. Res., 70, 2181-2186, 1965.

Kellogg, P.J., Flow of Plasma Around the Earth, J. Geophys. Res., 67, 3805-3811, 1962.

Kiepenheuer, K.O., Emission of Corpuscles From the Sun, J. Geophys. Res., 57, 113-120, 1952.

Konradi, A., and R.L. Kaufmann, Evidence for Rapid Motion of the Outer Boundary of the Magnetosphere, J. Geophys. Res., 70, 1627-1638, 1965.

Landau and Lifshitz, Fluid Mechanics, Addison-Wessley, Reading, Mass. 1959.

Large, L.N., Proc. Phys. Soc. (London) 81, 1101, 1963.

Lazarus, A.J., H.S. Bridge, J.M. Davis, and C.W. Snyder, Initial Results from the Mariner 4 Solar Plasma Experiment, COSPAR, Vienna, 1966a.

Lazarus, A.J., H.S. Bridge, and J. Davis, Preliminary Results from the Pioneer 6 M.I.T. Plasma Experiment, J. Geophys. Res., 71, 3787, 1966b.

Lerch, I., Validity of the Hydromagnetic Approach in Discussing Stability of the Magnetospheric Boundary, J. Geophys. Res., 71, 2365-2371, 1966.

Levy, R.H., H.E. Petschek and G.L. Siscoe, Aerodynamic Aspects of the Magnetosphere Flow, AVCO Corp. Res. Rep. 170, 1963.

Lin, R.P. and K.A. Anderson, Periodic Modulations of the Energetic Electron Fluxes in the Distant Radiation Zone, J. Geophys. Res. 71, 1827-1836, 1966.

Lincoln, J.V., Geomagnetic and Solar Data, J. Geophys. Res., 70, 4963, 5953, 1965.

Lüst, Rh., Interplanetary Plasma, Space Science Reviews, 1, 522-552, 1962.

Lyon, E., H. Bridge, A. Egidi and B. Rossi, IMP-1 Plasma Summary Data, Am. Geophys. Union, 45, 605 (Abstract), 1964.

Lyon, E.F., Explorer-18 Plasma Measurements, The Solar Wind, Edited by Mackin and Neugebauer, Pergamon Press, 1966a.

Lyon, E.F., A Study of the Interplanetary Plasma, M.I.T. Ph.D. Thesis, January, 1966b, unpublished.

Maer, K. and A.J. Dessler, Comments on paper by Conway W. Snyder, Marcia Neugebauer, and U.R. Rao, "The Solar Wind Velocity and its Correlation with Cosmic Ray Variations and with Solar and Geomagnetic Activity", J. Geophys. Res., 69, to be published, 1964.

McCracken, K.G., The Cosmic-Ray Flare Effect, 1., 2. and 3., J. Geophys. Res., 67, 423-458, 1962.

McIlwain, C.E., J. Geophys. Res., 66, 3681, 1961.

Mead, G.D., Deformation of the Geomagnetic Field by the Solar Wind, J. Geophys. Res., 69, 1181-1195, 1964.

Mead, G.D. and D.B. Beard, Shape of the Geomagnetic Field Solar Wind Boundary, J. Geophys. Res., 69, 1169-1180, 1964.

Medved, D.B., and Y.E. Strausser, Kinetic Ejection of Electrons from Solids, in Adv. in Electronics and Electron Phys., Vol. 21, Academic Press, N.Y., 1965.

Midgley, J.E. and L. Davis, Computation of the Bounding Surface of a Dipole Field in a Plasma by a Moment Technique, J. Geophys. Res., 67, 499-504, 1962.

Morawetz, C.S., Magnetohydrodynamic Shock Structure Without Collisions, Phys. Fluids, 4, 998-1006, 1961.

Morawetz, C.S., Modification for Magnetohydrodynamic Shock Structure Without Collisions, Phys. Fluids, 5, 1447-1450, 1962.

Morton, K.W., Large-amplitude Compression Waves in an Adiabatic Two-Fluid Model of a Collision-Free Plasma, J. Fluid Mech., 14, 369-384, 1962.

Morton, K.W., Finite Amplitude Compression Waves in a Collision-Free Plasma, NYO-10434, Courant Institute of Math. Sciences, New York Univ., 1964.

Nakada, M.P., and G.D. Mead, Diffusion of Protons in the Outer Radiation Belt, J. Geophys. Res., 70, 4777-4792, 1965.

Ness, N.F., C.S. Scearce, and J.B. Seek, Initial Results of the IMP-1 Magnetic Field Experiment, J. Geophys. Res., 69, 3531-3569, 1964.

Ness, N.F., and J.M. Wilcox, The Solar Origin of the Interplanetary Magnetic Field, Phys. Rev. Letters, 13, 461-464, 1964.

Ness, N.F., The Interplanetary Medium, in Introduction to Space Science, Ed. by W. Ness, Gordon and Breach, New York, 1965a.

Ness, N.F., C.S. Scearce, J.B. Seek, and J.M. Wilcox, A Summary of Results from the IMP-1 Magnetic Field Experiment, Buenos Aires, Argentina, COSPAR, submitted to Space Research VI, 1965.

Ness, N.F., The Earth's Magnetic Tail, J. Geophys. Res., 70, 2989-3006, 1965b.

Ness, N.F., The Magnetohydrodynamic Wake of the Moon, J. Geophys. Res., 70, 517-534, 1965c.

Ness, N.F. and J.M. Wilcox, Sector Structure of the Quiet Interplanetary Magnetic Field, Science, 148, 1592-1594, 1965.

Ness, N.F., C.S. Scearce, and S. Cantarano, Preliminary Results from the Pioneer 6 Magnetic Field Experiment, J. Geophys. Res., 71, 3305-3313, 1966.

Ness, N.F. and J.M. Wilcox, Extension of the Photospheric Magnetic Field Into Interplanetary Space, Astrophys. J., 143, 23-31, 1966.

Ness, N.F., Simultaneous Measurements of the Interplanetary Magnetic Field, J. Geophys. Res., 71, 3319-3324, 1966.

Neugebauer, M. and C.W. Snyder, The Mission of Mariner 2: Preliminary Observations, Solar Plasma Experiment, Science, 138, 1095, 1962.

Northrop, T.G., and E. Teller, Stability of the Adiabatic Motion of Charged Particles in the Earth's Field, Phys. Rev., 117, 215-225, 1960.

Northrop, T.G., The Adiabatic Motion of Charged Particles, John Wiley and Sons (Interscience) New York, 1963.

Obayashi, T., The Streaming of Solar Flare Particles and Plasma in Interplanetary Space, Space Science Reviews, 3, 79-108, 1964a.

Obayashi, T., Interaction of Solar Plasma Streams with the Outer Geomagnetic Field, J. Geophys. Res., 69, 861-868, 1964b.

Olbert, S. and G. Moreno, Analysis of the Solar Wind in the Transition Region, Am. Geophys. Union, 45, 605 (Abstract), 1964.

Olbert, S., Unpublished Notes, Cambridge, Mass., 1966.

Parker, E.N., Interaction of the Solar Wind with the Geomagnetic Field, Phys. Fluids, 1, 171-187, 1958a.

Parker, E.N., Dynamics of the Interplanetary Gas and Magnetic Field, Astrophys. J., 128, 664-676, 1958b.

Parker, E.N., Cosmic-Ray Modulation by Solar Wind, Phys. Rev., 110, 1445-1449, 1958c.

Parker, E.N., The Hydrodynamic Theory of Solar Corpuscular Radiations and Stellar Winds, Astrophys. J., 132, 821-866, 1960.

Parker, E.N., Sudden Expansion of the Solar Corona Following a Large Solar Flare and the Attendant Magnetic Field and Cosmic-Ray Effects, Astrophys. J., 133, 1014-1033, 1961a.

Parker, E.N., The Stellar-Wind Regions, Astrophys. J., 134, 20-27, 1961b.

Parker, E.N., Interplanetary Dynamical Processes, Interscience Publishers, a Division of John Wiley and Sons, Inc., New York, 1963.

Parker, E.N., Dynamical Theory of the Solar Wind, Space Sci. Rev., 4, 666-708, 1965a.

Parker, E.N., Dynamical Properties of Stellar Coronas and Stellar Winds, IV. The Separate Existence of Subsonic and Supersonic Solutions, Astrophys. J., 141, 1463-1478, 1965b.

Parker, E.N., On the Existence of Slow Solutions in Coronal Hydrodynamics, Astrophys. J., 141, 322-324, 1965c.

Parker, E.N., The Passage of Energetic Charged Particles Through Interplanetary Space, Planet, Space Sci., 13, 9-49, 1965d.

Parker, E.N., Dynamical Properties of Stellar Coronas and Stellar Winds. V. Stability and Wave Propagation, Astrophys. J., 143, 32-37, 1966.

Parker, L.W., A Computer Program for Calculating the Charge Distribution About a Space Vehicle, AAS, 2nd Symposium on Interaction of Space Vehicles with an Ionized Atmosphere, Miami Beach, Florida, Mov. 1965.

Petschek, H.E., Magnetic Field Annihilation, AVCO Corp, Report AMP 123, 1963.

Petschek, H.E., Magnetic Field Annihilation, in AAAS-NASA Symposium on the Physics of Solar Flares, NASA-SP-50, Edited by W.N. Hess, pp. 425-439, Washington, D.C., 1964.

Piddington, J.H., The Cis-Lunar Magnetic Field, Planet. Space Sci. 9, 305-318, 1962.

Razdan, H., D.S. Colburn, and C.P. Sonett, Recurrent SI+ and SI- Impulse Pairs and Shock Structure in M-Region Beams, Plant Space Sci., 13, 1111-1123, 1965.

Rossi, B., Interplanetary Plasma, Space Research III, 529-539, 1963.

Russian Report to COSPAR, Investigations of the Upper Atmosphere and Outer Space Carried out in the USSR in 1965, Ninth Plenary Meeting, Vienna, Austria, 1966.

Sarabhai, V., Some Consequences of Nonuniformity of Solar Wind Velocity, J. Geophys. Res., 68, 1555-1557, 1963.

Scarf, F.L., W. Berstein, and R.W. Bernstein, Electron Acceleration and Plasma Instabilities in the Transition Region, J. Geophys. Res., 70, 9-20, 1965.

Sen, A.K., Stability of the Magnetospheric Boundary, Planet. Space Sci., 13, 131-141, 1965.

Serbu, G.P. and E.J.R. Maier, Low Energy Electrons Measured on IMP-2, J. Geophys. Res., 71, 3755-3766, 1966.

Shen, C.S., and C.C. Chang, Fermi Acceleration of Charged Particles in the Transition Region Beyond the Magnetosphere, J. Geophys. Res., 71, 241-252, 1965.

Shklovsky, I.S., Moroz, V.I., and V.G. Kurt, The Nature of the Earth's Third Radiation Belt, Soviet Astronomy. A.J., 4, 871-873, 1961, (or, Astron Zhurnal, 37, 931-934, 1960).

Slutz, R.J., Numerical Method for Calculating the Equilibrium Configuration of Free-Surface Plasma, Bull. Am. Phys. Soc., 8, 165-167, 1963.

Snyder, C.W., M. Neugebauer, and V.R. Rao, The Solar Wind Velocity and Its Correlation with Cosmic-Ray Variations and with Solar and Geomagnetic Activity, J. Geophys. Res., 68, 6361-6370, 1963.

Snyder, C.W., and M. Neugebauer, Interplanetary Solar Wind Measurements by Mariner II, Space Research IV. Edited by P. Muller, pp. 89-113, Interscience Publishers, a Division of John Wiley and Sons, Inc., New York, 1964.

Snyder, C.W., and M. Neugebauer, The Relation of Mariner 2 Plasma Data to Solar Phenomena, in The Solar Wind, ed. by Mackin and Neugebauer, Pergamon Press, 1966.

Sonett, C.P., L. Davis, Jr., and P.J. Coleman, J. Phys. Soc. Japan, 17, Suppl. II-A, 524, 1962.

Sonett, C.P., D.S. Colburn, L. Davis, Jr., E.J. Smith, and P.J. Coleman, Jr., Evidence for a Collision-Free Magnetohydrodynamic Shock in Interplanetary Space, Phys. Rev. Letters, 13, 153-156, 1964.

Spitzer, Lyman, Jr., Physics of Fully Ionized Gases, 2nd Ed., Interscience Publishers, A Division of John Wiley and Sons, Inc., New York, 1962.

Spreiter, J.R. and B.R. Briggs, Theoretical Determination of the Form of the Boundary of the Solar Corpuscular Stream Produced by Interaction with the Magnetic Dipole of the Earth, J. Geophys. Res., 67, 37-51, 1962. Also NASA Tech. Report R-120, 1961.

Spreiter, J.R. and W.P. Jones, On the Effect of a Weak Interplanetary Magnetic Field on the Interaction Between the Solar Wind and the Geomagnetic Field, J. Geophys. Res., 68, 3555-3565, 1963.

Spreiter, J.R., A.L. Summers, and A.Y. Alkane, Hydromagnetic Flow Around the Magnetosphere, Planet. Space Sci., 14, 223-253, 1966.

Störmer, C., The Polar Aurora, Oxford Press, London, 1955.

Strong, I.B., J.R. Asbridge, S.J. Bame, and H.E. Felthauser, Electrons in the Transition Region Between the Bow Shock and the Magnetosphere, Am. Geophys. Union, 47, 142 (Abstract), 1966a.

Strong, I.B., J.R. Asbridge, S.J. Bame, H.H. Heckman, and A.J. Hundhausen, Measurements of Proton Temperatures in the Solar Wind, Phys. Rev. Letters, 16, 631-633, 1966b.

Sturrock, P.A., and J.R. Spreiter, Shock Waves in the Solar Wind and Geomagnetic Storms, J. Geophys. Res., 70, 5345-5352, 1965.

Sturrock, P.A., and R.E. Hartte, Two Fluid Model of the Solar Wind, Phys. Rev. Letters, 16, 628-631, 1966.

Sugiura, M. and J.P. Heppner, The Earth's Magnetic Field, in Introduction to Space Science, Edited by W. Hess, Gordon & Breach Science Publishers, New York, 1965.

Taylor, H.A., H.C. Brinton, and C.R. Smith, Positive Ion Composition in the Magnetoionosphere Obtained from the OGO-A Satellite, J. Geophys. Res., 70, 5769-5782, 1965.

Vasyliunas, V., Unpublished Notes, Cambridge, Mass., 1964.

Vasyliunas, V., Private Communication, Cambridge, Mass., 1966a.

Vasyliunas, V., Observations of 50 to 2000 ev Electrons With OGO-A, Am. Geophys. Union, 47, 142 (Abstract), 1966b.

Vasyliunas, V., Observations of Low Energy Electrons with the OGO-A Satellite, M.I.T., Ph.D. Thesis, Cambridge, Mass., Unpublished, 1966c.

Walters, G.K., Effect of Oblique Interplanetary Magnetic Field on Magnetosphere Shape and Behavior, J. Geophys. Res., 69, to appear, 1964.

Wilcox, J.M. and N.F. Ness, Quasistationary Co-Rotating Structure in the Interplanetary Medium, J. Geophys. Res., 70, 5793-5805, 1965.

Wilcox, J.M., Solar and Interplanetary Magnetic Fields, Science, 152, 161-166, 1966.

Wolfe, J.H., R.W. Silva, and M.A. Myers, Observations of the Solar-Wind-Geomagnetic Field Interaction Region on IMP-II and OGO-I, Proc. of the Sixth COSPAR Symp., Mar Del Plate, Argentina, 1965.

Wolfe, J.H., R.W. Silva, and Marilyn A. Meyers, Observations of the Solar Wind During the Flight of IMP-1, J. Geophys. Res., 71, 1319-1340, 1966a.

Wolfe, J.H., R.W. Silva, D.D. McKibbin, and R.H. Mason, The Compositional, Anistropic and Nonradial Flow Characteristics of the Solar Wind, J. Geophys. Res., 71, 3329-3335, 1966b.

BIOGRAPHICAL NOTE

The author was born on November 23, 1936 in New York City. After graduating from Regis High School in 1954, he attended Manhattan College where he received the Bachelor of Electrical Engineering degree, cum laude, in 1958. Upon graduation he joined the M.I.T. Lincoln Laboratory as a Staff Associate and began studies leading to the Master of Science degree in Electrical Engineering in 1960.

The following three years were spent in the U.S. Air Force at the Space Systems Division in Los Angeles, California. There he was actively involved with the Satellite Control Facility which serves as the ground-space communication link for the Air Force's many satellite programs. Having completed his tour of duty, he left the service as a 1st Lt. and returned to M.I.T. in 1963 to start the doctoral program with the support of the Staff Associate program of the Lincoln Laboratory.

Since returning to M.I.T., the author has been associated with the Cosmic Ray Group of the Laboratory for Nuclear Science and has been actively engaged in the plasma research program carried out under the direction of Dr. H.S. Bridge.

The author is a member of Eta Kappa Nu, Tau Beta Pi and Sigma Xi.